ตัวเร่งปฏิกิริยาซัลไฟด์ของโลหะแทรนซิชันแบบไม่มีตัวรองรับสำหรับ
ไฮโดรดีซัลเฟอไรเซชันเชิงลึกของเชื้อเพลิงไฮโดรคาร์บอน

นางสาว บุญญาวัณย์ อยู่สุข
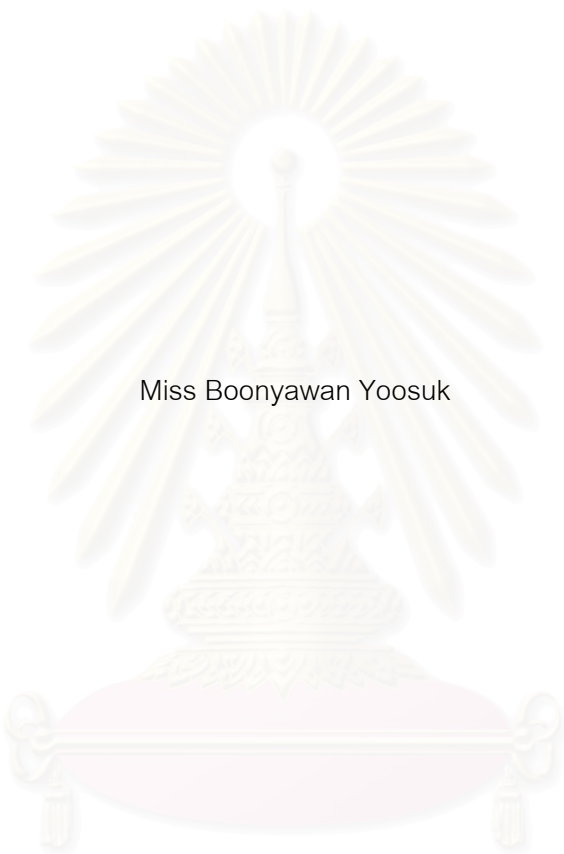
UNSUPPORTED TRANSITION METAL SULFIDE CATALYSTS FOR

DEEP HYDRODESULFURIZATION OF HYDROCARBON FUELS

Miss Boonyawan Yoosuk

A Dissertation Submitted in Partial Fulfillment of the Requirements

for the Degree of Doctor of Philosophy Program in Chemical Technology

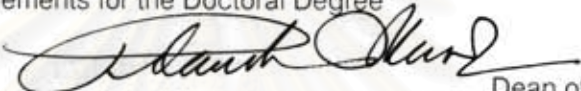Department of Chemical Technology

Faculty of Science

Chulalongkorn University

Academic Year 2007

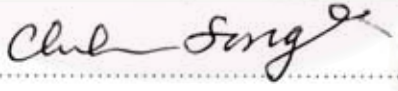|	
Thesis Title	UNSUPPORTED TRANSITION METAL SULFIDE CATALYSTS FOR DEEP HYDRODESULFURIZATION OF HYDROCARBON FUELS
By	Miss Boonyawan Yoosuk
Filed of study	Chemical Technology
Thesis Advisor	Professor Pattarapan Prasassarakich, Ph.D.
Thesis Co-advisor	Professor Chunshan Song, Ph.D.
Thesis Co-advisor	Chawalit Ngamcharussrivichai, Ph.D.

Accepted by the Faculty of Science, Chulalongkorn University in Partial Fulfillment of the Requirements for the Doctoral Degree

....Dean of the Faculty of Science

(Professor Piamsak Menasveta, Ph.D.)

THESIS COMMITTEE

....Chairman

(Associate Professor Tharapong Vitidsant, Ph.D.)
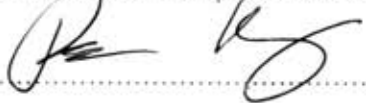
....Thesis Advisor

(Professor Pattarapan Prasassarakich, Ph.D.)

....Thesis Co-advisor

(Professor Chunshan Song, Ph.D.)

....Thesis Co-advisor

(Chawalit Ngamcharussrivichai, Ph.D)

.... Member

(Associate Professor Amorn Petsom, Ph.D.)

.... Member

(Associate Professor Pornpote Piumsomboon, Ph.D)

.... Member

(Associate Professor Paisan Kongkachuichay, Ph.D)

บุญญาวัณย์ อยู่สุข : ตัวเร่งปฏิกิริยาซัลไฟด์ของโลหะแทรนซิชันแบบไม่มีตัวรองรับสำหรับ ไฮโดรดีซัลเฟอไรเซชันเชิงลึกของเชื้อเพลิงไฮโดรคาร์บอน. (UNSUPPORTED TRANSITION METAL SULFIDE CATALYSTS FOR DEEP HYDRODESULFURIZATION OF HYDROCARBON FUELS) อ. ที่ปรึกษา : ศ.ดร.ภัทรพรรณ ประศาสน์สารกิจ, อ. ที่ปรึกษา ร่วม : Prof. Chunshan Song และ ดร.ขวลิต งามจรัสศรีวิชัย, 156 หน้า

ความต้องการของเชื้อเพลิงสะอาดส่งผลให้เกิดความพยายามทั่วโลกอย่างต่อเนื่องใน การลดระดับกำมะถันในเชื้อเพลิงอย่างมาก ก่อให้เกิดความต้องการของตัวเร่งปฏิกิริยาไฮโดรดีซัลเฟอ- ไรเซชันที่มีประสิทธิภาพสูง จุดประสงค์ของงานวิจัยนี้เพื่อศึกษาศักยภาพของตัวเร่งปฏิกิริยาโมลิบดีนัม พื้นฐานแบบไม่มีตัวรองรับซึ่งเตรียมจากวิธีไฮโดรเทอร์มอล ตัวเร่งปฏิกิริยาแบบไม่มีตัวรองรับมีแอกทิวิ- ตีสูงสำหรับไฮโดรดีซัลเฟอร์ไรเซชั่นของไดเบนโซไทโอฟีน และ 4,6-ไดเมทิลไดเบนโซไทโอฟีน แอกทิวิตี และพื้นที่ผิวของตัวเร่งปฏิกิริยา แปรผันอย่างมากกับอุณหภูมิและความดันในกระบวนการเตรียม ตัว ทำละลายอินทรีย์ที่เติมในกระบวนการเตรียมช่วยเพิ่มการกระจายตัวของโมเลกุลของสารตั้งต้น ตัวเร่ง ปฏิกิริยาโมลิบดีนัมพื้นฐานทั้งที่ไม่มีและมีตัวช่วยเร่งปฏิกิริยา (โคบอล หรือ นิกเกิล) มีความแตกต่าง กันทั้งสมบัติและแอกทิวิตี การเติมตัวช่วยเร่งปฏิกิริยาทำให้เกิดการลดลงของพื้นที่ผิวและปริมาตรรู- พรุน การวิเคราะห์เชิง TPR บงชี้ว่าตัวช่วยเร่งปฏิกิริยาลดความแข็งแรงของพันธะระหว่างโลหะ และซัลเฟอร์ ผลการวิเคราะห์เชิง HRTEM และ XRD แสดงว่าการเติบโตของอนุภาคตัวเร่งปฏิกิริยาถูก ชะลอเมื่อมีการเติมตัวช่วยเร่งปฏิกิริยา ตัวช่วยเร่งปฏิกิริยายังช่วยเพิ่มแอกทิวิตีการดีซัลเฟอร์ไรเซชัน ของโมลิบดีนัมซัลไฟด์ และเปลี่ยนสัดส่วนของเส้นทางไฮโดรดีซัลเฟอไรเซชันโดยตรง และเส้นทาง ไฮโดรจีเนชัน ผลที่สำคัญของตัวช่วยเร่งปฏิกิริยา คือ การเพิ่มอัตราการแตกของพันธะคาร์บอน และซัลเฟอร์ การดูดซับของไดเบนโซไทโอฟีน และ 4,6-ไดเมทิลไดเบนโซไทโอฟีนในวัฏภาคของเหลว ถูกใช้เพื่อศึกษาความสามารถการดูดซับและกลไกการดูด-ซับบนตัวเร่งปฏิกิริยาที่เตรียมได้ ผลการ ทดลองแสดงให้เห็นว่า ตัวช่วยเร่งปฏิกิริยาไม่เพียงแต่เพิ่มจำนวนตำแหน่งกัมมันต์ แต่ยังช่วยในการ เพิ่มแอกทิวิตีของตำแหน่งกัมมันต์ของโมลิบดีนัมซัลไฟด์

ภาควิชา	เคมีเทคนิค	ลายมือชื่อนิสิต	บุญญาวัณย์ อยู่สุข
สาขาวิชา	เคมีเทคนิค	ลายมือชื่ออาจารย์ที่ปรึกษา	
ปีการศึกษา	2550	ลายมือชื่ออาจารย์ที่ปรึกษาร่วม	
		ลายมือชื่ออาจารย์ที่ปรึกษาร่วม	

4673813623   : MAJOR   CHEMICAL TECHNOLOGY

KEYWORD: HYDRODESULFURIZATION / UNSUPPORTED SULFIDE CATALYST / MOLYBDENUM / COBALT / NICKEL / ULTRA-CLEAN FUELS

BOONYAWAN YOOSUK : UNSUPPORTED TRANSITION METAL SULFIDE CATALYSTS FOR DEEP HYDRODESULFURIZATION OF HYDROCARBON FUELS. THESIS ADVISOR : PROF. PATTARAPAN PRASASSARAKICH, THESIS COADVISOR : PROF. CHUNSHAN SONG AND CHAWALIT NGAMCHARUSSRIVICHAI, Ph.D., 156 pp.

The requirement of clean fuels has resulted in a continuing worldwide effort to dramatically reduce the sulfur levels. This is driving the need for more active hydrodesulfurization (HDS) catalysts. The purpose of this research is to study the potential of unsupported Mo based sulfide catalysts prepared from hydrothermal method. The unsupported catalysts exhibited the excellent activity for the simultaneous HDS of dibenzothiophene (DBT) and 4,6-dimethyldibenzothiophene (4,6-DMDBT). Activity and surface area of catalysts depend strongly upon the preparation temperature and pressure. Organic solvent added in catalyst preparation helps to improve the dispersion of the precursor molecules. The unpromoted and promoted (Co or Ni) Mo sulfide catalysts have different properties and activity. Addition of promoter decreased surface area and pore volume. TPR analysis suggested that promoter decrease metal sulfur bond strength. HRTEM and XRD results showed that the growth of catalyst particle was suppressed when promoter was added. The promoter increased HDS activity of MoS_2 and changed the contribution of the direct-desulfurization and of hydrogenation pathways. The main effect of the promoter was to increase the rate of C–S bond cleavage. The liquid-phase adsorption of DBT and 4,6-DMDBT was used to study the adsorption capacity and mechanism over the synthesized catalysts. The results showed that the promoters not only increase active site number, but also enhance activity of active sites of the Mo sulfide.

Department.....Chemical Technology......Student's signature....Boonyawan Yoosuk....

Field of study...Chemical Technology.....Advisor's signature........................

Academic year..........2007................Co-advisor's signature........................

                                Co-advisor's signature........................

ACKNOWLEDGMENTS

CONTENTS

LIST OF TABLES

LIST OF FIGURES

NOMENCLATURES

ATTM	:	Ammonium tetrathiomolybdate
B	:	Boron
BCH	:	Bicyclohexyl
BET	:	Brunauer-Emmet-Teller
BP	:	Biphenyl
BT	:	Benzothiophene
C_1-BT	:	Methyl-Benzothiophene
C/C_0	:	A ratio of the outlet concentration to the initial concentration
CHB	:	Cyclohexylbenzene
Co	:	Cobalt
Cr344	:	Commercial alumina supported CoMo sulfide catalyst
Cr424	:	Commercial alumina supported NiMo sulfide catalyst
CUS	:	Coordinative Unsaturated Sites
DBT	:	Dibenzothiophene
DDS	:	Direct desulfurization
DFT	:	Density Functional Theory
3,3,-DMBCH	:	Dimethylbicyclohexane
3,3'-DMBP	:	3,3'-Dimethylbiphenyl
2,3-DMBT	:	2,3-Dimethylbenzothiophene
2,4-DMDBT	:	2,4-Dimethyldibenzothiophene
2,6-DMDBT	:	2,6-Dimethyldibenzothiophene
2,7-DMDBT	:	2,7-Dimethyldibenzothiophene
2,8-DMDBT	:	2,8-Dimethyldibenzothiophene
3,6-DMDBT	:	3,6-Dimethyldibenzothiophene
3,7-DMDBT	:	3,7-Dimethyldibenzothiophene
4,6-DMDBT	:	4,6-Dimethyldibenzothiophene
FCC	:	Fluid Catalytic Cracking
GC-AED	:	Gas Chromatography Atomic Emission Detector
GC-FID	:	Gas Chromatography Frame Ionization Detector
GC-PFPD	:	Gas Chromatography - Pulsed Flame Photometric Detector
GC-MS	:	Gas Chromatography Mass Spectroscopy
HDS	:	Hydrodessulfurization

HDN	:	Hydrodenitrogenation
HDO	:	Hydrodeoxygenation
HDM	:	Hydrodemetallization
HHDBT	:	Hexa-hydrodibenzothiophene
HHDMDBT	:	Hexa-hydrodimethyldibenzothiophene
HTREM	:	High Resolution Transmission Electron Microscopy
HYD	:	Hydrogenation
k	:	Total rate constant
k_1	:	Rate constant of hydrogenation pathway
k_2	:	Rate constant of direct desulfurization pathway
LCO	:	Light Cycle Oil
LHSV	:	Liquid Hourly Space Velocity
MCHT	:	Methylcyclohexyltoluene
2-MDBT	:	2-Methyldibenzothiophene
3-MDBT	:	3-Methyldibenzothiophene
4-MDBT	:	4-Methyldibenzothiophene
Mo	:	Molybdenum
MT	:	Methylthiophene
Ni	:	Nickel
P	:	Phosphorus
PASCs	:	Poly-Aromatic Sulfur Compounds
Pd	:	Palladium
ppm	:	Part Per Million
PSU-SARS	:	The Pennsylvania State University - Selective Adsorption for Removing Sulfur
Pt	:	Platinum
Ru	:	Rutheniun
STM	:	Scanning Tunneling Microscope
THDBT	:	Treta-hydrodibenzothiophene
THDMDBT	:	Treta-hydrodimethyldibenzothiophene
2,3,5-TMBT	:	2,3,5-Trimethylbenzothiophene
2,3,6-TMBT	:	2,3,6-Trimethylbenzothiophene
2,3,7-TMBT	:	2,3,7-Trimethylbenzothiophene

TMDBT	:	Trimethyldibenzothiophene
TOF	:	Turn Over Frequency
TPR	:	Temperature Programmed Reduction
W	:	Tungsten
XRD	:	X-Ray Diffraction

CHAPTER I

INTRODUCTION

1.1 Motivation

The challenge of fulfilling the world's growing transportation energy needs is no longer a simple issue of producing enough liquid hydrocarbon fuels. This challenge is accentuated by a complex interplay of environmental and operational issues. Environmental issues include societal demands that liquid hydrocarbon fuels be clean and least emission of pollutants upon utilization. The emergence of new refining processes and the increasing use of new forms of energy conversion, e.g. fuel cells, exemplify operational issues.

The requirement of ultra-clean transportation fuels, particularly, gasoline, diesel, and jet fuels, has resulted in a continuing worldwide effort to dramatically reduce the sulfur levels [1-5]. Sulfur content in diesel fuel is an environmental concern because upon combustion, sulfur is converted to SOx, which not only contributes to acid rain, but also poisons the catalytic converter for exhaust emission treatment. Sulfur content is usually expressed as the weight percent (wt %) of sulfur in the fuel, since there are many different sulfur-containing compounds in petroleum-derived fuels.

The government agencies in various countries have implemented more stringent regulations for refineries to produce cleaner gasoline and diesel fuels with reduced sulfur content. The US Clean Air Act Amendments of 1990 and the new regulations by the US Environmental Protection Agency (EPA), and government regulations in many countries call for the production and use of more environmentally friendly transportation fuels with lower contents of sulfur and aromatics. Recently, the fuel specifications for all highway diesel fuels in the US, Japan, and Western Europe requied the sulfur content of the diesel fuels to be less than 0.05 wt.% or 500 parts per million by weight (ppmw). The new government regulations in many countries further lowered the contents of sulfur and aromatics during 2004–2007 [6]. In most countries, the sulfur content in diesel will be restricted to 50 ppm within another 5 years [7, 8]. In the

European Union, the maximum permissible sulfur content of diesel will be reduced from 50 ppm to 10 ppm in the year 2009 (4). Now, the sulfur content of diesel fuel is down to 50 ppm in USA and 15 ppm in Japan. In Thailand, the Ministry of Energy plans to further reduce sulfur in diesel to below 350 ppm and 50 ppm in 2010.

The problem of deep removal of sulfur has become more serious due to the lower and lower limit of sulfur content in the finished fuel products by regulatory specifications, and the higher and higher sulfur contents in the crude oils. A survey of the data on crude oil sulfur content and API gravity for the past two decades reveals a trend that US refining crude continue towards higher sulfur contents and heavier feeds [9, 10]. Together, these trends are driving the need for better catalysts for deep desulfurization. Conventional catalysts used in the hydrotreating process include mainly Ni or Co promoted Mo- or W-based catalysts supported by γ-Al$_2$O$_3$ [11]. They are active in converting thiophene and benzothiophenes, but not active enough to desulfurize efficiently the most refractory sulfur-containing poly-aromatic compounds, e.g. dibenzothiophene (DBT) and its alkyl-substituted derivatives which are the major portion of sulfur in the high-boiling fraction of crude oil, i.e. heavy naphtha, diesel, and light FCC naphtha. Such a demand for more active hydrodesulfurization catalysts has triggered a significant increase in research activity on HDS catalysts [1, 2, 12]. These studies have shown that one way to improve the MoS$_2$-based catalysts could be to increase the amount of active phase or to use bulk sulfides. The emergence of highly loaded sulfide catalysts demonstrates that sulfide-based systems still have great potential for improvement.

1.2 Hydrotreating

Hydrotreating or hydroprocessing refers to a variety of catalytic hydrogenation processes which saturate unsaturated hydrocarbons and remove S [by hydrodesulfurization (HDS)], N [by hydrodenitrogenation (HDN)], O [by hydrodeoxygenation (HDO)] and metals [by hydrodemetallization (HDM)] from different petroleum streams in a refinery. Hydrotreating processes have been developed from the cracking and hydrogenation processes introduced in petroleum refineries in the 1930s [13]. Hydrotreating is a group of very important processes and has been studied extensively for many decades. Hydrotreaters now occupy a central role in modern refineries. It can affect a refinery's product by strategic placement within the overall refinery processes as shown in Figure 1.1.

The distinguishing feature of the hydroprocesses is that although the composition of the feedstock is relatively complex and a variety of reactions may occur simultaneously, the final product may actually meet all the required specifications for its particular use. Some of the main purposes of hydrotreating of different refinery streams are summarized in Table 1.1.

In hydrotreating, the feedstock is reacted with hydrogen at elevated temperatures in the range of 300 – 450 ^{o}C, and elevated pressures in the range of 0.7 – 15 MPa in the presence of a hydrogenation catalyst. Typical hydrotreating process conditions used in industry are shown in Table 1.2. Commercial hydrotreating catalysts are, typically, sulfides of molybdenum (Mo) or tungsten (W) supported on γ-Al$_2$O$_3$ and promoted by ether Co or Ni. Nickel, known for its high hydrogenation activities, is preferred as a promoter when feedstocks contain high amounts of nitrogen and aromatics. The composition ranges and physical properties of typical hydrotreating catalysts in the oxidic phase are summarized in Table 1.3. Hydrotreating catalysts are, typically, sold in the oxidic phase although the active phase is a metal sulfide. Prior to their use, the oxide catalysts are converted to sulfide form in the reactor using either hydrogen sulfide or a sulfur containing hydrocarbon feedstock. HDS has frequently been the most important objective of hydrotreating and has, therefore, been the focus of most scientific and technologic research.
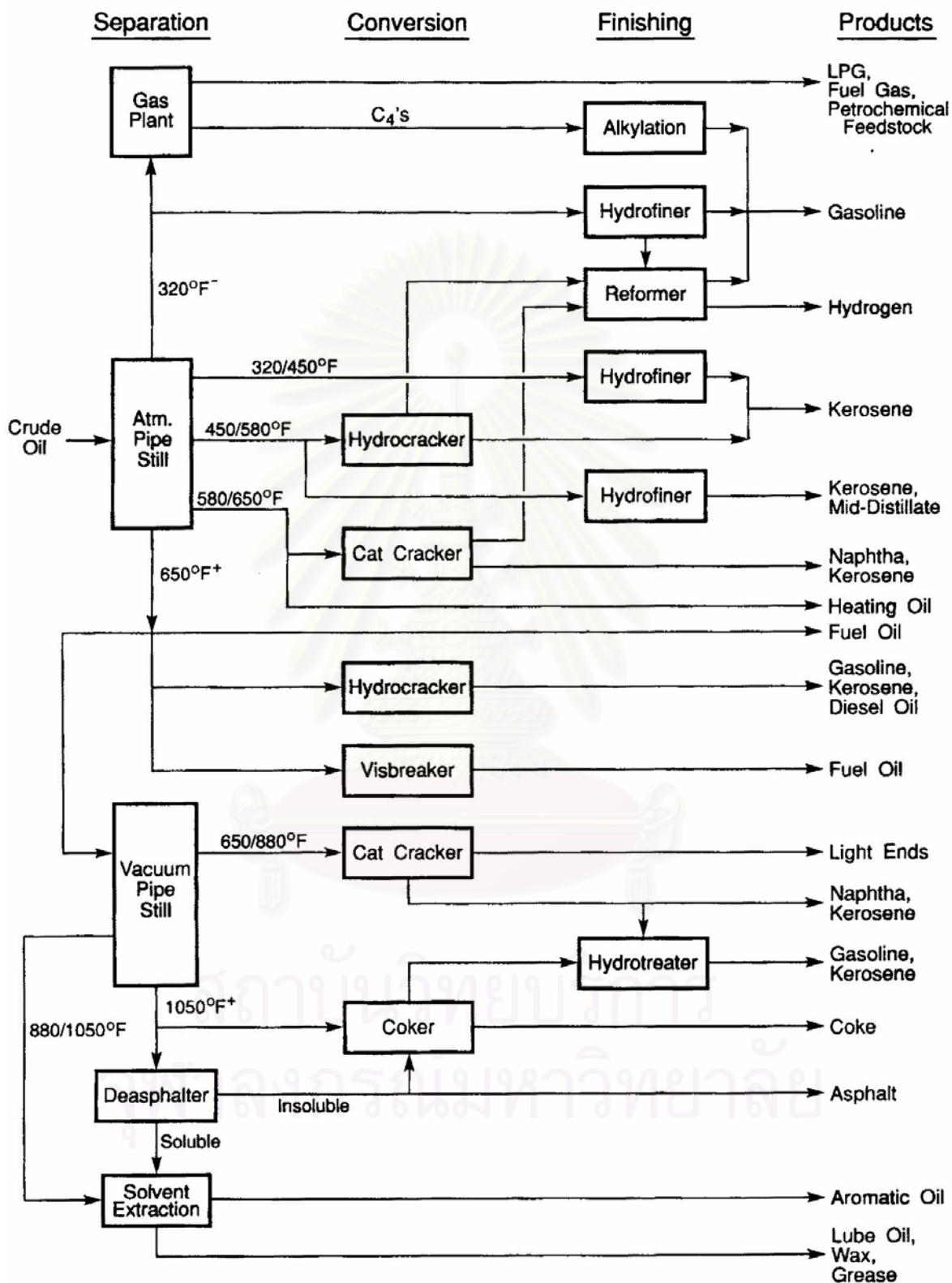
Figure 1.1 Refinery schematic showing the placement of hydrotreating units [11].

Table 1.1 Main Purposes for Hydrotreating of Different Refinery Streams [13].

Hydrotreating reaction	Stream being treated	Main purpose
HDS	Catalytic reformer feeds	Avoid catalyst poisoning
	Diesel	Meet environmental limits
	Distillate fuel oils	Meet environmental limits
	FCC feeds	Avoid sulfur oxides release during regeneration
	Various streams	Reduce corrosion during refining and handling
	Straight run products	Improve odor
	HCR feeds	Reduce catalyst poisoning
	Resids	Meet fuel oil specifications or pretreated feedstocks
	Steam reformer feeds	Avoid catalyst poisoning
	Coker feeds	Reduce sulfur content of coke
HYD	Diesel	Hydrogenation of aromatics to improve cetane index and meet environmental limits
	Kerosene, jet fuel	Improve smoke point (aromatic reduction)
	FCC feeds	Partial saturation of polyaromatic compounds to improve cracking reactivity/selectivity; reduce coking of FCC catalyst
	Cracked feeds	Olefin/diolefin hydrogenation to increase stability (reduce gum formation in diesel and kerosene)
HDN	Lube oils	Polishing (improve stability)
	FCC and HCR feeds	Avoid poisoning of acid sites
	Hydrocracking feeds	Avoid poisoning of acid sites
HCR	VGO, resides	Conversion to lighter fractions
Dewaxing	Diesel, VGO	Improve flow properties
Mild HCR	VGO	Conversion to lighter fractions
HDM	FCC and HCR feeds	Avoid metal deposition, non-selective cracking, coke build-up, and zeolite destruction
	Resids	Reduce metal deposition
CCR reduction	FCC feeds, resids	Reduce coking on FCC catalyst

Table 1.2 Typical Hydrotreating Process Conditions Used in Industry [14].

Fuel type and historical conditions	Temperature (^{o}C)	Hydrogen pressure (MPa)	LHSV (h^{-1})
Recent history			
Naphtha	290-370	1.38-3.45	2-8
(gasoline)	315-400	3.45-8.27	2-4
Kerosene/gas oil			
(jet/diesel fuels)	370-425	5.17-13.80	1.0-3.0
FCC feed pretreated			
Current trends			
Naphtha	290-370	1.38-5.17	2-6
(gasoline)	315-400	3.45-10.30	0.5-3.0
Kerosene/gas oil			
(jet/diesel fuels)	370-425	6.90-20.70	0.5-2.0
FCC feed pretreated			

Table 1.3 Composition and Properties of Typical Hydrotreating Catalysts [15].

Composition and properties	Range	Typical values
Active phase precursors (wt%)		
MoO_3	13-20	15
CoO	2.5-3.5	3.0
NiO	2.5-3.5	3.0
Promoters (wt%)		
SiO_2	0.5-1	0.5
B, P	0.5-1	0.5
Physical properties		
Surface area (m^2/g)	150-500	180-300
Pore volume (cm^3/g)	0.25-0.8	0.5-0.6
Pore diameter (nm)		
Mesopores	3-50	7-20
Macropores	100-5000	600-1000
Extrudate diameter (mm)	0.8-4	3
Extrudate length/diameter	2-4	3
Bulk density (g/ml)	0.5-1.0	0.7
Average crush strenght/length (kg/mm)	1.0-2.5	1.9

*Active phase precursors are supported on a γ-Al_2O_3 carrier

1.3 Hydrodesulfurization

Hydrodesulfurization is catalytic hydrogenation processes which remove sulfur in petroleum. The hydrodesulfurization process had been developed in the 1960s to remove high concentration of sulfur in fuel [16]. The main aims of hydrodesulfurization are to prevent poisoning of sulfur-sensitive metal catalysts used in subsequent reactions and the catalytic converter in an automobile, to remove the unpleasant odor, to minimize the amount of sulfur oxides introduced into the atmosphere (contribution to acid rain) by combustion of petroleum-based fuels in catalytic cracking to meet environmental restrictions and to reduce corrosion problem in the refining process.

For hydrodesulfurization process, hydrocarbon feed-stocks and hydrogen are passed through a catalyst bed at elevated temperature and pressure. Some of the sulfur atoms attached to hydrocarbon molecules react with hydrogen on the surface of the catalyst forming hydrogen sulfide (H_2S). H_2S is removed as a gas. The reaction of an aliphatic compound is schematically shown in eq. (1.1), where R stands for alkyl.

$$R-SH+H_2 \rightarrow R-H+H_2S \qquad (1.1)$$

A similar reaction applies to aromatic and polyaromatic sulfur compounds, where a desulfurized hydrocarbon and H_2S again are the final products. However, the mechanism of the reaction of sulfur compounds containing aromatic ring(s) is not as simple as presented in eq. (1.1), but can proceed through several reaction pathways. More details will be presented in Section 1.6 and it will be shown that a similar reaction network exists for all poly-aromatic sulfur compounds.

Hydrotreater feedstocks are highly complex mixtures. In contrast to a model feed of one or a few organo-sulfur compounds in a solvent of choice, a real fuel consists of a cocktail of hundreds of paraffins, naphthenes, polycyclic aromatics, organo-sulfur and nitrogen compounds. Deep HDS is known to be affected by components in the reaction mixture such as organic hetero-compounds and poly-aromatic hydrocarbons [13, 17, 18].

1.4 Sulfur Compounds
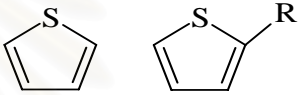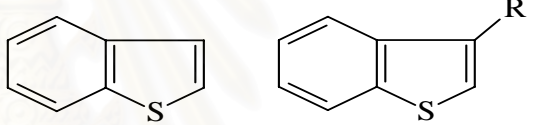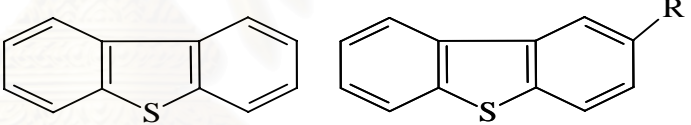
Petroleum is not a uniform substance, and its chemical and physical composition varies not only with the location and age of the oil field but also with the depth of the individual well. On a molecular basis, petroleum is a complex mixture of hydrocarbons with small amounts of organic compounds containing sulfur, oxygen, and nitrogen as well as compounds containing metallic constituents, particularly vanadium, nickel, iron and copper. The elemental compositions of crude in a whole series of crude oils vary over fairly narrow limits as shown in Table 1.4.

Table 1.4 Elemental Composition of Petroleum [11].

Element	% wt
Carbon	83.0 – 87.0
Hydrogen	10.0 – 14.0
Nitrogen	0.1 – 2.0
Oxygen	0.05 – 1.5
Sulfur	0.05 – 6.0
Metals (Ni and V)	< 1000 ppm

The sulfur compounds found in petroleum or synthetic oils are generally classified into two types: nonheterocycles and heterocycles. The former comprises thiols, sulfides and disulfides. The heterocycles are mainly composed of thiophenes with one to several aromatic rings and their alkyl or aryl substitutents. Examples of sulfur compounds are shown in Table 1.5.

Table 1.5 Sulfur Containing Molecules in Petroleum [16].

Compound class	Structure
Nonheterocycles	
Thiols (mercaptan)	RSH
Sulfides	RHR'
Disulfides	RSSR'
Heterocycles	
Thiophenes	
Benzothiophenes	
Dibenzothiophenes	

Since the new regulations of transportation fuel require very low concentration of sulfur compounds, a good understanding of the compositional features of transportation fuel in the terms of sulfur species that have to be desulfurized is important to aid their deep desulfurization. There are three major types of transportation fuels i.e. gasoline, diesel and jet fuel that are different in composition and properties. The common types of sulfur compounds in liquid fuels are listed below.

    1. Gasoline range: naphtha and fluid catalytic cracking (FCC)–naphtha

        - mercaptanes (RSH); sulfides (R_2S); and disulfides (RSSR)

        - thiophene and its alkylated derivatives

        - benzothiophene.

    2. Jet fuel range: heavy naphtha and middle distillate

        - benzothiophene (BT) and its alkylated derivatives.

3. Diesel range: middle distillate and light cycle oil (LCO)
    - alkylated benzothiophenes
    - dibenzothiophene (DBT) and its alkylated derivatives.
4. Boiler fuel feeds: heavy oils and distillation residues
    - ≥3-ring polycyclic sulfur compounds, including DBT benzonaphthothiophene (BNT)
    - phenanthro[4,5-*b,c,d*]thiophene (PT) and their alkylated derivatives.

Ma et al. (2001) conducted a detailed analysis to identify the type of sulfur compounds and their alkylated isomers in a commercial gasoline, diesel and jet fuel sample by using Gas Chromatography - Pulsed Flame Photometric Detector (GC–PFPD) [19]. From Figure 1.2, in each fuel, the sulfur compounds left in the finished products are those that have lower reactivity among all the sulfur compounds. Sulfur compounds tend to become larger in ring size and higher in number of substitutes as the fuel becomes higher in boiling point ranges from gasoline to jet fuels to diesel.
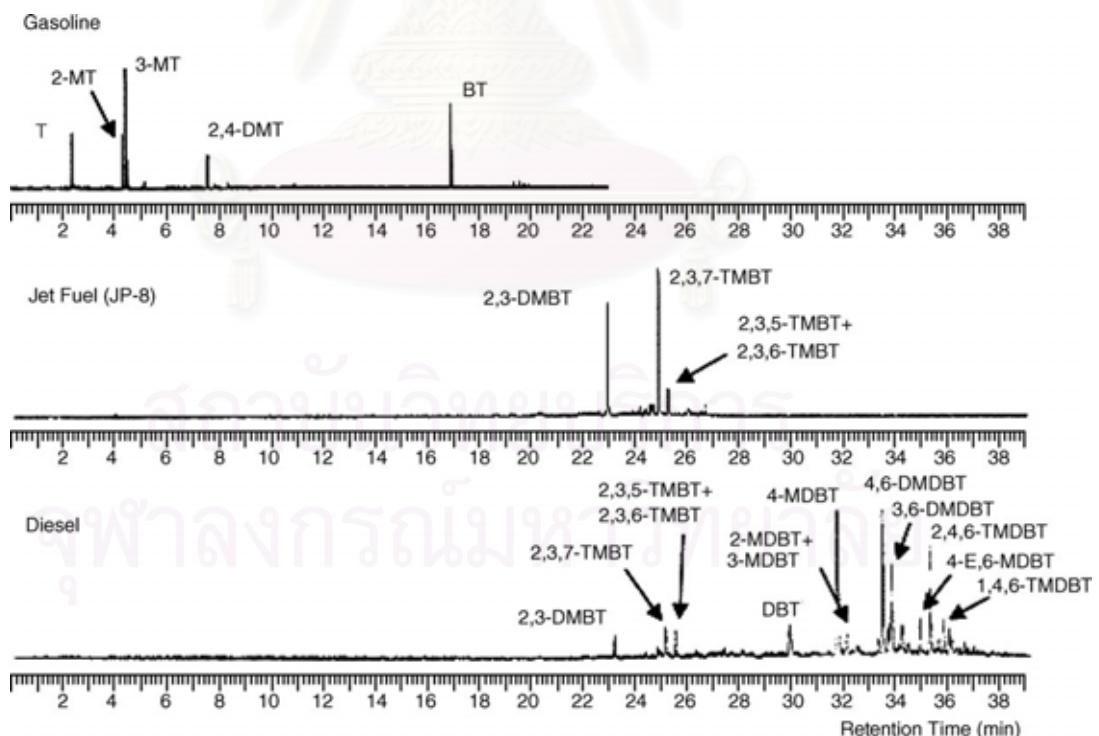
Figure 1.2 Sulfur compounds in commercial gasoline, jet fuel and diesel identified by GC-PFPD analysis coupled with GC-MS and reaction kinetic analysis [19].

1.5 Reactivity of Poly-Aromatic Sulfur Compounds (PASCs)

The organic sulfur compounds present in petroleum vary widely in their reactivities in catalytic hydrodesulfurization. Figure 1.3 presents a qualitative relationship between the type and size of sulfur molecules in various distillate fuel fractions and their relative reactivities. For the sulfur compounds without a conjugation structure between the lone pairs on S atom and the π-electrons on aromatic ring, including disulfides, sulfides, thiols, and tetra-hydrothiophene, HDS occurs directly through hydrogenolysis pathway (more details in each pathway described in Section 1.6). These sulfur compounds exhibit higher HDS reactivity than that of thiophene by an order of magnitude, because they have higher the electron density on the S atom and weaker C–S bond [20]. The reactivities of the 1- to 3-ring sulfur compounds decrease in the order: thiophenes > benzothiophenes > dibenzothiophenes [17, 21-24]. In naphtha, thiophene is so much less reactive than the thiols, sulfides, and disulfides that the latter can be considered to be virtually infinitely reactive in practical high-conversion processes [25, 26]. Similarly, in gas oils, the reactivities of (alkyl-substituted) 4-methyldibenzothiophene (4-MDBT) and 4,6-dimethyldibenzothiophene (4,6-DMDBT) are much lower than those of other sulfur-containing compounds [26-29]. Consequently, in deep HDS, the conversion of these key substituted dibenzothiophenes largely determines the required conditions. In 1997, Gates and Topsoe [26] pointed out that 4-MDBT and 4,6-DMDBT are the most appropriate compounds for investigations of candidate catalysts and reaction mechanisms.
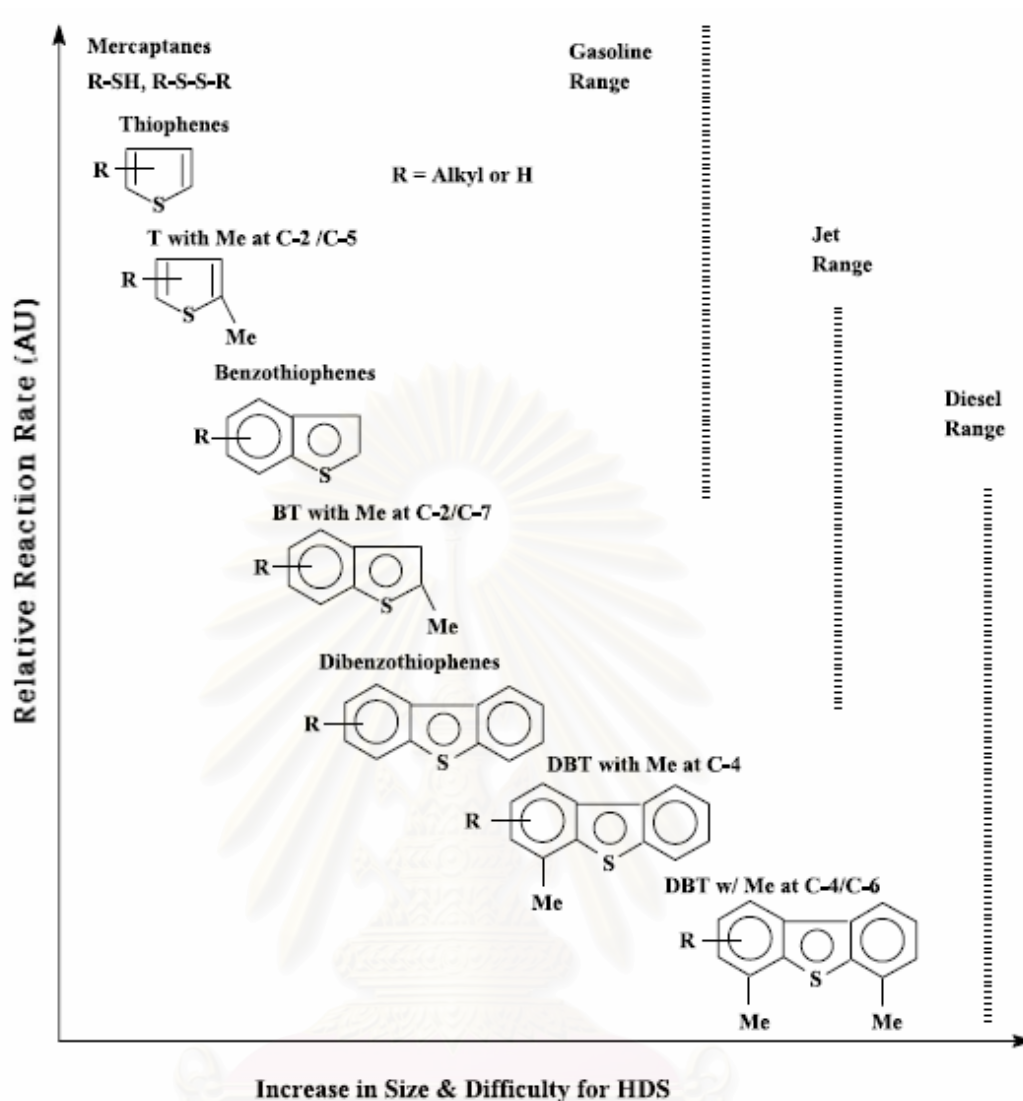
Figure 1.3 Relative reactivity of various organic sulfur compounds in HDS versus their ring sizes and positions of alkyl substitutions on the ring [1].

HDS reactivities of heterocyclic sulfur compounds in a diesel fuel are governed basically by the types of C-S bonds and the position of alkyl substituents. The first factor is related to the strength of C-S bonds, and the second is related to the steric hindrance as well as the electron density on the sulfur atom [30]. Ma et al. [28] identified individual sulfur species in a diesel fuel of boiling range 232 – 365 ^{o}C and quantified their reactivities by studying the desulfurization over a commercial NiMo/γ-Al$_2$O$_3$ catalyst at 360 ^{o}C and 45 atm hydrogen pressure. The kinetics for the HDS of these species was determined by lumping the rate constants for the individual sulfur species into four groups listed in decreasing order of reactivity as below:

Group 1 - Benzothiophenes with no substituents in the 2- or 7- position
(39 %wt)
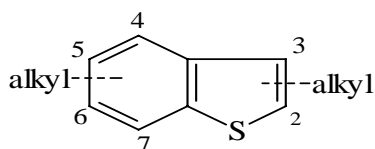
Relative k = 1

Group 2 - Dibenzothiophenes with no substituents in the 4- or 6- position
(20 %wt)
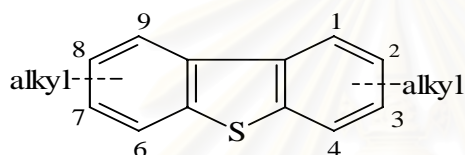
Relative k = 0.230

Group 3 - Dibenzothiophenes with one substituents in the 4- position
(26 %wt)
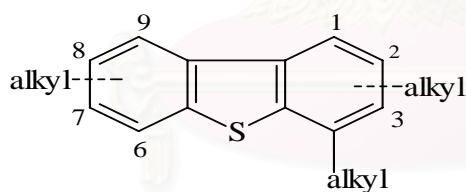
Relative k = 0.080

Group 4 - Dibenzothiophenes with two substituents in the 4- or 6-
position (15 %wt)
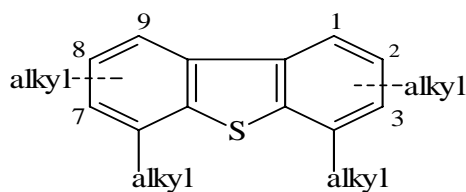
Relative k = 0.028

The relative contribution of each group to the net sulfur content of the diesel (shown in parentheses) clearly indicates that the bulk sulfur in diesel feedstocks is dibenzothiophenic in nature. Deep desulfurization will require that all compounds of groups 1, 2 and 3 are completely desulfurized and at least half of those in the least reactive fourth group are also converted.

It has been known for many years that the desulfurization of benzothiophenes (BTs) and dibenzothiophenes (DBTs) is affected by the presence of alkyl substituents. Three decades ago, Givens and Venuto [31] demonstrated that the position and number of substituents present on benzothiophene (BT) strongly influenced the overall reactivity of the molecule and thus, the degree of desulfurization. However, not all substituted dibenzothiophenes are difficult to be desulfurized. Houalla et al. [23, 32] reported that ring substitution in remote position such as 2-, 3-, 7- and 8- on DBT did little to reduce reactivity. However, they did establish that substitution in the 4- and 6- positions decreases the molecular reactivity by one order of magnitude. Thus, this is clearly demonstrated in four groups which provide molecular structures of poly-aromatic sulfur compounds (PASCs) along with their relative reaction rate constants. The refractory nature of 4-MDBT and 4,6-DMDBT has been further confirmed by some recent studies [33-36].

1.6 HDS Reaction Mechanism for Poly-Aromatic Sulfur Compounds (PASCs)

Hydrodesulfurization of organic sulfur compounds generally proceeds through two possible pathways (direct desulfurization and hydrogenation) as shown in Figure 1.4.
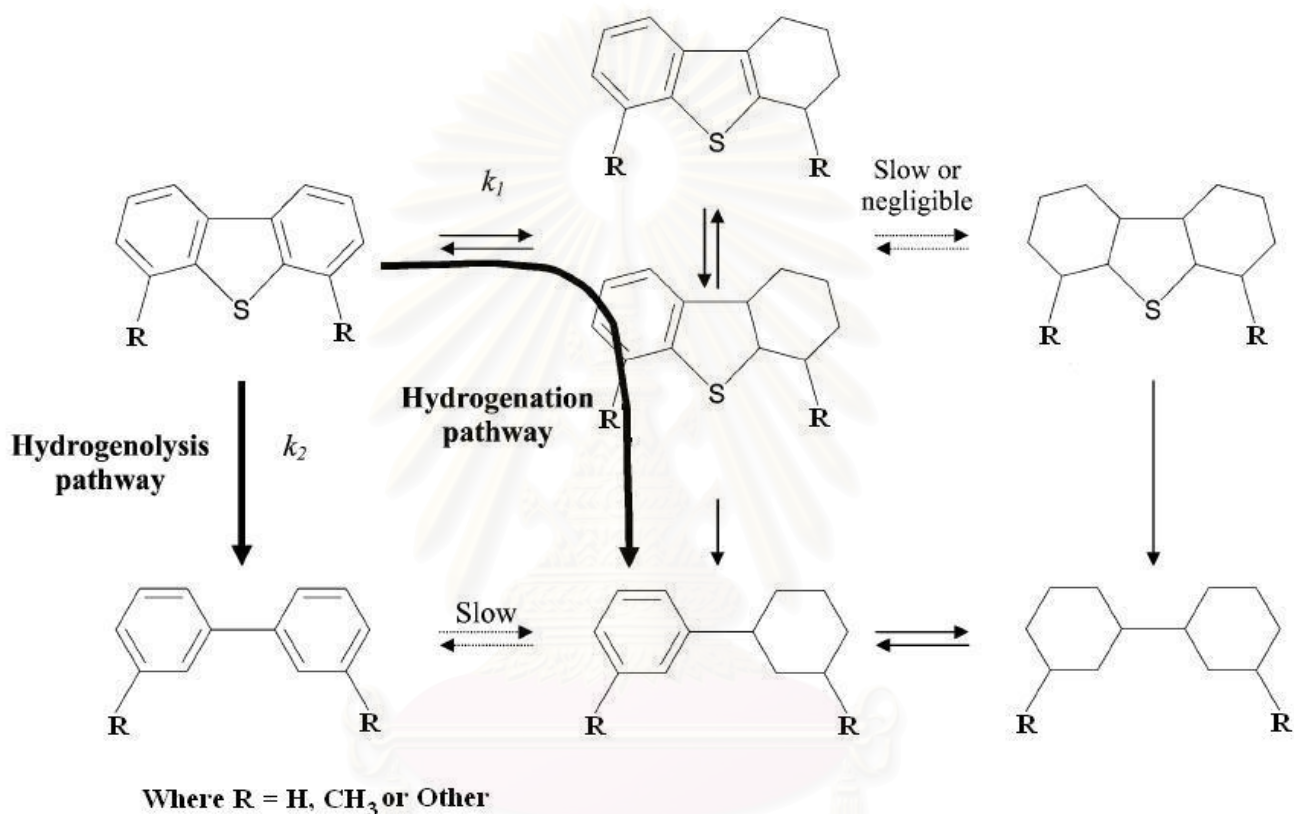
Figure 1.4 Mechanistic pathways of desulfurization of poly-aromatic sulfur compounds via a ring hydrogenation network (denoted by the rate constant k_1) and a direct C-S bond hydrogenolysis network (denoted by the rate constant k_2) [13].

1.6.1 Direct Desulfurization Pathway

Direct-desulfurization (DDS) or hydrogenolysis pathway involves chemisorption of the sulfur atom in molecule on an exposed Mo ion at a sulfur vacancy through a one-point attachment as shown in Figure 1.5 (a). This is followed by hydrogen transfer and sulfur elimination to complete desulfurization [37]. The HDS of DBT occurs predominantly via the DDS pathway. However, hydrogenolysis does not saturate the benzene rings in 4,6-DMDBT.

1.6.2 Hydrogenation Pathway

The second pathway is called hydrogenation (HYD), involving the adsorption of sulfur compounds on the MoS_2 stack through the π - electrons on the aromatic rings as shown in Figure 1.5 (b). This is followed by hydrogenation of one of the aromatic rings and sulfur elimination to complete desulfurization. 4,6-DMDBT is generally desulfurized through the HYD pathway because the direct adsorption of sulfur atom in 4,6-DMDBT on the active sites is hindered by the two methyl groups at the 4- and 6-positions. If 4,6-DMDBT is first hydrogenated to hexahydro-DMDBT, the steric hindrance is reduced and the electron density on the S atom is increased. As a result, the hydrogenated 4,6-DMDBT is easily desulfurized [38-40].

1.6.3 Difficulty in HDS Reaction of Poly-Aromatic Sulfur Compounds

It is well known that DBT with alkyl substitutents are difficult to be desulfurized because their HDS reactivity in both direct desulfurization and hydrogenation pathways are inhibited. Gates and Topsoe [26] pointed out that 4-MDBT (4-methyldibenzothiophene) and 4,6-DMDBT are the most appropriate compounds for investigation of candidate catalysts and reaction mechanism. The sulfur atom in 4-MDBT and 4,6-DMDBT is difficult to be adsorbed on to Mo cations with sulfur vacancies in MoS_2 because of steric hindrance caused by the methyl groups in the 4- and 6- positions [22, 32]. The difficulty in the adsorption of the sulfur atom on to the Mo cation significantly inhibits the direct desulfurization pathway.
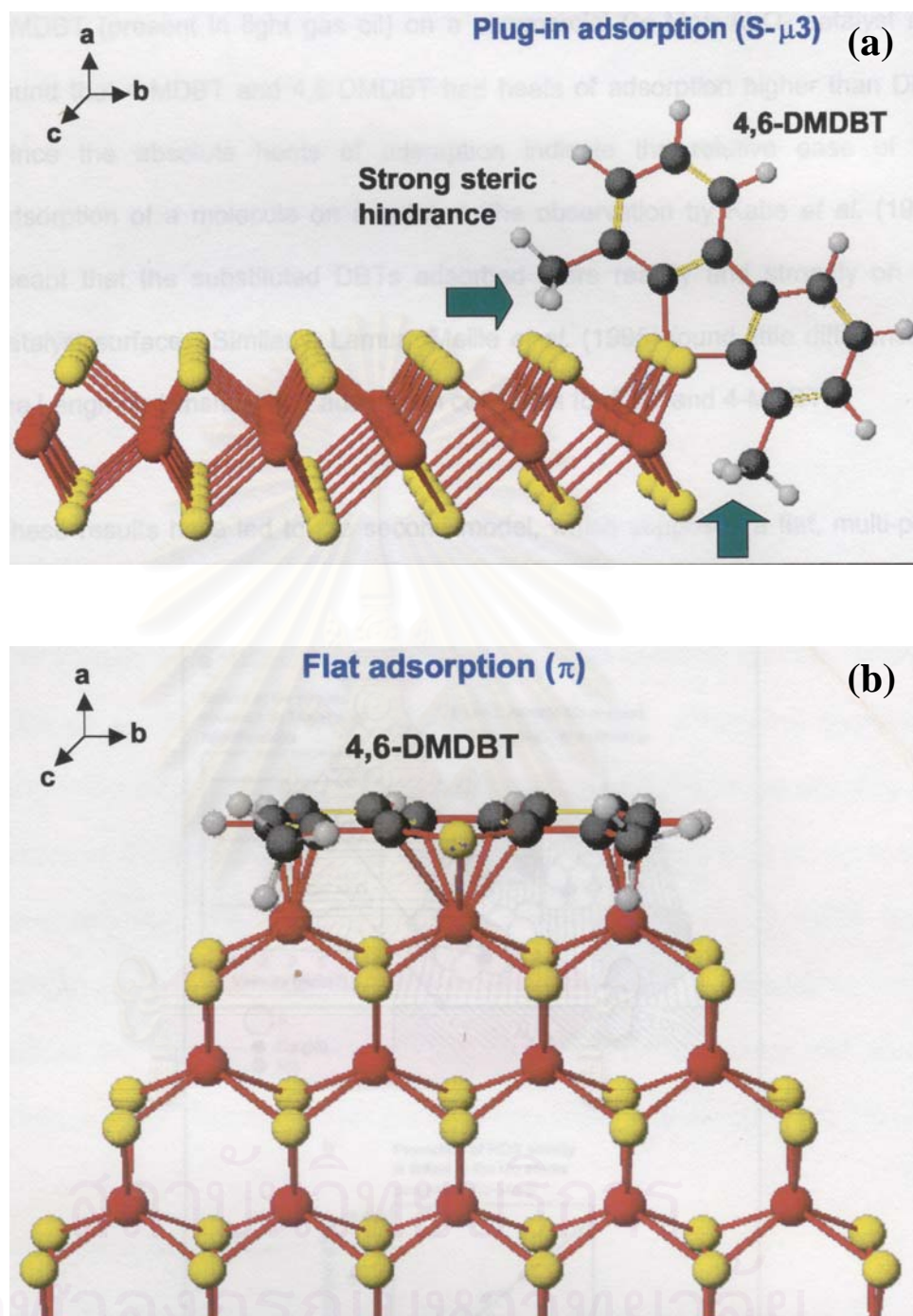
Figure 1.5 Adsorption conformations of 4,6-DMDBT at (a) the hydrogenolysis active site and (b) the hydrogenation active site. There is a strong steric hindrance in the plug-in adsorption [2].

Computer modeling and simulation of the active sites on the catalyst surface and their interaction with sulfur compounds have also been applied to understand the reaction pathways and mechanisms [41-43]. Figure 1.5 shows two types of chemisorption patterns of 4,6-DMDBT on MoS_2, the S-μ3 type adsorption (Figure 1.5(a)) and flat adsorption (Figure 1.5(b)). In the flat adsorption, the sulfur compound is adsorbed flat on the adsorption site through π electron on the aromatic rings where as the sulfur atom in the thiophenic compound interacts directly with the adsorption site in the plug-in adsorption. Semi-empirical calculations have been carried out to illustrate the difference in chemisorption patterns between DBT and 4,6-DMDBT. Both DBT and 4,6-DMDBT can interact well with MoS_2 catalyst by flat chemisorption. The S-μ$_3$ type chemisorption of 4,6- DMDBT, differently from that of the DBTs without any alkyl group at both 4- and 6-positions, is difficult due to the steric hindrance of the alkyl groups adjacent to the sulfur atom. This steric hindrance is expected to increase with increasing molecular size of the alkyl groups (from methyl to ethyl to propyl).

Kabe et al. [45] proposed that 4-MDBT or 4,6-DMDBT can be adsorbed on the catalyst through π-electron in the aromatic rings more strongly than that of DBT and the C–S bond cleavage of adsorbed DBTs is disturbed by steric hindrance of the methyl group. Previous studies by Mochida's group [46-49] have demonstrated that, over the industrial HDS catalysts, the refractory sulfur compounds, particularly 4,6-DMDBT, are desulfurized dominantly via the hydrogenation pathway as the alkyls at the 4- and/or 6-position of DBT strongly block the hydrogenolysis pathway. Quantum chemical calculation on the conformation and electron property of the various sulfur compounds and their HDS intermediates by Ma et al. [29, 47, 50] shows that the hydrogenation pathway favors desulfurization of the refractory sulfur compounds as a result of both decreasing the steric hindrance of the methyl groups and increasing the electron density on the sulfur atom in the sulfur compounds. When the desulfurization of the refractory sulfur compounds occurs dominantly through the hydrogenation pathway, the inhibition of the coexistent aromatics towards the HDS by competitive adsorption on the hydrogenation active sites becomes stronger in deep HDS [51]. H_2S produced in the early stage of the reaction is one of the main inhibitors for HDS of the unreactive species [52, 53].

1.7 Hydrodesulfurization Catalysts

The catalyst selection for a certain process is based on studies of activity, selectivity and lifetime. This is usually a very long and difficult task. Once the suitable catalyst giving the desired product quality at a reasonable cost is found, the search for a better catalyst starts immediately. In hydroprocessing, the selection of a catalyst depends mainly on the desired conversion and characteristics of the processed feedstock. As mentioned above, the characteristics of feed vary widely. The amount of impurities and the physical properties thus determine the choice of the catalyst. This suggests that a universal catalyst or a catalytic system suitable for hydroprocessing of the feeds from different crudes does not exist. With respect to the chemical and physical properties, a wide range of hydroprocessing catalysts has been developed for commercial applications.

1.7.1 Commercial HDS Catalysts

Hydrodesulfurization catalysts consist of metals impregnated on a porous alumina support. Almost all of the surface area is found in the pores of alumina, and the dispersed metals appear in a thin layer over the entire alumina surface within the pores. Cobalt, molybdenum and nickel are the most commonly used metals for desulfurization catalysts. The catalysts are manufactured with the metals in an oxide state. They are converted to the active sulfide form by sulfiding the catalyst either prior to use or in situ during the HDS reaction. Any catalyst that exhibits hydrogenation activity will catalyze hydrodesulfurization to some extent. However, the group VIB metals (chromium, molybdenum and tungsten) are highly active for desulfurization, especially when promoted with metals from the iron group (iron, cobalt, nickel).

Cobalt-molybdenum catalysts are by far the most popular choice for desulfurization, particularly for straight-run petroleum fractions. Nickel-molybdenum catalysts are often chosen instead of cobalt-molybdenum catalysts when higher activity is required for saturation of polynuclear aromatic compounds or removal of nitrogen compounds or desulfurization of more refractory sulfur compounds, such as those in cracked feedstock. In some applications, nickel-cobalt-molybdenum (Ni-Co-Mo) catalysts offer a useful balance of hydrotreating activity. Nickel-tungsten (Ni-W) is

usually chosen only when very high activity for aromatic saturation is required along with activity for desulfurization and denitrogenation. The catalysts are available in several different compositions as shown in Table 1.6. Co-Mo and Ni-Mo catalysts resist poisoning and are the most universally applied catalysts for HDS of every fraction from naphtha to residue. For practical applications, Ni–Mo catalysts generally have higher hydrogenation ability for saturating aromatic ring that is connected to thiophenic sulfur, while Co–Mo catalysts generally have higher selectivity towards C–S bond cleavage without hydrogenation of neighboring aromatic rings. For HDS under high H_2 pressure, Ni–Mo catalysts tend to be more active than Co–Mo catalysts.

Table 1.6 Representative Metal Content of Commercial Catalyst [11].

	Co-Mo	Ni-Mo	Ni-Co-Mo	Ni-W
Metal (%wt)				
Cobalt (Co)	2.5	-	1.5	-
Nickel (Ni)	-	2.5	2.3	4.0
Molybdenum (Mo)	10.0	10.0	11.0	-
Tungsten (W)	-	-	-	16.0

The catalyst development has been one of the focuses of industrial research and development for deep HDS [54]. For example, new and improved catalysts have been developed and marketed by Akzo Nobel, Criterion, Haldor-Topsoe, IFP, United Catalyst/Sud-Chemie, Advanced Refining, ExxonMobil, Nippon Ketjen in Japan, and RIPP in China. Recently, NEBULA catalyst has been developed jointly by ExxonMobil, Akzo Nobel and Nippon Ketjen and commercialized in 2001 [55]. NEBULA stands for New Bulk Activity, a bulk base metal catalyst without using a porous support. Figure 1.6 shows the recent results published by Akzo Nobel on relative activity of the new NEBULA and STARS catalysts compared to the conventional CoMo/Al_2O_3 developed over the last 50 years [56]. The physical appearance of NEBULA is shown in Figure 1.7.
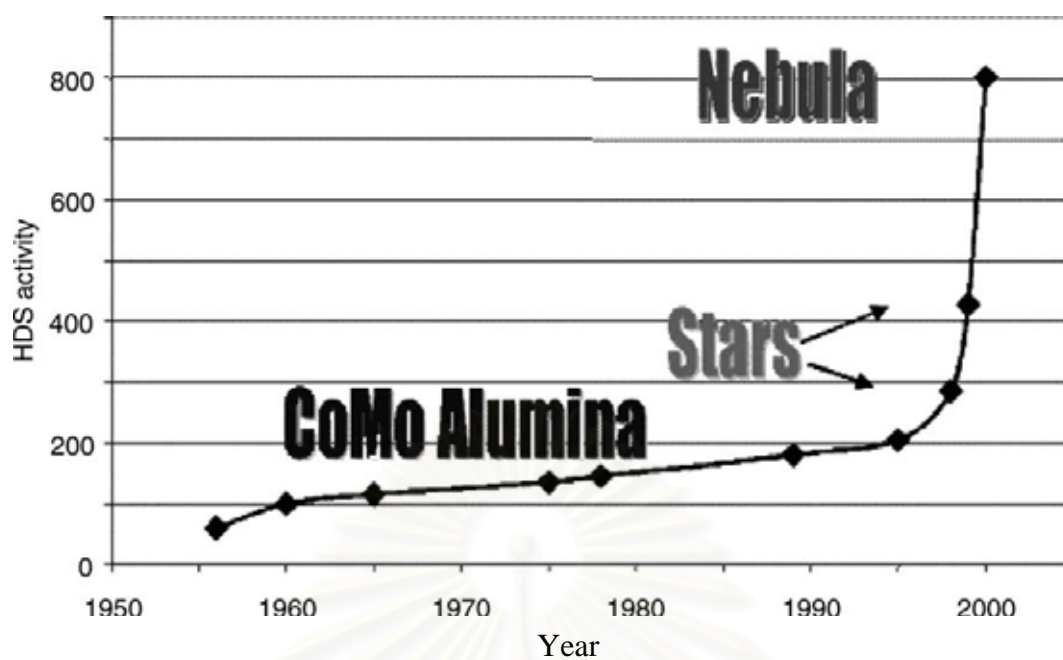
Figure 1.6 Development of HDS catalysts over the past 50 years [56].

Figure 1.7 Physical appearance of NEBULA-1 catalyst [57].

1.7.2 Molybdenum Sulfide Catalyst

Molybdenum disulfide (MoS_2), the main active phase in hydrotreating catalysts, has a layered structure and could be visualized as a sandwich of the metal between two sulfur layers. A layer compound consists of stacks of S-Mo-S slabs held together by Van der Waals interactions. Each slab composes of two hexagonal planes of S atoms and an intermediate hexagonal plane of Mo atoms, which are trigonal prismatically coordinated to the S atoms as shown in Figure 1.8. The morphology of the MoS_2 nanocluster is determined by the relative stability of two types of edge terminations, i.e., the S-edge and the Mo-edge. Molybdenum cations at the corners and edges terminating the layered structure of MoS_2 are responsible for its catalytic activity [59, 60].
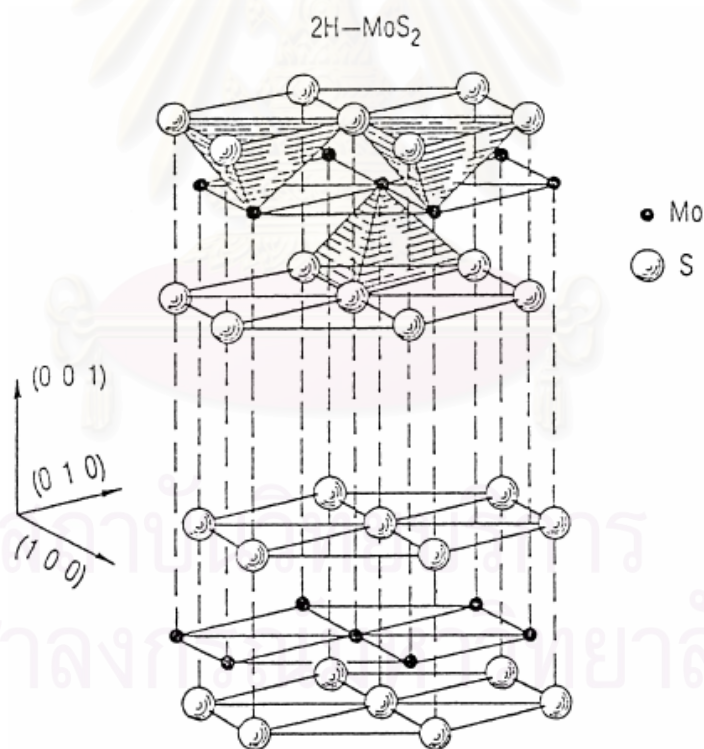
Figure 1.8 2H-MoS_2 hexagonal structure showing the S-Mo-S sandwiches and
the interlayer or Van der Waals gap [58].

The importance of the edges and corners of MoS_2 was first reported by Voorhoeve [61] and Farragher [62]. Sulfur anions in the basal planes of MoS_2 are more difficult to be removed than anions at the corners and edges since the latter has a lower degree of coordination. Therefore, there will be a greater number of sulfur vacancies and exposed Mo ions at the edges and corner of the MoS_2 sandwich. These sulfur vacancies, because of their unsaturated state, are the crucial active sites responsible for catalyzing the desulfurization of sulfur compounds. Figure 1.9 shows molecular simulation depicting sulfur vacancies in a stack of MoS_2 and the adsorption modes of DBT [63].
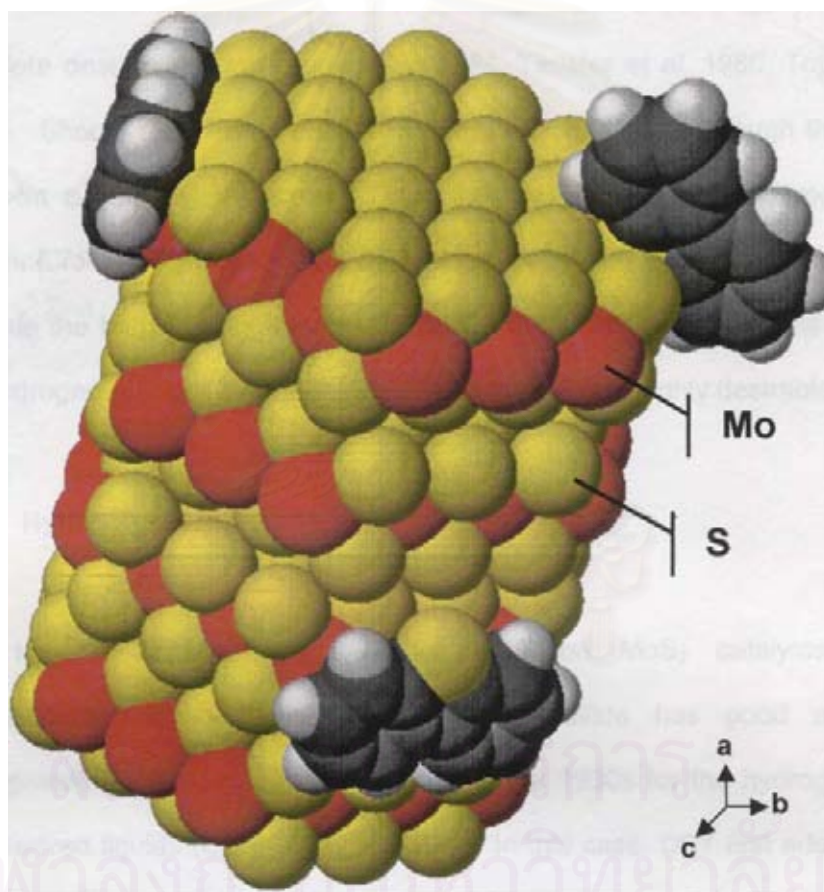
Figure 1.9 Molecular simulation depicting sulfur vacancies in a stack of MoS_2 and the adsorption modes of DBT [63].

In 1994, Daage and Chianelli [64] proposed the first and famous model correlating the structure of MoS_2 with its reactivity for large poly-aromatic sulfur compounds (PASCs). It is called "Rim-Edge Model". This laid the fundamental basis for understanding deep HDS of diesel feedstocks. The rim-edge model is particularly relevant for the HDS of large PASCs e.g., DBT, 4-MDBT and 4,6-DMDBT where steric hindrance is present. In the rim-edge model, the MoS_2 catalyst particle can be described as a stack of several discs. The top and bottom discs are associated with the rim sites. The discs "sandwiched" between the top and bottom discs are associated with the edge sites as shown in Figure 1.10. According to this model, only the rim layers (top and bottom layers of the slabs) provide active sites for hydrogenation. Hydrogenation cannot be catalyzed on the edge plane because aromatic rings cannot be adsorbed via the π coordination due to the steric hindrance. Sulfur hydrogenolysis is promoted on both the rim and edge sites. Thus, the rim-edge model predicts that rim sites dominate hydrogenation and the selectivity for hydrogenation is related to the ratio of rim to edge site. Furthermore, the model clarifies the importance of the attacking of MoS_2 to the interaction of PASCs and thus, their HDS. It should be noted that the rim-edge model was never extended to promoted catalytic systems.
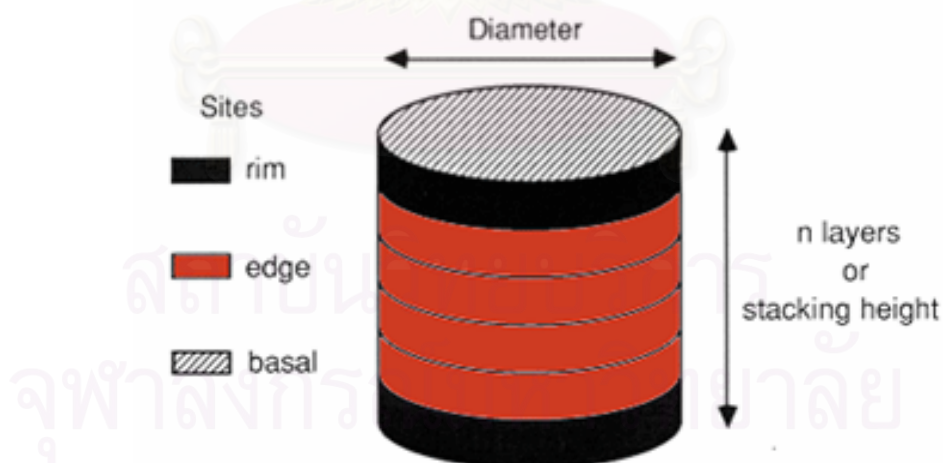
Figure 1.10 Rim-Edge model of a MoS_2 catalyst particle [64].

1.7.3 Role of Promoter.

The promotion of the HDS activity, which is observed when elements such as Co or Ni are added to Mo- or W- based catalysts, is probable the single topic which has attracted the most attention in many studies of HDS catalysts. Figure 1.11 demonstrates as a plot of the HDS rate constant against increasing Co content in the catalytic active phase. This discovery drove extensively research and debate on the role of promoters in the HDS active phase. In order to explain the promotional behaviors, over many years, numerous models and proposals have been suggested as follows:

- Formation of Co species in alumina
- Formation of intercalation structures
- Formation of pseudo intercalation structures
- Formation of Co-Mo-S structures and sites different from those in MoS_2
- An increase in stability/dispersion of Mo phase
- A decrease in deactivation by coke
- An increase in acidity
- Contact synergism; Co_9S_8 (or Co-Mo-S) providing H_2 spillover to MoS_2
- Formation of Co_9S_8 like structures with no role of MoS_2
- Formation of other interaction structures of sulfide Co species
- Prevention of $Al_2(MoO_4)_3$ formation
- An increase in number of sulfur vacancies
- A decrease in number of MoS_2 sulfur vacancies
- An increase in exposure of MoS_2 basal planes
- Influences on MoS_2 morphology
- Changes in reducibility of MoS_2
- Introduced p-type conductivity
- Electron transfer
- An increase in electron density of sulfur
- Coexistence of tetrahedral and octahedral Co species
- Enhancement of H_2 chemisorption
- Modification adsorbate vibrational frequencies

- Creation of non-stoichiometry molybdenum sulfide
- Averaging of heat of formations of Co_9S_8 and MoS_2
- Changed in sulfur-sulfur interaction
- A decrease in metal sulfur bond energies
- Activation of thiophene on promoter atoms in Co-Mo-S and transfer of hydrogen from neighbor Mo sites
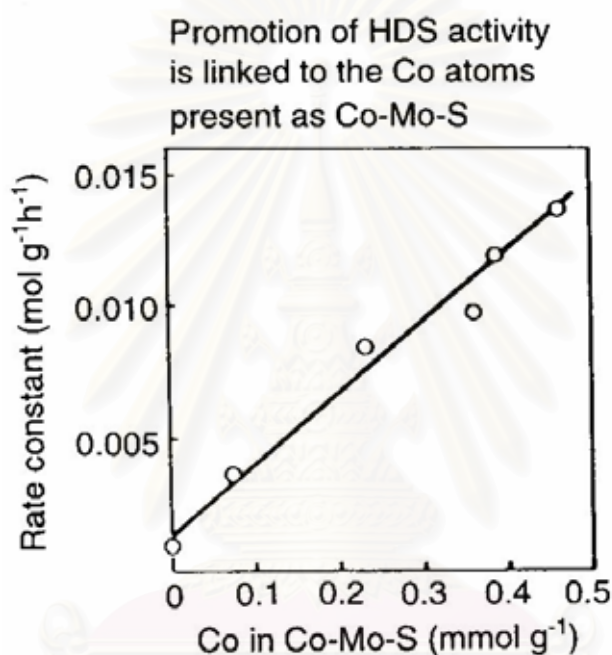
Figure 1.11 A visual description of the promotional effect of Co in Co-Mo/γ-Al$_2$O$_3$ [65].

It is seen that the proposals ranged from Co(Ni) having an indirect textural role to special kinetic effects or specific structures. These different views reflect the difficulties in establishing definitive structure-activity correlations.

Although the HDS catalysts have been used commercially for more than 70 years, the exact chemical nature and structure of the active species are still unclear. Several models have been proposed to explain the HDS active phase in hydrotreating catalysts. A few of the most important models are described here.

1.7.3.1 Monolayer Model

The monolayer model, proposed by Schuit and coworkers [66-71], was the first attempt to explain the structural basis for the activity of CoMo/γ-Al$_2$O$_3$ catalysts as shown in Figure 1.12. The molybdenum species were assumed to be bonded to the surface of the alumina, forming a monolayer. Interaction of the Mo with the alumina was believed to occur via oxygen bridges resulting from reaction with surface OH groups. The incorporation of Mo^{6+} ions was proposed to be compensated by a "capping layer" of O^{2-} ions on top of the monolayer. Cobalt (present as Co^{2+}) was assumed to be in tetrahedral positions on the surface of the alumina, replacing Al^{3+} ions. The promotional effect of cobalt was suggested to result from an increase in the stability of the Mo monolayer caused by the presence of replaced aluminum cations on the surface adjacent to the monolayer. According to this model, sulfide ions (S^{2-}) replace the oxygen ions (O^{2-}) in the "capping layer" upon sulfidin and, due to the larger size of the sulfur ions, a maximum incorporation in the monolayer may be only one sulfur per two oxygen ions. The presence of hydrogen in the catalysis system causes removal of some S^{2-} ions, resulting in reduction of adjacent molybdenum ion to Mo^{3+}. These were believed to be the catalytically active sites for HDS. A modified version of the monolayer model, in which molybdenum species form one-dimensional chains on the surface of the alumina, has been proposed by Massoth [72]. The location of cobalt was not included in this proposal, but Mitchell and Trifiro [73] suggested that Co may be present in the surface layers. It has also been proposed that the monolayer model describes the initial stages of a catalyst during sulfiding and that intercalation structures may be evolved during operation [74].
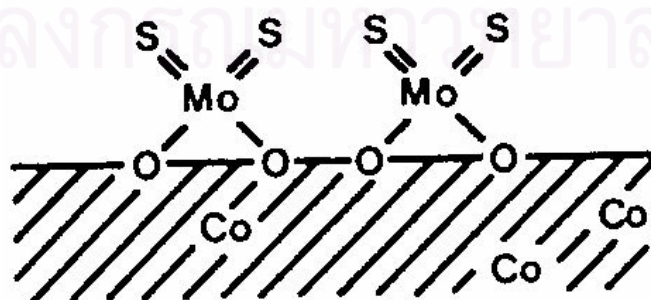
Figure 1.12 Schematic representation of the monolayer model [66].

1.7.3.2 Intercalation Model

Voorhoeve and Stuiver [75, 76] proposed that the MoS_2 structures consist of slabs, each of which comprises a plane of Mo atoms sandwiched between two hexagonal close-packed planes of sulfur atoms. The Co or Ni ions are believed to occupy octahedral intercalation position in the Van der Waal's gap between slabs. Farragher and Cossee [62, 77] later pointed out that intercalation of cobalt and nickel in ideal crystals of MoS_2 is not energetically possible [78]. They modified the model such that the intercalation was assumed to be restricted to the edge surfaces of the MoS_2 lattice. Figure 1.13 presents a schematic drawing of the intercalation model. The promotion was related, via and induced surface reconstruction, to an increase in the concentration of Mo^{3+} ions caused by the presence of the promotion atoms. Provided MoS_2 is present as very small crystals, this model may explain the relatively high Co/Mo ratios necessary to achieve maximum catalytic activity. The intercalation and pseudo-intercalation models implicitly assume the presence of three-dimensional multilayer structures of MoS_2 in order for intercalation to take place.
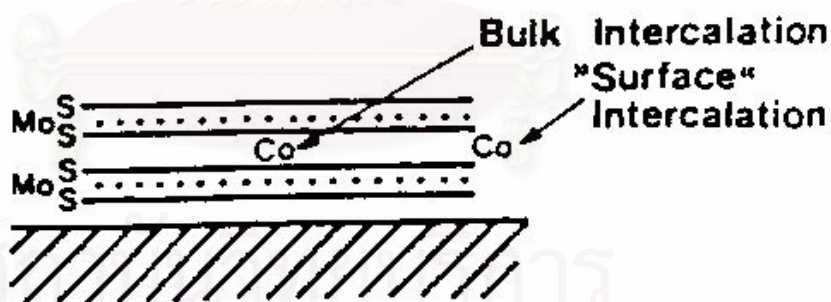
Figure 1.13 Locations of the promoter atoms in the MoS_2 structure as proposed by the intercalation and pseudo intercalation models [75].

1.7.3.3 Contact Synergy Model

The contact synergy model, also known as the remote control model, was proposed by Delmon and coworker [79-81] as shown in Figure 1.14. It is another model based on Mo being present as MoS_2. Due to the problems in characterizing supported catalysts, they studied a number of unsupported CoMo catalysts that exhibited comparable promoting effects to the supported catalysts. The unsupported catalyst showed the presence of bulk Co_9S_8 and MoS_2 phases. The contact of these two phases was suggested to result in spill-over of hydrogen from Co_9S_8 to MoS_2, thereby enhancing the intrinsic activity of the MoS_2 [81, 82]. Figure 1.15 illustrates the proposal of Delmon et al. The particles of cobalt sulfide adsorb and dissociate hydrogen. The H species are mobile enough in the conditions of catalysis to attack the MoS_2 particles, and create coordinative unsaturations at the edges. The active sites are then operating in the diverse reactions to proceed. The remote control mechanism appears general in HDS catalysis and influences activity and selectivity patterns for selected reactions. It has also been evidenced when mechanical mixtures of different solids are used. In relation to this model, it should be noted that the Co_9S_8 and MoS_2 are the thermodynamically stable pure sulfides under reaction conditions [83].
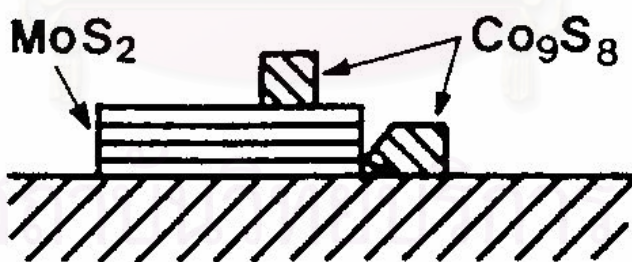
Figure 1.14 Illustration of the structural features of the active phases in CoMo catalysts as proposed by the contact synergy model [81].
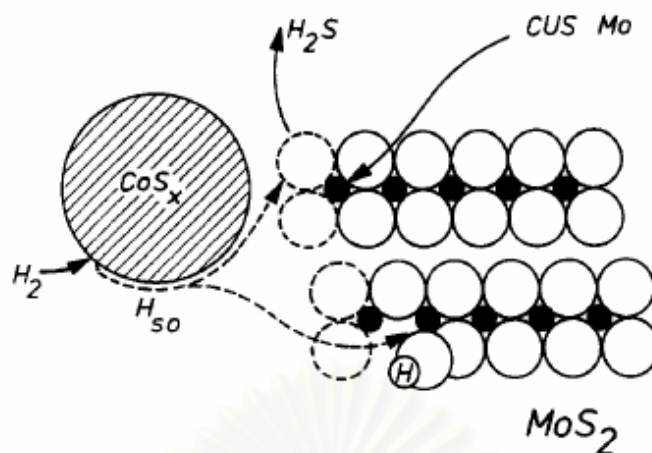
Figure 1.15 Schematic representation of the formation of coordinative unsaturated site (CUS) at MoS_2 by action of H species [81].

1.7.3.4 Co-Mo-S Model

One of the most widely accepted models for the active phase of HDS is the Co-Mo-S model postulated on the studies of Mössbauer spectroscopy, extended X-ray absorption spectroscopy and infrared spectroscopy by Topsoe and coworkers [84-92]. The Co-Mo-S phase was shown to be MoS_2 like structures with the promoter atoms located at the edges in five-fold coordinated sites (tetragonal pyramidal-like geometry) at the edge plans of MoS_2 as shown in Figure 1.16.

The Co-Mo-S structure is not a single bulk phase with a fixed overall Co:Mo:S stoichiometry. Rather, it should be regarded as a family of local structures with a wide range of Co concentrations, from pure MoS_2 to essentially full coverage of the MoS_2 edges by Co. All Co atoms in Co-Mo-S may not have identical properties due to such effects giving different edge-site geometries [93], Co-Co interactions [87, 88] and sulfur coordinations [94].
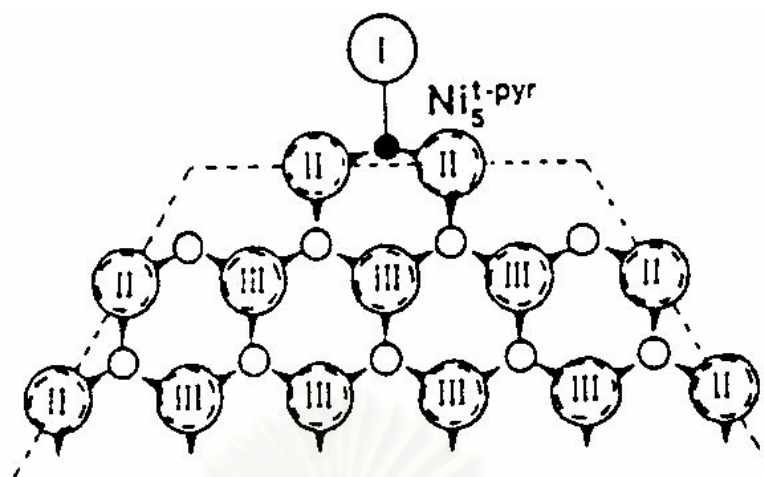
Figure 1.16 Schematic drawing of the Ni-Mo-S type structure illustrating the local

environment (Ni_5^{t-pyr}) of the promoter atoms at the edge plane of MoS_2.

The single-bonded sulfur atom, I, is located in the plane of Mo. II and III

denote doubly and triply bonded sulfur atoms which are present both

in the top and bottom sulfur layers [84].

The Co-Mo-S phase has subdivisions to further explain differences in the activities of catalysts for hydrogenation and hydrogenolysis. Typically, for alumina supported catalysts, two types of the Co-Mo-S phase can be formed during catalyst sulfidation [95, 96]. Type I Co-Mo-S phase consists of single or monolayer slabs of MoS_2 which interact strongly with the support, probably via Mo-O-Al linkages located at the edges. Type II Co-Mo-S phase, on the other hand, consists of multiple slabs of MoS_2. These interactions are small. In carbon supported catalysts, where the support interactions are weaker, the single slab structures may exhibit Type II Co-Mo-S phase. The structural differences between alumina supported Type I Co-Mo-S and alumina-silica and carbon supported Type II Co-Mo-S catalysts have been dealt with in several studies [96, 97]. The Type I Co-Mo-S phase is less active than Type II Co-Mo-S for large PASCs like DBT. This is expected because the large PASCs like DBT have dimensions of approximately 3 x 8 x 12.2 Å and are severely constrained in terms of geometric interaction with a type I Co-Mo-S monolayer whose thickness is estimated to be 6 Å [65]. Type II Co-Mo-S phases, on the other hand, are 20 – 30 Å high stacks and more suitable for handle the adsorption and HDS of the large PASCs. Figure 1.17

illustrates Type I and Type II crystallites in the presence of 4,6-DMDBT. Chianelli et al. [65] was one of the first who pointed out the importance of crystal geometry when considering desulfurization of large molecules such as DBT.
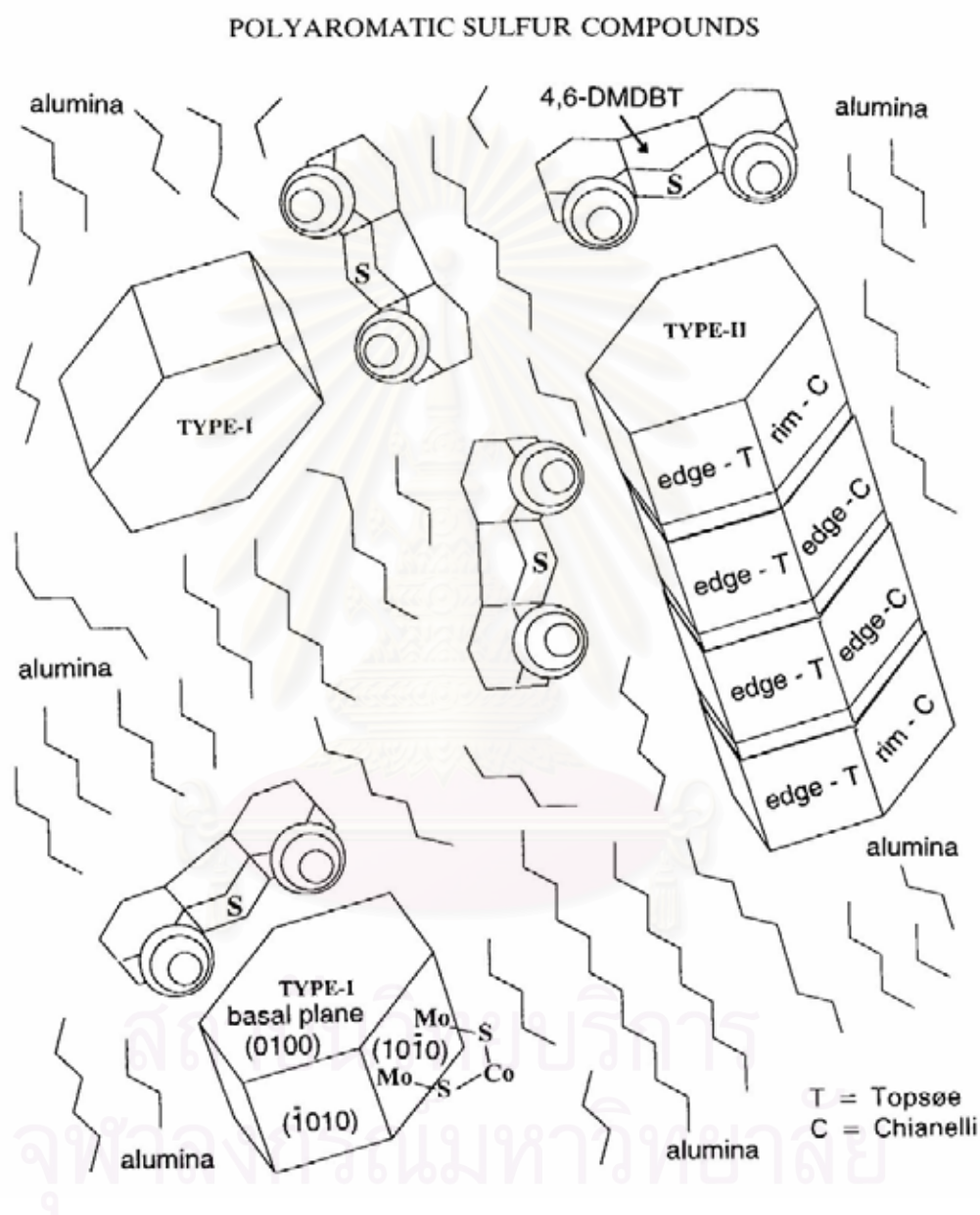
Figure 1.17 Potential geometric considerations in the interaction of PASCs with catalytic active sites [65].

The combined results from reaction test, Mössbauer and IR spectroscopic studies of both supported and unsupported catalysts have shown that most of the catalytic activity is linked to the presence of the promoter atoms in the Co-Mo-S phase. Such structures appear to be quite general and present in other promoted Mo (Fe-Mo-S and Ni-Mo-S) catalysts. The in-situ studies showed that other phases than Co-Mo-S (e.g., Co_9S_8 and Co in the alumina lattice ($Co:Al_2O_3$)) may be presented in typical alumina supported CoMo catalysts as shown in Figure 1.18

The Co-Mo-S model is now generally favored since, among the above models, it is only the one which is based on the direct in-situ physicochemical measurements of the active state of the promoted hydrotreating catalysts. A particular advantage of the model is the possibility to quantitatively link the promotion to the measured amount of Co atoms in the Co-Mo-S phase.
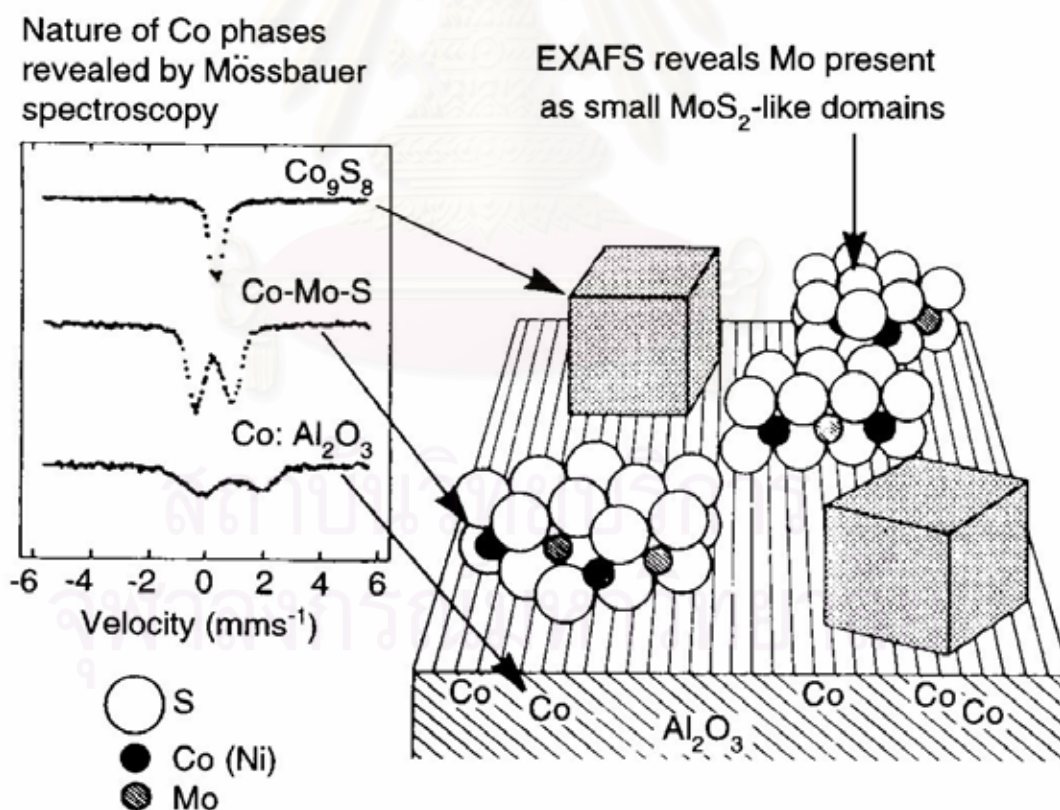
Figure 1.18 Schematic view of the different phases present in a typical alumina supported catalyst [13].

1.7.4 Atomic Scale Structure of MoS$_2$ and Co-Mo-S Nanoclusters

In order to continue improving HDS catalysts, a detailed understanding of the MoS$_2$ clusters including their morphology, edge structures, active sites, and interactions with typical sulfur molecules, is necessary. To further advance the understanding of the catalyst structure, new insight has been gained from detailed surface science studies. Recently, the scanning tunneling microscope (STM) has emerged as a new tool to directly image the catalytically relevant surface structures on the atomic scale. By studying model systems for catalysts, such investigations have helped to solve surface structures with catalytic relevance and have, in particular, emphasized the catalytic importance of edges, kinks, atom vacancies, or other surface defects, which other surface-averaging techniques often fail to discover.

Recently, the first successful atom-resolved scanning tunneling microscopy (STM) studies performed on a realistic HDS model catalyst were reported. The studies have presented the first direct structural information for both unpromoted MoS$_2$ [98] and promoted Co–Mo–S structures [99], and have recently been used to explore the interaction with thiophene (C$_4$H$_4$S) [100]. The studies showed, quite surprisingly, that the morphology of MoS$_2$ nanoclusters in the catalyst may, in fact, be very complex, since they do not seem to have a fixed shape [101]. Rather, the clusters adapt their shape according to the conditions under which they are synthesized, e.g., triangles under heavy sulfiding conditions (catalyst activation) or truncated hexagons under more sulforeductive conditions resembling HDS conditions. The STM images of both MoS$_2$ structures are shown in Figure 1.19.
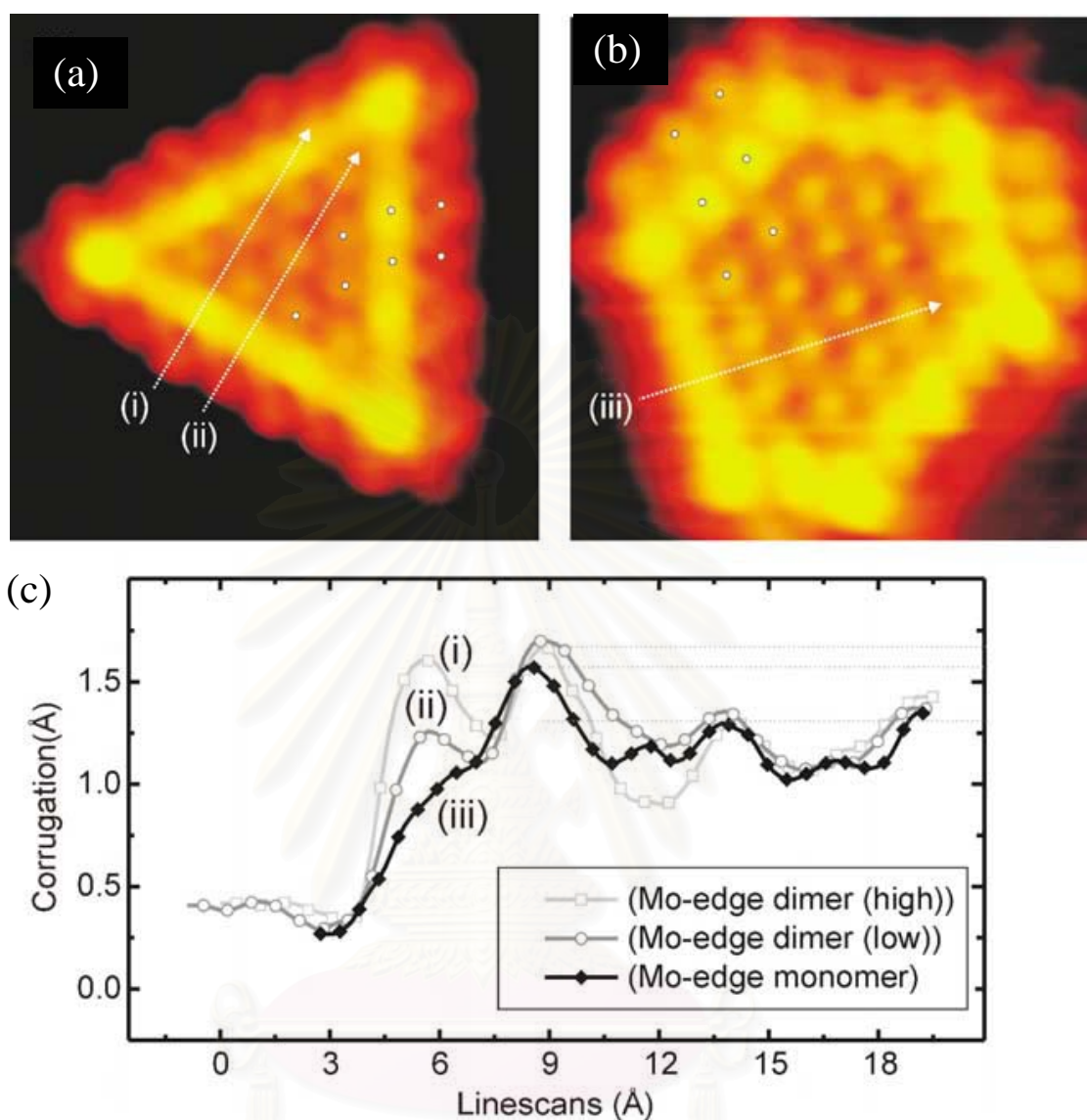
Figure 1.19 Atom-resolved STM image of (a) a triangular single-layer MoS$_2$ nanocluster
(b) a hexagonal single-layer MoS$_2$ nanocluster. White dots indicate the
registry of protrusions at the edges. (c) STM corrugation measurements
across the Mo edges of the triangle and hexagonal. The scan orientations are
indicated by white lines on both STM images. For the MoS$_2$ triangle two
lines, (i) and (ii), are indicated since the fully saturated Mo edge exhibits a
superstructure along the edge protrusions resulting in an alternating high/low
pattern [101].

The detailed atomic-scale structure of the catalytically important edges in MoS$_2$ was solved by combining the experimental STM images and simulations from theoretical density functional theory (DFT) calculations, which included the effect of hydrogen adsorption on the edges and the potential influence of the gold model substrate [101]. Figure 1.20 shows the ball model of hexagonal and triangular MoS$_2$ nanoclusters. The triangular MoS$_2$ nanoclusters synthesized under sulfidation conditions were found to be terminated by fully saturated Mo edges. The dominant presence of triangular morphology implies that one of the edge terminations is more stable than the other [98]. It was concluded that the edge termination is a Mo-edge. A possible model with one S atom per Mo-edge atom arranged in a reconstructed geometry is shown in Figure 1.20 (b). However, another low-energy structure with S dimers at the Mo-edge may be possible [102, 103]. Another structure is the hexagonal clusters (Figure 1.20 (a)). The morphology of the MoS$_2$ nanocluster is determined by the relative stability of two different types of edge terminations, Mo edges covered with S monomers and fully sulfur-saturated S edges with H atoms adsorbed (i.e., S–H groups). This is the first direct evidence for the exact location of S–H groups, which are believed to be important in HDS as a source of hydrogen atoms. In Figure 1.20 (a), the two edge terminations are illustrated for a hypothetical MoS$_2$ cluster, where the edges are simple terminations of the bulk MoS$_2$ structure.
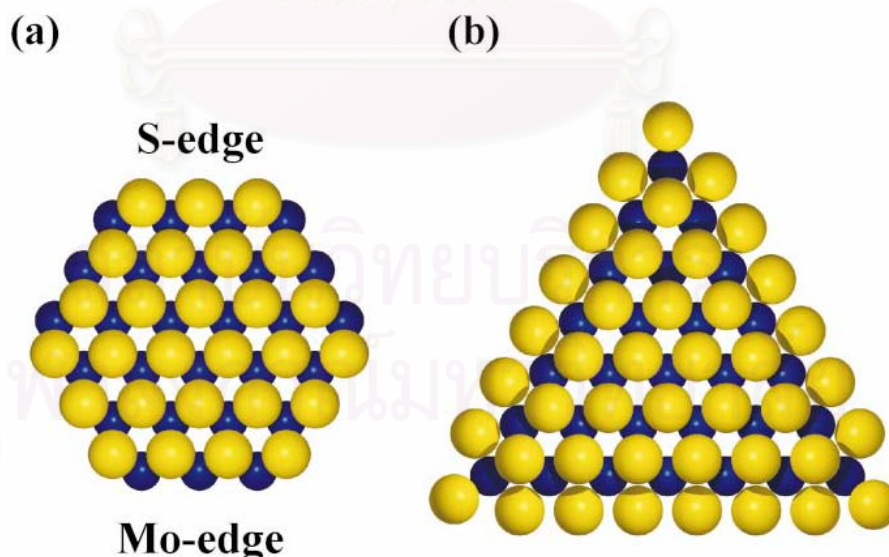
Figure 1.20 (a) Ball model (top view) of a hypothetical bulk truncated MoS$_2$ hexagonal exposing both Mo- and S-edges. (b) Triangular MoS$_2$ cluster exposing Mo-edges with edge sulfur atoms located out of registry with the basal plane. [101].

In 2001, Lauritsen and coworkers [99] showed STM image of Co-Mo-S which is possible to obtain the first atomic-scale images of the Co–Mo–S structure present in hydrodesulfurization (HDS) catalysts. It was observed that the presence of the Co promoter atoms causes the shape of the MoS_2 nanoclusters to change from triangular to hexagonally truncated. The change in morphology appears to be driven by a preference of Co for the S-edge of MoS_2. Figure 1.21 shows STM images and ball models of MoS_2 cluster and Co-Mo-S structure. The observed hexagonal truncated morphology of the Co–Mo–S nanoclusters (Figure 1.21 (a)) implies that both edge terminations, i.e., S- and Mo-edges, must be presented. The identity of the two edges is inferred from the high-resolution STM images of the Co–Mo–S edges. They found that the longer edges are identical with those observed for the triangular MoS_2 nanoclusters with the protrusions being imaged out of registry with the basal plane [98]. These edges are thus attributed to sulfided Mo-edges. The Co promoter atoms appear to have little effect on the Mo-edges. Therefore, the short edges are attributed to S-edges. The result of cobalt addition to stabilize the S-edge is in good agreement with the DFT calculations, showing a preference of Co to be located at the S-edge [102]. The Co edge atoms appear to enhance electronic density at the nearby S atoms as suggested by the brighter image. It is possible that the perturbed electronic environment of the sulfur atoms neighboring the Co atoms is a key to understanding the increased activity of the Co–Mo–S structures. A single Co atom substituted a Mo atom in the basal plane metal lattice, and in analogy with the situation at the Co-substituted S-edges, this induces an enhanced electron density at the three neighboring sulfur atoms.

On the basis of atom resolved STM technique, it is concluded that the Co atoms are located exclusively at the S-edges of the Co–Mo–S nanoclusters with a full edge substitution by Co. The presence of the Co atoms is found to induce structural, morphological, and electronic changes.
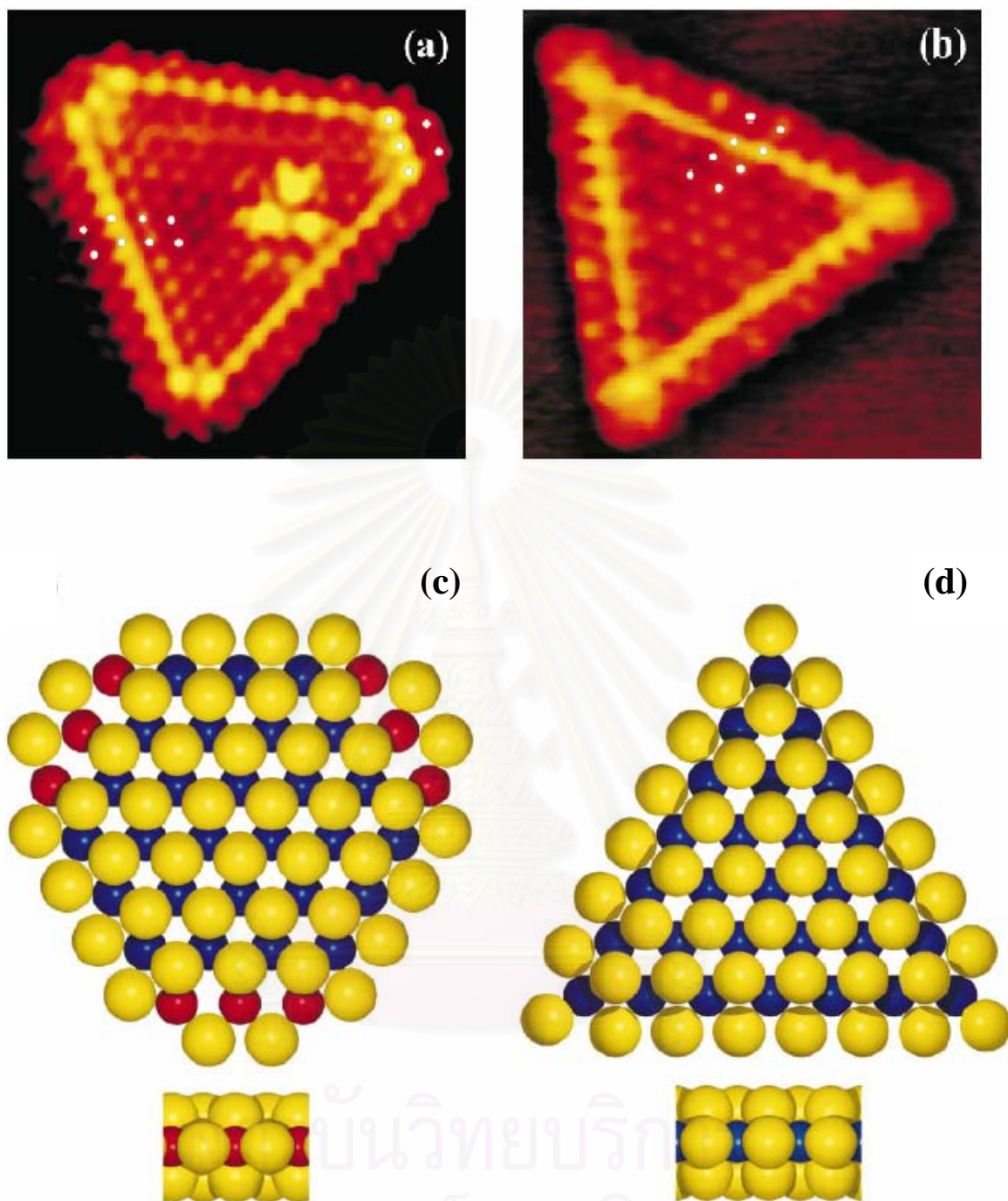
Figure 1.21 STM image of (a) a single-layer Co–Mo–S nanocluster. (b) Triangular
single-layer MoS_2 nanocluster. In both images the small white dots
illustrate the position of the protrusions. (c) Ball model of the proposed
hexagonally truncated Co–Mo–S structures with Co fully substituted at the
S-edges. (d) Ball model of Triangular MoS_2 cluster exposing Mo-edges with
edge sulfur atoms located out of registry with the basal plane. Color code:
Mo, blue; S, yellow; Co, red [99].

1.8 Objective and Scope

Due to the increasingly stringent environmental regulations for fuel sulfur content and high sulfur contents in the crude oils, the highly active HDS catalyst is required in order to improve performance of HDS process and reduce sulfur content in the finished fuel products to meet regulatory specifications. Hydrothermal synthesis is a challenging method to prepare new catalysts with high HDS activity towards the most refractory sulfur compounds (DBT and 4,6-DMDBT). Moreover, the catalyst prepared by the hydrothermal method does not need further sulfidation before HDS reaction. The HDS activity of Mo based sulfide catalysts by the hydrothermal method was studied under the following hypotheses:

- The well mixing of water accompanied with organic solvent at the appropriate temperature and pressure would provide the resulting unsupported Mo based sulfide catalyst with high dispersion and high activity for HDS reaction.

- Unsupported Mo based sulfide catalyst with its nano size particles and high activity prepared by the hydrothermal method is a promising HDS catalyst capable of hydrodesulfurization of the refractory sulfur compounds.

- Unsupported Mo based sulfide catalyst properly prepared has superior activity to commercial catalyst in the deep HDS.

Chapter 1 of this thesis provides a review of relevant literatures. The general information and condition of the hydrotreating process including hydrodesulfurization were given. The HDS reactivities and HDS reaction mechanism of sulfur compound were reported. The proposed model of HDS catalyst were also mentioned. Detail of materials, experimental procedures and analytical method are given in Chapter 2.

The effects of catalyst preparation conditions on the HDS activity of the unsupported NiMo sulfide catalysts were reported in Chapter 3. Four catalyst preparation parameters (temperature, pressure, amount of organic solvent and Ni/(Mo+Ni) ratio) were investigated. The influence of four parameters on the simultaneous hydrodesulfuization of DBT and 4,6-DMDBT were evaluated. The characterization of the unsupported NiMo sulfide catalysts at various with difference Ni/(Mo+Ni) ratios was also studied. The appropriate conditions of the hydrothermal method for the preparation of the highly active HDS catalyst were determined.

In Chapter 4, the promoter (Ni or Co) was added into the unsupported Mo sulfide catalyst to improve hydrodesulfurization activity and product selectivity. The chemical and physical properties of the synthesized catalysts with and without promoter were investigated using Brunauer-Emmet-Teller (BET), X-Ray Diffraction (XRD), Temperature Programmed Reduction (TPR) and High Resolution Transmission Electron Microscopy (HRTEM). The kinetic studies were carried out to demonstrate the effects of Co or Ni on Mo sulfide catalyst regarding the activity and product selectivity for the simultaneous HDS of DBT and 4,6-DMDBT. The HDS activity of potential of unsupported Mo based sulfide catalysts prepared from hydrothermal method in the deep hydrodesulfurization catalyst was compared with two commercial alumina supported sulfide catalysts (CoMo and NiMo).

In order to deeply understand the nature of the active sites on the surface of the unsupported Mo based sulfide catalysts, the simultaneous liquid-phase adsorption of DBT and 4,6-DMDBT was performed using the Pennsylvania State University the Selective Adsorption for Removing Sulfur (PSU-SARS) and reported in Chapter 5. The adsorption capacities, selectivities and mechanism of DBT and 4,6-DMDBT on the unsupported Mo based sulfide catalysts was studied. Subsequently, Chapter 6, the hydrodesulfurization of light cycle oil (LCO) over the unsupported Mo based sulfide catalysts was investigated to study the activity of synthesized catalysts in the real liquid fuel. The commercial catalysts were continued for comparative purposes.

Finally, the important conclusions from this research and recommendations for the future work are provided in Chapter 7. Thus, the results of this research will contribute the deep understanding and useful guidance to the development of Mo based sulfide catalysts for hydro-treatment processes.

CHAPTER II

EXPERIMENTAL AND CHARACTERIZATION

2.1 Materials

Ammonium tetrathiomolybdate (ATTM) ($(NH_4)_2MoS_4$), nickel nitrate hexahydrate ($Ni(NO_3)_2 \cdot 6H_2O$), cobalt nitrate hexahydrate $Co(NO_3)_2 \cdot 6H_2O$, dibenzothiophene (DBT), 4,6-dimethyldibenzothiophene (4,6-DMDBT) and decahydronaphthalene (decalin, used as solvent) were purchased from Aldrich Chemical Company and were used without further purification. It was noted in the previous work in this laboratory that a long-time storage of ATTM in a closed vial that has been exposed to air may lead to degradation of the reagent resulting in deviations in the observed activity of in situ generated MoS_2 catalysts from different bottles of ATTM reagent. In the present work, a bottle of newly purchased ATTM was used in syntheses, and the reagent bottle was stored in a refrigerator in order to minimize the oxidative degradation.

2.2 Catalyst Preparation

The synthesis procedure of the unsupported Mo based sulfide catalysts used this study was modified from the method reported by Song et al. [104-106]. The objective of this modification was to improve the HDS activity and product selectivity of the catalysts to the most refractory sulfur compounds.

The unsupported Mo based sulfide catalysts were synthesized by using hydrothermal method. The catalyst synthesis was carried out in a 25 ml batch reactor as shown in Figure 2.1. ATTM was dissolved in 10 g of de-ionized water and organic solvent (decalin) was then added to this solution. A required amount of $Co(NO_3)_2 \cdot 6H_2O$ or $Ni(NO_3)_2 \cdot 6H_2O$ was dissolved in the minimum amount of water and added to the solution. The atomic ratio of Me/(Me+Mo) was in the range of 0 - 0.56 (Me = Ni or Co). The reactor was purged before being pressurized with

hydrogen gas to a desired initial pressure and placed in a preheated fluidized sand bath at desired temperature for 2 h. Subsequently, the reactor was removed from the sand bath and immediately quenched in water bath. The unsupported catalysts synthesized were separated and immerged under an organic solvent. The effects of catalyst preparation conditions on the HDS activity of the unsupported NiMo sulfide catalysts were investigated. Table 2.1 shows the catalyst preparation conditions in this study.

Figure 2.1 Batch reactor.

The commercial supported catalysts CoMo/Al$_2$O$_3$ (Cr344) and NiMo/Al$_2$O$_3$ (Cr424) obtained from the Criterion Catalyst Company, Houston, TX. USA were used to compare activity for the HDS of 4,6-DMDBT and DBT with the synthesized unsupported Mo based sulfide catalysts. The commercial catalysts were crushed to a particle size of <1 mm and presulfided at 350 $^{\circ}$C for 4 h in a flow of 5 vol % H$_2$S-H$_2$ at a flow rate of 150 ml/min. These catalysts were subsequently stored in decalin to minimize oxidation.

Table 2.1 Catalyst Preparation Conditions.

Parameters	Temperature (^{o}C)	Pressure (MPa)	Solvent amount (g)	Ni/(Mo+Ni)
Temperature	300	2.8	1	0.43
	325	2.8	1	0.43
	350	2.8	1	0.43
	375	2.8	1	0.43
Pressure	350	1.4	1	0.43
	350	2.1	1	0.43
	350	2.8	1	0.43
	350	3.4	1	0.43
Solvent amount	350	2.8	0	0.43
	350	2.8	1	0.43
	350	2.8	3	0.43
Ni/(Mo+Ni)	350	2.8	1	0
	350	2.8	1	0.2
	350	2.8	1	0.33
	350	2.8	1	0.43
	350	2.8	1	0.5
	350	2.8	1	0.56
	350	2.8	1	1

2.3 Catalysts Evaluation.

2.3.1 Hydrodesulfurization of Model Fuel

Catalytic performance of a metal sulfides was evaluated with a simultaneous HDS of DBT and 4,6-DMDBT in a horizontal tubing 25 ml micro reactor. The reactor was loaded with 0.023 g synthesized catalyst and 4 g reactant mixture (0.4% mole 4,6-DMDBT and 0.4% mole DBT in decalin). The sealed reactor was purged with hydrogen, then pressurized up to 2.8 MPa and placed in a fluidized sand bath which was preheated up to 350 ^{o}C for 30 min. The reactor was agitated at a rate of 200 strokes/min, which reaction was not diffusion controlled. The temperature inside the reactor was monitored by a thermocouple. After the reaction, the reactor was removed from the sand bath and immediately quenched in a cold-water bath. Finally, liquid products and the catalysts were collected.

2.3.2 Hydrodesulfurization of Light Cycle Oil

Light cycle oil (LCO) was obtained from United Refining Company, Warren, Pennsylvania USA. The HDS of LCO was carried out in a horizontal tubing 25 ml. micro-reactor. 3 g LCO and 0.09 g synthesized or commercial catalysts were loaded in the reactor. The reactor was purged eight times with hydrogen gas. Finally, it was pressurized to 2.8 MPa hydrogen pressure and placed in a fluidized sand bath which was preheated up to 350 ^{o}C for 30 min. The reactor was agitated at a rate of 200 strokes/min. After the reaction, the reactor was removed from the sand bath and immediately quenched in a cold-water bath. Finally, liquid products and the catalysts were collected.

2.3.3 Liquid Phase Adsorption

In order to compare the DBT and 4,6-DMDBT adsorption capacity of unsupported Mo, CoMo and NiMo sulfide catalysts, the fixed bed adsorption system was performed by using the method of Selective Adsorption for Removing Sulfur recently proposed and established at the Pennsylvania State University (PSU-SARS) [1, 2, 107-111]. A schematic of the liquid phase adsorption system is shown in Figure 2.2. The model fuel contained 0.045 % mole of DBT and 0.045 % mole of 4,6-DMDBT in decalin. The adsorption experiment was carried out at ambient temperature and pressure of nitrogen. The unsupported catalyst was packed in a stainless steel column having a bed dimension of 4.6 mm i.d. and 37.5 mm length as shown in Figure 2.3. The model fuel was fed into the column by HPLC pump and flowed up through the bed at a liquid hourly space velocity (LHSV) of 1.04 h^{-1}. The effluent from the top of the column was collected periodically for analysis.
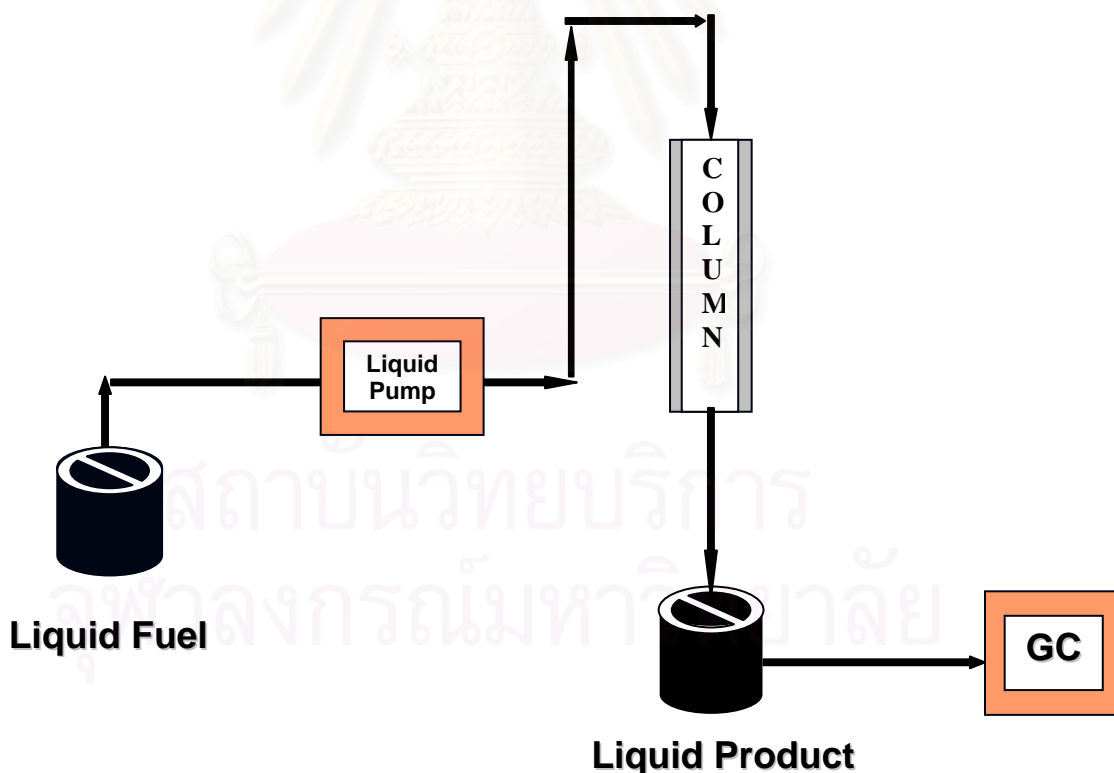
Figure 2.2 A schematic of the liquid-phase adsorption flow system.
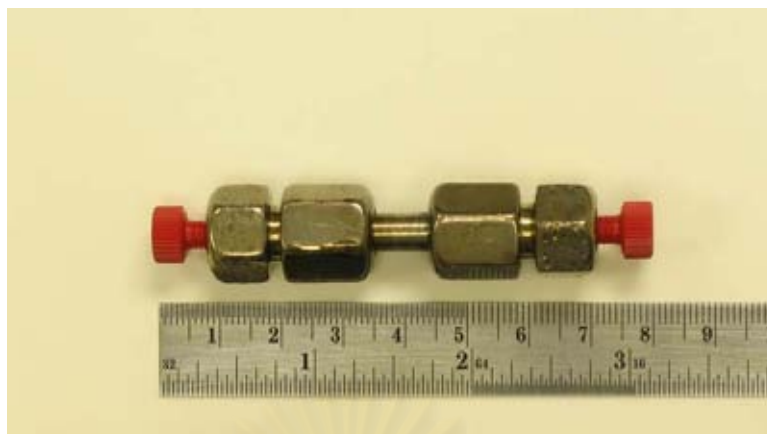
Figure 2.3 A stainless steel column for liquid-phase adsorption experiment.

2.4 HDS Product Analysis

2.4.1 Model Fuel

The liquid products were analyzed qualitatively with a Shimadzu GC/MS (GC12A/QP-500) and quantitatively with a HEWLETT PACKARD GC-FID (HP5890) with a XTI-5 column (Restek). Both GC/MS and GC-FID were programmed from 55°C to 240 $^{\circ}$C at heating rate of 5 $^{\circ}$C/min. The response factors (RF) of the compounds were determined by injecting a known amount of some reagent together with a known amount of internal standard. The GC response factors for DBT, 4,6-DMDBT and four of the products (biphenyl (BP), cyclohexylbenzene (CHB), bicyclohexyl (BCH) and 3,3'-dimethylbiphenyl (3,3'-DMBP)) were determined using authentic samples. The product analysis using GC-FID is described in detail in Appendix A. Conversion (% wt) and selectivity (% mole) of each product were defined in Appendix B.

2.4.2 Light Cycle Oil

The liquid products from HDS of LCO were analyzed for total sulfur and individual sulfur compounds. The total sulfur concentration was determined using an Antek 9000S Total Sulfur Analyzer. The instrument was calibrated in our laboratory at four different sulfur concentration ranges: 0–6, 6–60, 60–300 and 300–900 ppmw sulfur using dibenzothiophene (DBT) in n-decane and linear calibration curves were obtained for each calibration range. The linearity of the calibration in each range was also cross-checked using sulfur standard samples supplied by Antek. The sulfur detection limit of the total sulfur analyzer in the normal working range is 0.5 ppmw sulfur. The Gas Chromatography - Pulsed Flame Photometric Detector (GC-PFPD) was used to determine individual sulfur compound in LCO before and after the HDS reaction. A Hewlett-Packard 5890 series II gas chromatograph with a capillary column, XTI-5 (Restek, bonded 5%, 30 m x 0.25 mm i.d. x 0.25 mm film thickness) and a split mode injector (ratio 100:1) was used with ultra-high purity helium as a carrier gas. The conditions and temperature program for GC-PFPD are described in Appendix A.

2.5 Catalyst Characterization

2.5.1 Adsorption Desorption Isotherms of Nitrogen

N_2 adsorption-desorption isotherms were measured on a Micromeritics ASAP 2020 (Accelerated Surface Area and Porosimetry System) instrument. The Brunauer-Emmet-Teller (BET) specific surface area was determined using adsorption data in the relative pressure range of 0.06 to 0.3. Pore size distributions of the samples were calculated from the isotherms by the Barrett–Joyner–Hallenda (BJH) method. The BJH pore size distributions were calculated from the desorption branch of the isotherms. Fresh samples were vacuum dried before the adsorption measurement.

2.5.2 Temperature Programmed Reduction

Temperature-programmed reduction (TPR) measurements were conducted with a Micromeritics AutoChem 2910 Automated Catalyst Characterization System. About 0.1 g of sample was charged in the reactor and heated up to 500 ∘C at the rate of 10 ∘C/min, held at that temperature for 30 min and cooled to room temperature under Ar flow to remove the adsorbed materials. A mixture of 4.8 vol% H_2/Ar was introduced at 50 ml/min into the sample loop. The heat treated sample was heated at a rate of 10 ∘C /min to 650 ∘C. The effluent gas was passed through a viscous solution of isopropanol cooled by liquid N_2 to remove the water produced during reduction and analyzed using a thermal conductive detector.

2.5.3 X-Ray Diffraction

Crystalline structure of the synthesized catalysts was characterized using X-ray diffraction (XRD) on a Scintag Powder Diffractometer with Cu-Kα emission at 30 mA 35 KV. Diffractograms were obtained from 5° to 80° 2θ with a scanning speed of 2 ^{o}/min. Diffractograms were analyzed using the standard JCPDS files.

2.5.4 High Resolution Transmission Electron Microscopy

High resolution transmission electron microscopy (HRTEM) was performed on a JEOL JEM-2010F transmission electron microscope. A small amount of sample was ground with a mortar and pestle. The sample was then suspended in ethanol and sonicated. A drop of the suspension was put on a lacey carbon film supported by a Cu grid.

CHAPTER III

HIGHLY ACTIVE UNSUPPORTED NiMo SULFIDE CATALYSTS FOR DEEP HDS OF DBT AND 4,6-DMDBT: EFFECT OF CATALYST PREPARATION CONDITIONS

Conventional catalysts used in the hydrotreating process include mainly Ni or Co promoted Mo- or W-based catalysts supported by γ-Al_2O_3 [11]. They are active in converting thiophene and benzothiophenes, but not active enough to desulfurize efficiently the most refractory sulfur-containing polyaromatic compounds, e.g. dibenzothiophene (DBT) and its alkyl-substituted derivatives which are the major portion of sulfur in the high-boiling point fraction of crude oil, i.e. heavy naphtha, diesel, and light FCC naphtha.

It is well established that the Mo based catalysts used for HDS are promoted by the addition of cobalt or nickel in much more than trace amounts. The synergetic effects of the promoters on catalytic activity of the Mo sulfides have been reported by many research groups [13, 112, 113]. The effect of promoter over the Mo sulfide catalysts for HDS reactions has been attributed to the amount of promoter atoms that can be accommodated on the edges of MoS_2 layers and also to the electronic transfer from promoter atom that induces on Mo atoms located at these sites [114, 115].

Generally, the Mo sulfide catalysts are prepared by an impregnation of aqueous solution of oxide precursors on Al_2O_3 support, followed by drying, calcination and pre-sulfidation with either H_2/H_2S or an organic sulfur compound such as dimethyldisulfide (DMDS) [16]. An alternative to the oxide-sulfide transformation is to use precursor compounds already sulfided like ammonium thiometalates precursors $(NR_4)_2MeS_4$ (R: H or alkyl; Me: Mo or W). Some researchers have proposed more effective preparation of Mo sulfide catalysts from different precursors such as ammonium tetrathiomolybdate (ATTM) [112, 113, 116-119]. These Mo sulfide catalysts can be synthesized directly via a thermal decomposition method of ATTM and do not need further sulfidation. Deyers and

coworkers [120] observed relatively high activity of Mo sulfide catalysts prepared via hydrothermal method compared with Mo sulfide catalysts prepared by thermal decomposition. Recently, Song et al. [104-106] reported a new hydrothermal synthesis method for preparing highly dispersed unsupported Mo sulfide catalyst from aqueous ATTM solution in the presence of organic solvent under hydrogen atmosphere. The use of organic solvent helps to improve dispersion of the precursor molecules. However, even if unsupported Mo sulfide catalysts have been often used as model catalysts for hydrotreating reactions, their high volumetric activities tend to be more and more attractive for commercial applications.

All unsupported catalysts in this work were prepared via the hydrothermal method developed from the procedure reported by Song et al. [104-106]. It is well known that conditions and atmospheres during the catalyst preparation have strongly affected the activity of catalysts. In this chapter, the effect of catalyst preparation conditions on the HDS activity of the unsupported NiMo sulfide catalysts was studied. The parameters studied included catalyst preparation temperature, the catalyst preparation pressure, organic solvent (decalin) and Ni/(Mo+Ni) mole ratios.

3.1 HDS of DBT and 4,6-DMDBT

As described in Chapter 2, the HDS reaction of DBT and 4,6-DMDBT proceeds through direct desulfurization (DDS) pathway and hydrogenation (HYD) pathway.

The two pathways of DBT HDS are shown in eq. (3.1) and (3.2)

1. Biphenyl (BP) represents the product from DDS pathway

(3.1)
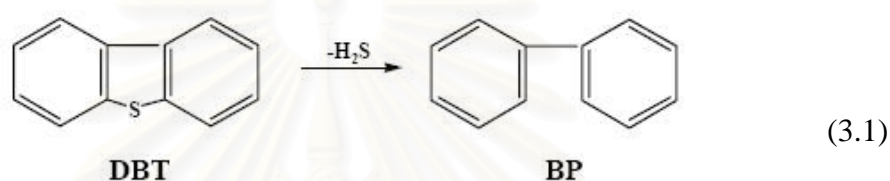
2. Tetra-hydrodibenzothiophene (THDBT), cyclohexylbenzene (CHB) and bicyclohexane (BCH) represents the products from HYD pathway.
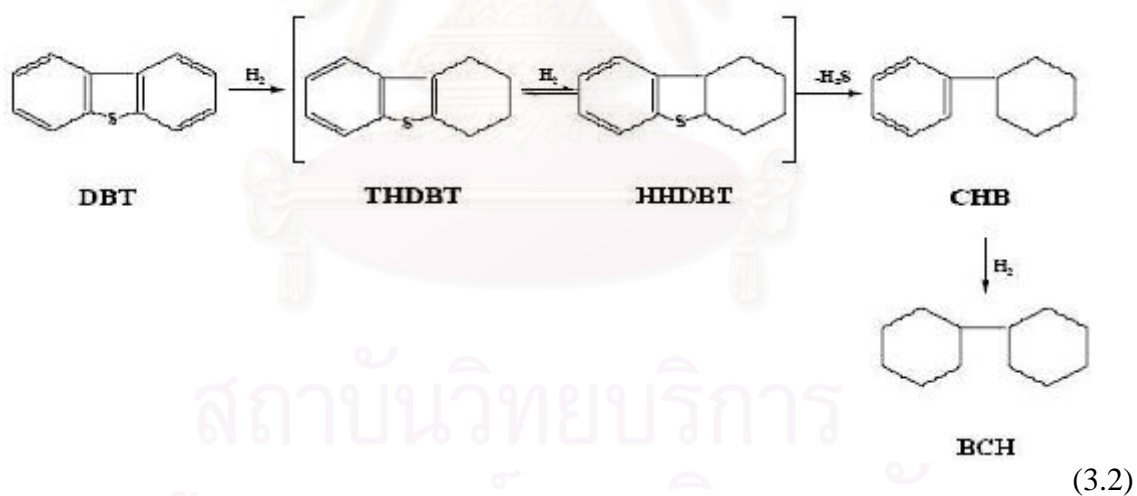
(3.2)

Since DDS and HYD pathways are parallel, the ratio between HYD and DDS can be approximated in term of the product selectivity by the following equation.

$$\text{HYD/DDS} = \frac{\text{selectivity to}(\text{THDBT} + \text{CHB} + \text{BCH})}{\text{selectivity to BP}}$$

(3.3)

The two pathways of 4,6-DMDBT HDS are shown in eq. (3.4) and (3.5)

1. 3,3'Dimethylbiphenyl (3,3'-DMBP) represents the product from DDS pathway

$$(3.4)$$
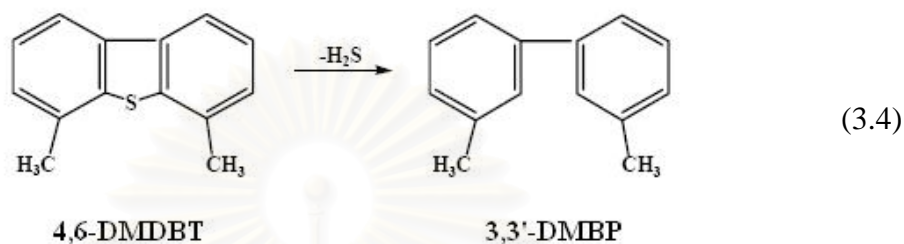
2. Tetra-hydrodimethyldibenzothiophene (THDMDBT), methylcyclohexyltoluene (MCHT) and dimethylbicyclohexane (3,3'-DMBCH) represent the products from HYD pathway.
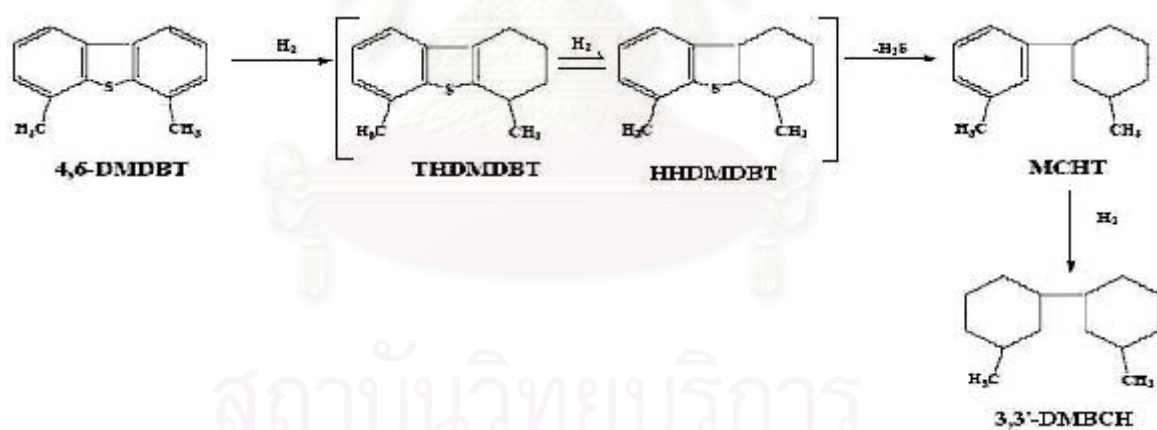
$$(3.5)$$

Since DDS and HYD pathways are parallel, the ratio between HYD and DDS can be approximated in term of the product selectivity by the following equation.

$$\text{HYD/DDS} = \frac{\text{selectivity to(THDMDBT + MCHT + DMBCH)}}{\text{selectivity to 3,3'-DMBP}} \qquad (3.6)$$

3.2 Effect of Catalyst Preparation Temperature

Figure 3.1 shows the effect of catalyst preparation temperature on the activity of unsupported NiMo sulfide catalysts for the DBT and 4,6-DMDBT HDS. When the preparation temperature was increased from 300 ^{o}C to 375 ^{o}C, the conversion of DBT and 4,6-DMDBT increased gradually from 50.3% to 63.9% and from 41.6% to 51.9%, respectively. The DBT conversion was approximately 1.2 times the 4,6-DMDBT conversion. Table 3.1 presents the product distribution in the DBT and 4,6-DMDBT HDS over NiMo sulfide catalysts prepared at various temperatures. The selectivity to biphenyl (BP) and cyclohexylbenzene (CHB) which were the major products of DBT HDS showed the different trend. The CHB selectivity (product from HYD pathway) increased while the BP selectivity (product from DDS pathway) decreased when the catalyst preparation temperature was increased. However, the selectivity to tetra-hydrodibenzothiophene (THDBT) and bicyclohexane (BCH), as the minor products, did not change significantly.
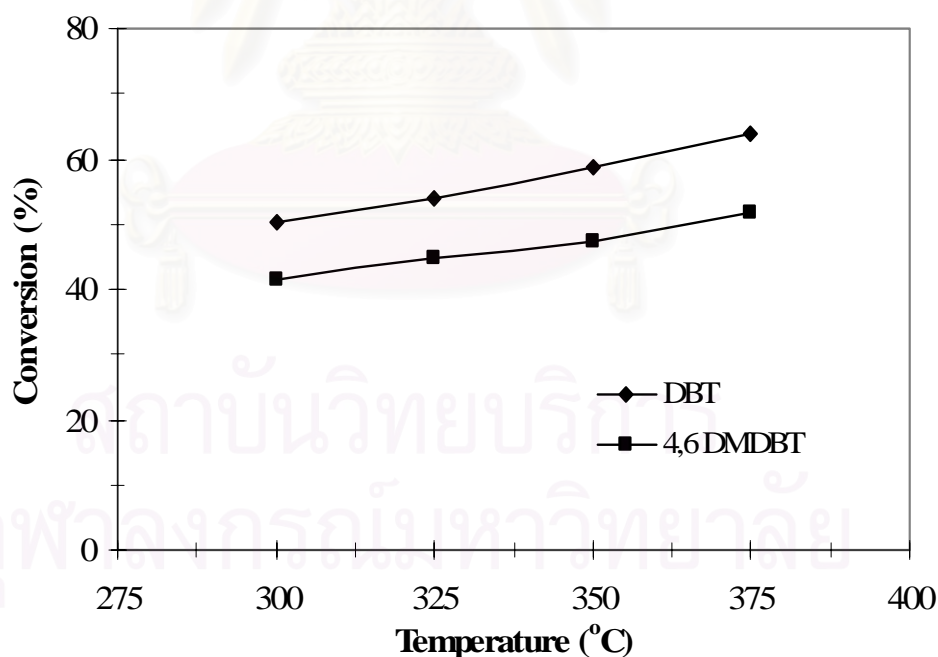
Figure 3.1 Effect of preparation temperature on simultaneous HDS of DBT and 4,6-DMDBT over unsupported NiMo sulfide catalysts. (other preparation parameters: pressure = 2.8 MPa, solvent amount = 1 g and Ni/(Mo+Ni) = 0.43).

Table 3.1 Effect of Preparation Temperature on HDS of 4,6-DMDBT and DBT over NiMo Sulfide Catalysts.(Other catalyst preparation parameters: pressure = 2.8 MPa, solvent amount = 1 g and Ni/(Mo+Ni) = 0.43)

Preparation Temperature (^{o}C)	300	325	350	375
DBT Conversion (wt%)	50.3	53.8	58.5	63.9
Selectivity (%)				
BP	46.5	43.4	41.1	38.7
THDBT	5.2	5.4	6.2	4.9
CHB	39.6	42.0	42.6	47.1
BCH	8.7	9.2	10.1	9.3
HYD/DDS[a]	1.2	1.3	1.4	1.6
4,6-DMDBT Conversion (wt%)	41.6	44.8	47.3	51.9
Selectivity (%)				
3,3'-DMBP	40.6	37.1	33.2	25.4
THDMDBT	33.7	35.6	37.8	41.8
MCHT	24.0	25.8	27.0	31.0
3,3'-DMBCH	1.7	1.5	2.0	1.8
HYD/DDS[b]	1.5	1.7	2.0	2.9

[a] HYD/DDS = [selectivity to (THDBT+CHB+BCH) / selectivity to BP].

[b] HYD/DDS = [selectivity to (THDMDBT+MCHT+ 3,3'-DMBCH) / selectivity to 3,3'-DMBP].

For the product selectivity of 4,6-DMDBT HDS, unlike the DBT HDS, tetra-hydrodimethyldibenzothiophene (THDMDBT) was the major hydrogenation product accompanied with 3,3'-dimethylbiphenyl (3,3'-DMBP) and methylcyclohexyltoluene (MCHT). The 3,3'-DMBP selectivity decreased from 40.6% to 25.4% when the catalyst preparation temperature was increased from 300 ^{o}C to 375 ^{o}C. Similarly to the product distribution of DBT HDS, 3,3'-DMBP, a product from the DDS pathway, decreased when the catalyst preparation temperature was increased, while the products from the HYD pathway (THDMDBT and MCHT)

increased. The selectivity to 3,3'-DMBCH, as the minor product, did not change. Consequently, the HYD/DDS ratio increased from 1.2 to 1.6 for the DBT HDS and from 1.5 to 2.9 for the 4,6-DMDBT HDS when the catalyst preparation temperature was increased.

From these results, it can be concluded that the high preparation temperature not only increase the HDS activity of the unsupported NiMo sulfide catalyst but also enhance the hydrogenation activity. It has been reported that the catalytic activity of Mo based sulfide catalyst is related to the coexistence of two different sites and each site drives the HDS reaction through the DDS pathway and the HYD pathway [64].The predominant pathway may be directly dependent upon the relative concentration of these active sites. According to the result of preparation temperature effect, it seems that there are more HYD sites than the DDS sites on the unsupported NiMo sulfide catalysts prepared at high temperature. This result also agrees very well with the ratio of HYD/DDS in the product selectivity. Although the selectivity to MCHT and 3,3'-DMBP was not much different, the selectivity to hydrogenation products was significantly higher than that to hydrogenolysis product.

In addition, the high activity of catalyst prepared at higher preparation temperatures could also be explained by N_2 adsorption measurement. The specific surface area of the unsupported NiMo sulfide catalyst prepared at 375 ^{o}C (249 m^2/g) was much higher than that of catalyst prepared at 300°C (121 m^2/g) as shown in Table 3.2. The high pore volume also supported the high catalyst activity of catalysts for HDS.

Table 3.2 Surface Area and Pore Volume of NiMo Sulfide Catalysts Prepared
at Various Preparation Temperatures. (Other catalyst preparation
parameters: pressure = 2.8 MPa solvent amount = 1 g and Ni/(Mo+Ni)
= 0.43)

Preparation Temperature (^{o}C)	Surface Area (m^2/g)	Pore volume (cm^3/g)
300	121	0.19
325	158	0.21
350	201	0.28
375	249	0.39

3.3 Effect of Catalyst Preparation Pressure

Figure 3.2 shows the effect of catalyst preparation pressure on the subsequent hydrodesulfurization. Similarly to the catalyst preparation temperature effect, a gradual increase in the conversion of 4,6-DMDBT and DBT was observed when H$_2$ pressure in the catalyst preparation was increased. Thus, H$_2$ pressure in the catalyst preparation showed a remarkable strong effect on the HDS activity of the resulting catalyst. For the pressure range of 1.4 to 2.8 MPa, the DBT and 4,6-DMDBT conversion increased from 39.8% to 58.5% and from 29.4% to 47.3%, respectively. However, when the preparation pressure increased further up to 3.4 MPa, the increase of HDS activity was not significant for both sulfur compounds.
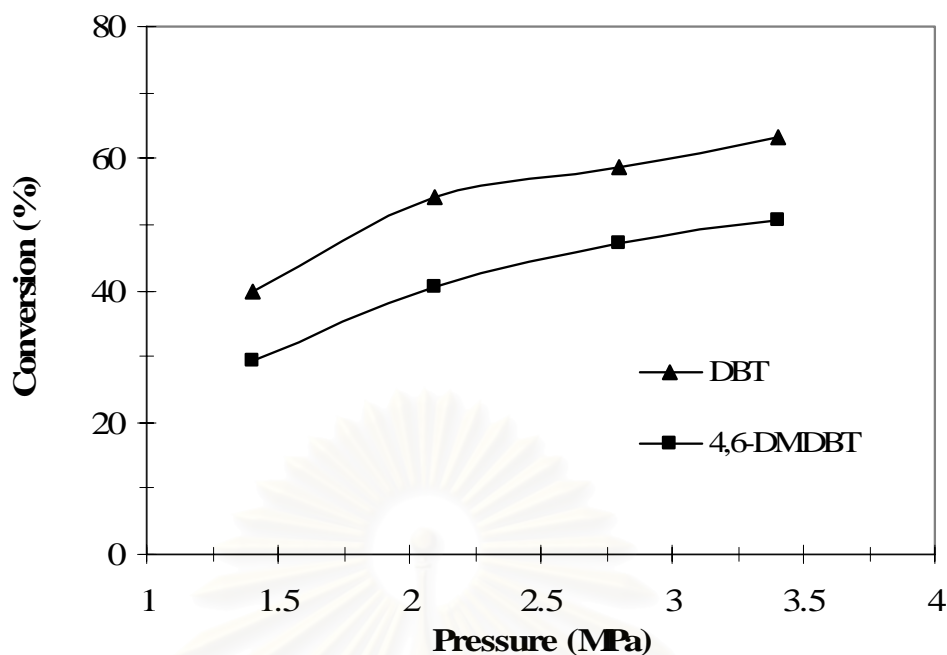
Figure 3.2 Effect of preparation pressure of H_2 on HDS of DBT and 4,6-DMDBT
over NiMo sulfide catalysts. (other preparation parameters: temperature
$= 350^{o}C$, solvent amount $= 1$ g and Ni/(Mo+Ni) $= 0.43$).

Product distribution in the DBT and 4,6-DMDBT HDS are presented
in Table 3.3 For the DBT HDS, generally, BP was a major product from the DDS
pathway. A small amount of THDBT from the HYD pathway and a trace amount of
BCH were also detected. However, it is very interesting that the major product was
CHB while the BCH amount was detected around 10%. Consequently, the HYD/DDS
ratio was over 1.0 for all catalysts, except for the NiMo sulfide prepared at 1.4 MPa
H_2 pressure (HYD/DDS ratio $= 0.9$). For the 4,6-DMDBT HDS, THDMDBT, 3,3'-
DMBP and MCHT were the major products. Unlike the preparation temperature
effect, the 3,3'-DMBP selectivity did not show a considerable change but the
selectivity to THDMDBT decreased significantly when the catalyst preparation
pressure was increased. The HYD/DDS ratio of both DBT and 4,6-DMDBT HDS also
decreased when the preparation pressure was increased. It can be concluded that the
unsupported NiMo sulfide catalysts prepared at high H_2 pressure became less active
for HYD pathway, but more active for DDS pathway.

Table 3.3 Effect of Preparation Presssure on HDS of 4,6-DMDBT and DBT over NiMo Sulfide Catalysts. (Other catalyst preparation parameters: temperature = 350 ^{o}C, solvent amount = 1 g and Ni/(Mo+Ni) = 0.43)

Preparation Pressure (MPa)	1.4	2.1	2.8	3.4
DBT Conversion (wt%)	39.8	54.2	58.5	63.4
Selectivity (%)				
BP	51.4	37.4	41.1	45.0
THDBT	10.9	9.5	6.2	5.6
CHB	31.6	43.1	42.6	40.8
BCH	6.1	10.0	10.1	8.6
HYD/DDS[a]	0.9	1.7	1.4	1.2
4,6-DMDBT Conversion (wt%)	29.4	40.4	47.3	50.5
Selectivity (%)				
3,3'-DMBP	29.4	31.4	33.2	32.8
THDMDBT	45.6	41.9	37.8	35.3
MCHT	21.7	24.5	27.0	28.9
3,3'-DMBCH	3.3	2.2	2.0	3.0
HYD/DDS[b]	2.4	2.2	2.0	2.0

[a] HYD/DDS = [selectivity to (THDBT+CHB+BCH) / selectivity to BP].

[b] HYD/DDS = [selectivity to (THDMDBT+MCHT+3,3'-DMBCH) / selectivity to 3,3'-DMBP].

Based on these results, the H_2 pressure significantly affects the HDS activity of NiMo sulfide catalysts. The higher H_2 pressure increased the activity of NiMo sulfide catalysts for both DBT and 4,6-DMDBT HDS. The low H_2 pressure might not provide enough hydrogen for the decomposition and the reaction of ATTM. Possibly, the high pressure assists ATTM to be converted and synthesized to NiMo sulfide with an active phase for DBT and 4,6-DMDBT HDS.

Table 3.4 Surface Area and Pore Volume of NiMo Sulfide Catalysts Prepared

at Various Preparation Pressures. (Other catalyst preparation

parameters: temperature = 350 $^{\circ}$C, solvent amount = 1 g and Ni/(Mo+Ni)

= 0.43)

Preparation Pressure (MPa)	Surface Area (m^2/g)	Pore volume (cm^3/g)
1.4	83	0.17
2.1	161	0.22
2.8	201	0.28
3.4	231	0.37

Similarly to the preparation temperature effect, the high activity of catalyst prepared at high pressure can be explained by N_2 adsorption measurement as presented in Table 3.4. The unsupported NiMo sulfide catalyst prepared at 1.4 MPa has surface area of 83 m^2/g while the catalyst prepared at 3.4 MPa has higher surface area (231 m^2/g). Thus, the active NiMo sulfide catalyst with high specific surface area and pore volume could be synthesized at high preparation pressure.

3.4 Effects of Organic Solvent in Catalyst Preparation

The effect of organic solvent was studied by addition of various amount of decalin to the aqueous solution of ATTM and Ni precursor. Table 3.5 reveals the effect of decalin amount on the activity of NiMo sulfide catalysts for the HDS of DBT and 4,6-DMDBT. Both the DBT and 4,6-DMDBT conversions increased significantly when the solvent added during the catalyst preparation was increased from 0 to 3 g. The NiMo sulfide catalyst prepared in the presence of 3 g organic solvent has much higher activity for the HDS of DBT (73.5% conversion) and 4,6-DMDBT (59.3% conversion). For the NiMo catalyst prepared without the solvent, BP was the predominant product of the DBT HDS. With increasing the amount of solvent, however, the BP selectivity slightly decreased. Moreover, the selectivity to CHB became more significant than the BP selectivity. The similar trends were

observed in the 4,6-DMDBT HDS. When the catalyst prepared with the high solvent amount was used, the increase in the MCHT selectivity was more pronounced than that in the 3,3'-DMBP selectivity.

Table 3.5 Effect of Organic Solvent Amount on HDS of 4,6-DMDBT and DBT over NiMo Sulfide Catalysts. (Other catalyst preparation parameters: temperature = 350 ^{o}C, pressure = 2.8 MPa and Ni/(Mo+Ni) = 0.43)

Solvent amount(g)	0	1	3
DBT Conversion (wt%)	52.4	58.5	73.5
Selectivity (%)			
BP	46.7	41.1	40.7
THDBT	7.7	6.2	3.4
CHB	38.4	42.6	46.2
BCH	7.2	10.1	9.7
HYD/DDS[a]	1.1	1.4	1.5
4,6-DMDBT Conversion (wt%)	35.8	47.3	59.3
Selectivity (%)			
3,3'-DMBP	31.2	33.2	36.0
THDMDBT	46.2	37.8	31.0
MCHT	20.9	27.0	31.1
3,3'-DMBCH	1.7	2.0	1.9
HYD/DDS[b]	2.2	2.0	1.8

[a] HYD/DDS = [selectivity to (THDBT+CHB+BCH) / selectivity to BP].

[b] HYD/DDS = [selectivity to (THDMDBT+MCHT+3,3'-DMBCH) / selectivity to 3,3'-DMBP].

Table 3.6 Surface Area and Pore Volume of NiMo Sulfide Catalysts Prepared

at Various Solvent Amounts. (Other catalyst preparation parameters:

temperature = 350 $^{\circ}$C, pressure = 2.8 MPa and Ni/(Mo+Ni) = 0.43)

Solvent Amount (g)	Surface Area (m^2/g)	Pore volume (cm^3/g)
0	75	0.16
1	201	0.28
3	258	0.43

Table 3.6 presents the specific surface area and pore volume of unsupported NiMo sulfide catalysts prepared with and without adding solvent. The results of BET analysis show that the NiMo sulfide catalyst prepared in the presence of solvent has much higher surface area (258 m^2/g) than that without solvent (75 m^2/g). The pore volume of catalyst also increased with increasing the solvent amount. Therefore, it is clear that the organic solvent addition led to a highly active unsupported NiMo sulfide catalyst with high surface area. Compared with the catalyst prepared with no solvent addition, the catalysts prepared in the presence of organic solvent have larger surface area for gas-liquid-solid contact, and therefore more active hydrogen species (such as H atom) could be produced for the HDS reaction. This may partially rationalize much higher activity of the catalyst prepared with solvent addition than one prepared in the absence of solvent.

The beneficial effect of organic solvent in this study is consistent with the results reported by Yoneyama and Song [105]. They reported that the addition of solvent in the preparation of MoS_2 from ATTM provided the high activity for cleavage of C-C bond and hydrogenation of naphthalene, and the additional water led to much higher activity. Probably, the presence of the organic solvent helps to disperse ATTM containing water droplet during the preparation with vigorous agitation resulting in a fine molecular dispersion of precursor molecules in the aqueous solution isolated by organic solvent prior to and during the decomposition

and hydrogen reduction. Afanasiev [121] also reported that the presence of organic matter decreased MoS_2 layer stacking and textural stabilization. The carbonaceous matter of any origin prevents the crystallization of the sulfide. The role of the organic molecule is rather that of scaffolding and preventing an agglomeration of layered sulfide fringes.

3.5 Effect of Ni/(Mo+Ni) Ratios

Based on the above results of preparation condition effect on catalytic activity, the unsupported NiMo sulfide catalysts with various Ni/(Mo+Ni) ratios were prepared under suitable conditions of 350 °C and 2.8 MPa H_2 pressure in the presence of 1 g organic solvent.

3.5.1 Specific Surface Area

The BET specific surface areas of the unsupported NiMo sulfide catalyst are summarized in Table 3.7. The surface area of all catalysts was measured before the HDS reaction. The results showed that the unsupported Mo sulfide catalyst prepared by the hydrothermal method has high surface area. However, it was reduced after being deposited by the promoter. The decrease in the surface area of sulfide catalyst after the promoter addition was previously observed for bimetallic sulfide catalysts by some researches [112, 122]. They found that the surface area was decreased from 50 m^2/g to 15 – 25 m^2/g after the addition of promoter to Mo sulfide catalyst [123]. The surface area of unsupported Mo sulfide catalysts was affected by the Ni content, indicating that the Ni content influenced the morphology and/or the degree of aggregation of the Ni-Mo phase. This suggests that the number of active sites in the NiMo sulfide catalysts was not increased but rather that the effectiveness of the active site may be enhanced.

Table 3.7 Surface Area and Pore Volume of NiMo Sulfide Catalysts Prepared with Various Ni/(Mo+Ni) Ratios. (Other catalyst preparation parameters: temperature = 350°C, pressure = 2.8 MPa and solvent amount= 1 g)

Ni/(Mo+Ni)	Surface Area (m^2/g)	Pore volume (cm^3/g)
0	320	0.72
0.20	245	0.39
0.33	207	0.28
0.43	201	0.28
0.50	187	0.25
0.56	159	0.21
1	4	0.01

3.5.2 Crystalline Structure

The XRD patterns of the NiMo sulfided catalyst series are shown in Figure 3.3. Comparison with a commercial MoS_2 powder, all unsupported Mo based sulfide catalysts exhibited broad diffraction peaks, indicating a very poorly crystallized MoS_2 structure, particularly when the promoter was presented. The catalyst with the Ni/(Mo+Ni) ratio of 0.33 showed the diffraction peaks of poorly crystalline MoS_2 only, indicating that the MoS_2 maintains its structure in the presence of amorphous Ni, as reported earlier [89]. For the catalysts with the Ni/(Mo+Ni) ratio above 0.43, the diffraction peaks of the second metal sulfide appeared progressively. Ni_3S_4 was presented in the catalysts with the Ni/(Mo+Ni) ratio of 0.43, 0.50 and 0.56. Moreover, NiS existed in the catalysts with the Ni/(Mo+Ni) ratio of 0.50 and 0.56. In most case, the ternary Mo-Ni-S phases did not appear clearly. It is probably due to the fact that there is overlapping of diffraction peaks from MoS_2 and Mo-Ni-S phase. Another reason is that the active structures (Mo-Ni-S phase) are possibly presented as small nano-crystals, which cannot be characterized by X-ray diffraction method [113].
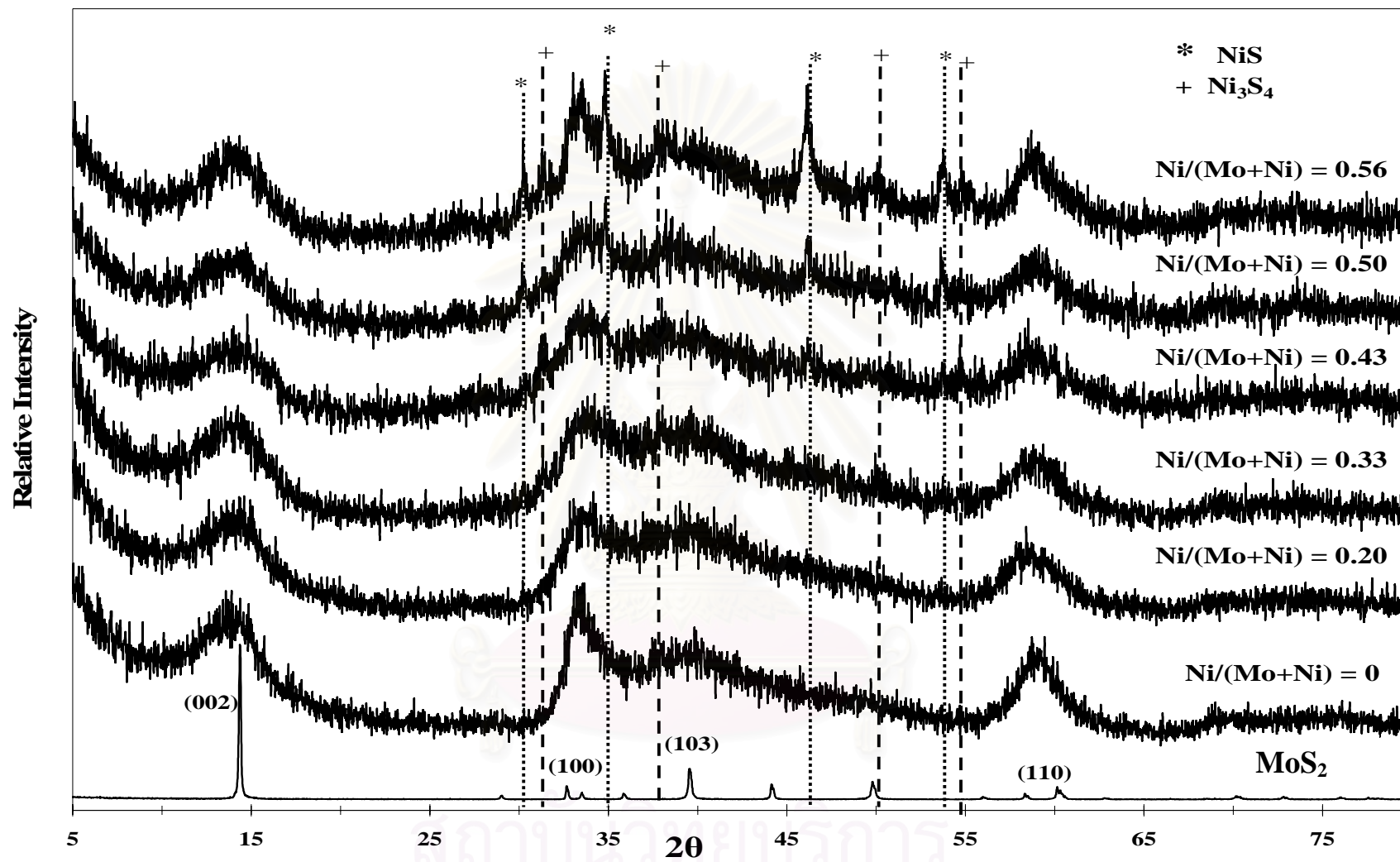
Figure 3.3 XRD patterns of unsupported NiMo sulfide catalysts with various Ni(Mo+Ni) ratios (MoS$_2$ represents Aldrich MoS$_2$ reagent).

3.5.3 Catalytic Activity and Selectivity

The effect of the Ni/(Mo+Ni) atomic ratio on the HDS activity of unsupported NiMo sulfide catalysts is presented in Table 3.8. The Mo sulfide catalyst was prepared by the same procedure as the NiMo sulfide catalysts, but without the Ni precursor. For the Ni sulfide catalyst, the same procedure was followed without the addition of ATTM and CS_2 was used as a sulfur source to provide sulfur for nickel [124]. The main purpose is to prepare a catalyst with high activity in converting the refractory sulfur compounds while the conventional catalysts are not active enough to desulfurize efficiently. The results in Table 3.8 show obviously that the unsupported NiMo sulfide catalysts had very high HDS activity compared with the commercial alumina supported NiMo catalysts (Cr424). Moreover, all unsupported NiMo sulfide and MoS_2 catalysts gave higher 4,6-DMDBT conversion than Cr424.

Surprisingly, 4,6-DMDBT is slightly more reactive than DBT over the unsupported Mo sulfide (31.8% 4,6-DMDBT conversion and 27.7% DBT conversion). This is mainly due to the higher activity in the HYD pathway as the prominent pathway for both sulfur compounds on this catalyst. As seen in Table 3.8, the HYD/DDS ratio for both DBT and 4,6-DMDBT HDS was very high (2.4 for DBT HDS and 11.8 for 4,6-DMDBT HDS). However, if we consider the HDS activity for the products with no sulfur (3,3'DMBP, MCHT and DMBCH for 4,6-DMDBT HDS and BP, CHB and BCH for DBT HDS), DBT reactivity is about twice of 4,6-DMDBT. The conversion of DBT and 4,6-DMDBT increased and reached maximum when Ni incorporated was increased up to the Ni/(Mo+Ni) ratio of 0.5. However, the conversion decreased when the ratio was further increased. These results indicated that there is a significant synergetic effect of Ni on the Mo catalysts for both DBT and 4,6-DMDBT HDS. The HYD/DDS ratio was above 1 for all catalysts even if the HDS of DBT which the hydrogenolysis pathway is generally predominant. It also indicated that the HDS of DBT and 4,6-DMDBT over unsupported Mo and NiMo sulfide catalysts mainly takes the route of hydrogenation. The HYD/DDS ratio decreased significantly when Ni was added into Mo sulfide catalyst. For example, the HYD/DDS ratio in the 4,6-DMDBT HDS is 11.8 for the Mo sulfide catalyst and 2.0 for the catalyst with the Ni/(Mo+Ni) ratio of 0.5. These results suggested that the promoting effect was essentially due to the enhancement of the rate of DDS pathway.

Table 3.8 Effect of Ni/(Mo+Ni) Ratios on HDS of 4,6-DMDBT and DBT over NiMo Sulfide Catalysts. (Other catalyst preparation parameters: temperature = 350°C, pressure = 2.8 MPa and solvent amount = 1 g)

Catalysts	MoS$_2$	NiMoS-0.20	NiMoS-0.33	NiMoS-0.43	NiMoS-0.50	NiMoS-0.53	NiS	Cr424[c]
Ni/(Mo+Ni)	0	0.20	0.33	0.43	0.50	0.53	1	0.31
DBT Conversion (wt%)	27.7	46.3	51.3	58.5	67.8	57.1	11.2	53.6
Selectivity (%)								
BP	29.2	46.6	44.9	41.1	39.5	44.8	56.7	64.3
THDBT	44.5	10.1	7.0	6.2	4.2	6.4	26.5	4.0
CHB	19.7	36.4	39.9	42.6	45.6	40.5	7.9	28.6
BCH	6.6	6.9	8.2	10.1	10.7	8.3	8.9	3.1
HYD/DDS[a]	2.4	1.1	1.2	1.4	1.5	1.2	0.8	0.6
4,6-DMDBT Conversion (wt%)	31.8	34.3	41.0	47.3	54.0	44.4	7.5	26.0
Selectivity (%)								
3,3'DMBP	7.8	26.6	26.3	33.2	33.4	31.2	10.7	32.6
THDMDBT	87.1	45.0	45.4	37.8	33.9	42.1	84.6	40.6
MCHT	3.8	26.8	26.6	27.0	30.6	25.2	4.3	26.6
3,3'-DMBCH	1.3	1.6	1.7	2.0	2.1	1.4	0.4	0.2
HYD/DDS[b]	11.8	2.8	2.8	2.0	2.0	2.2	8.4	2.1

[a]HYD/DDS = [selectivity to (THDBT+CHB+BCH) / selectivity to BP]. [b]HYD/DDS = [selectivity to (THDMDBT+MCHT+ 3,3'-DMBCH) / selectivity to 3,3'-DMBP]. [c]Commercial NiMo sulfide alumina supported catalyst.

The remarkable increase in the catalytic activity by the addition of Co or Ni to Mo sulfide catalyst has been reported by many research groups. Upon increasing the concentration of the promoter atoms, the activity may increase significantly. The other promoting effects may be highly dependent on the catalysts preparation procedure. The variation in the optimum Me/(Me+Mo) (Me = Co, Ni) atomic ratios reported in the literatures may be explained. In the case of the unsupported catalyst, the optimum Me/(Me+Mo) atomic ratios are in the range of 0.3 to 0.54 for CoMo sulfide catalysts [123, 125, 126] and 0.4 to 0.55 for Ni-Mo sulfide catalysts [127, 128]. In the case of the supported catalyst, the optimum Me/(Me+Mo) atomic ratios are in the range of 0.2 to 0.4 for CoMo and NiMo sulfide catalysts [13, 129]. In this study, the activity of the catalyst with the Ni/(Mo+Ni) ratio of 0.2 and 0.33 was much higher than MoS_2 and NiS sulfide catalysts. The NiMo sulfide catalyst with the Ni/(Mo+Ni) ratio of 0.50 had highest activity among all catalysts tested. This optimum Ni/(Mo+Ni) ratio agrees very well with the previous results reported for the unsupported NiMo sulfide catalysts.

During the catalyst preparation, the reaction occurring between ATTM and $Ni(NO_3)_2$ in the environment of hydrogen to form the bimetallic sulfide catalyst was suggested as follows [130].

$$2(NH_4)_2MoS_4 + Ni(NO_3)_2 \rightarrow (NH_4)_2\{Ni(MoS_4)_2\} + 2NH_4NO_3 \qquad (3.7)$$
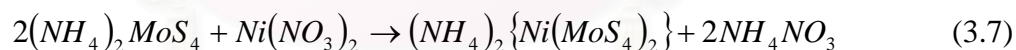
The presence of hydrogen gives the bimetallic sulfide according to the following reactions

$$Ni(MoS_4)_2 + H_2 \rightarrow Ni(MoS_3)_2 + H_2S \qquad (3.8)$$

$$Ni(MoS_3)_2 + H_2 \rightarrow Ni(MoS_2)_2 + H_2S \qquad (3.9)$$
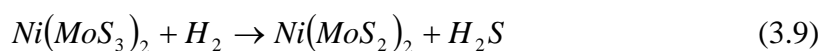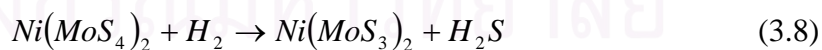
The chemical interaction among Ni and Mo atoms after the decomposition implies that a good dispersion of the promoter in MoS_2 is obtained,

resulting in the formation of a large number of NiMo sites. It has been reported that the presence of Ni promoter atoms causes the change of the shape of the MoS_2 nanoclusters from triangular to hexagonally truncated structure as mentioned in Chapter 1 [99]. Ni atoms may be placed at the edge of MoS_2 crystallites, forming Ni–Mo–S structure which is considered to provide a major HDS active site [13, 65, 131]. The hydrothermal method assists the formation of very small size of NiMo sulfide cluster in the unsupported catalyst. It is postulated that the organic solvent may be finely dispersed in the aqueous solution (close to supercritical fluid) of ATTM and Ni precursor at high H_2 pressure, facilitating the decomposition of ATTM and the reaction between Mo Species with the Ni precursor. Subsequently, very fine particles (nano-size) of NiMo sulfide catalyst could be synthesized. In addition, more Ni atoms would be incorporated into smaller Mo sulfide crystallites, forming more NiMoS phases.

From Table 3.8, the conversion of both sulfur compounds increased when the Ni/(Mo+Ni) atomic ratio was increased up to 0.5 because more active NiMoS phase was formed in the small crystallites of Mo sulfide. However, for the catalyst with Ni/(Mo+Ni) atomic ratio above 0.5, excess Ni atoms may occupy the active phase of NiMoS instead of reactants, leading to the decrease in the conversion of sulfur compounds. Although the separate phases of the Ni_3S_4 and NiS were presented in the catalysts with Ni/(Mo+Ni) ratio between 0.43 and 0.5 (Figure 3.3), there was no detrimental effect on the conversion of DBT and 4,6-DMDBT. What role does this separate metal sulfide play is a matter of debate. If these metal (Ni and Co) sulfide particles are indeed catalytically active, they might help adsorb and dissociate hydrogen molecule. The resulting H species could attack the MoS_2 particles and create coordinative unsaturated site at the edges [132, 133].

3.6 Effect of Co/(Mo+Co) Ratios

As mentioned above, Ni is the effective promoter that enhances and maintains the performance of the unsupported MoS_2 catalyst. However, Co is another promoter that widely accepted for promoting the HDS activity of MoS_2. Thus, in order to investigate the effect of Co on the unsupported MoS_2 catalysts, the unsupported CoMo sulfide catalysts with various Co/(Mo+Co) ratios were prepared at suitable conditions of 350 °C and 2.8 MPa H_2 pressure in the presence of 1 g organic solvent. Then the activity of CoMo sulfide catalysts was evaluated by the simultaneous HDS of DBT and 4,6-DMDBT and compared with the commercial catalysts.

Table 3.9 presents the effect of the Co/(Mo+Co) atomic ratio on the HDS activity of unsupported CoMo sulfide catalysts. Similar to NiMo sulfide, Co shows the significant synergetic effect on the Mo sulfide catalyst. The conversion of DBT and 4,6-DMDBT increased and reached maximum at the Co/(Mo+Co) ratio of 0.5. The effect of Co was slightly higher than that of Ni on the activity of MoS_2 for both DBT and 4,6-DMDBT HDS. However, over CoMo sulfide, the HYD/DDS ratio of DBT HDS was lower than 1.0 while this ratio of 4,6-DMDBT HDS is higher than 1.0. These results suggested that the DDS pathway was the main pathway for HDS of DBT whereas HDS of 4,6-DMDBT favored the HYD pathway over the unsupported CoMo sulfide catalysts.

Table 3.9 Effect of Co/(Mo+Co) Ratios on HDS of 4,6-DMDBT and DBT over CoMo Sulfide Catalysts. (Other catalyst preparation parameters:

temperature = 350°C, pressure = 2.8 MPa and solvent amount = 1 g)

Catalysts	MoS_2	CoMoS-0.20	CoMoS-0.33	CoMoS-0.43	CoMoS-0.50	CoMoS-0.53	Cr344[c]
Co/(Mo+Ni)	0	0.20	0.33	0.43	0.50	0.53	0.30
DBT Conversion (wt%)	27.7	55.4	58.9	63.5	68.0	65.4	44.3
Selectivity (%)							
BP	29.2	76.3	77.0	78.1	79.0	78.0	88.1
THDBT	44.5	4.6	5.5	4.0	2.7	4.2	2.0
CHB	19.7	14.5	13.2	12.9	11.9	12.1	8.1
BCH	6.6	4.6	4.3	5.0	6.3	5.7	1.8
HYD/DDS[a]	2.4	0.31	0.30	0.28	0.27	0.28	0.1
4,6-DMDBT Conversion (wt%)	31.8	38.9	47.7	56.5	61.7	56.8	17.8
Selectivity (%)							
3,3'DMBP	7.8	31.7	35.0	43.1	49.8	42.7	35.4
THDMDBT	87.1	42.9	41.3	33.4	27.0	33.8	36.7
MCHT	3.8	25.1	21.7	20.1	19.3	21.2	27.7
3,3'-DMBCH	1.3	0.3	2.0	3.4	3.9	2.3	0.3
HYD/DDS[b]	11.8	2.15	1.86	1.32	1.01	1.34	1.8

[a]HYD/DDS = [selectivity to (THDBT+CHB+BCH) / selectivity to BP]. [b]HYD/DDS = [selectivity to (THDMDBT+MCHT+ 3,3'-DMBCH) / selectivity to 3,3'-DMBP]. [c]Commercial CoMo sulfide alumina supported catalyst.

CHAPTER IV

COMPARATIVE STUDY ON PHYSICOCHEMICAL PROPERTIES AND CATALYTIC ACTIVITY OF MoS$_2$, CoMoS$_2$ AND NiMoS$_2$ UNSUPPORTED CATALYSTS

Catalysts based on molybdenum or tungsten have been used extensively for hydrodesulfurization (HDS) in petroleum refining for several decades and increasing attention is directed towards more effective catalysts for deep desulfurization [1, 2]. The increase in the HDS activity by addition of Co or Ni into Mo or W based catalysts has attracted the most attention in the studies of HDS catalysts. The synergetic effects of promoters on the catalytic activity of the Mo sulfides have been reported in the literatures [13, 112, 113]. The effect of promoter in Mo sulfide catalysts has been attributed to the amount of promoter atoms that can be accommodated on the edges of MoS$_2$ layers and also to the electronic transfer that promoter atom induces on Mo atoms located at these sites [114, 115]. The exact nature of the active sites in Co–Mo or Ni–Mo sulfide catalysts is still a subject of debate, but the Co–Mo–S model or Ni–Mo–S model is currently one of the most widely accepted [13, 134]. According to the model, the Co–Mo–S structure or Ni–Mo–S structure is responsible for the catalytic activity of the Co-promoted or Ni-promoted MoS$_2$ catalyst.

Throughout this chapter, the rate constant of a model fuel HDS is used as a quantitative measurement of activity of unsupported Mo based sulfide catalysts. Commercial available Co-Mo/γ-Al$_2$O$_3$ (Cr344) and Ni-Mo/γ-Al$_2$O$_3$ (Cr424) were used to compare the activities with the unsupported Mo based sulfide catalysts. The key components of these two catalysts as provided by Criterion Catalyst Corporation, were 13.5 wt % MoO, 2.9 wt % CoO for Cr344 and 13.0 wt % MoO, 3.0 wt % NiO for Cr424. The specific surface area of Cr344 and Cr424 are 183.3 m^2/g and 163.2 m^2/g, respectively. Although Cr344 and Cr424 are not state-of-the-art commercial HDS catalysts, they were available freely with no restrictions regarding its characterization and analysis. More recent and state-of-the-art commercial hydrotreating catalysts required secrecy and non-disclosure agreements to prevent the

complete examination necessary for a scientific study. For comparison, Cr344 and Cr424 were a better alternative than γ-Al$_2$O$_3$ supported catalyst synthesized in house.

In Chapter 3, the hydrothermal method was found to be very effective for the synthesis of highly active unsupported NiMo sulfide catalysts. Physical properties and activity of sulfide catalysts strongly depend upon the catalyst preparation conditions. Moreover, the organic solvent added in the catalyst preparation step assisted the dispersion of the precursor molecules. In this chapter, the appropriate preparation condition (350 ^{o}C, 2.8 MPa, 1 g of organic solvent and Me/(Me+Mo) = 0.43 (Me=Co or Ni)) was selected for synthesis of unsupported Mo, CoMo and NiMo catalysts. The purpose of the work in this chapter is to study the effect of Co and Ni on the HDS activity of unsupported Mo sulfide catalyst, prepared by hydrothermal method of ammonium tetrathiomolybdate (ATTM) in the simultaneous HDS of DBT and 4,6-DMDBT under typical hydrotreating conditions. The promoter effect on physicochemical properties and morphology of catalyst are also studied.

4.1 Catalyst Characterizations

4.1.1 N$_2$ Adsorption-Desorption Measurement

Table 4.1 presents the physical properties of unsupported Mo based sulfide catalysts. The surface area of catalysts was measured before the HDS reaction. The unsupported Mo sulfide catalyst had high surface area (320 m^2/g) and large pore volume (0.72 cm^3/g). After the addition of promoters, a significant decrease in the surface area and pore volume was observed. The NiMo and CoMo sulfide catalysts have the surface area of 201 and 196 m^2/g, respectively. These results indicate that the promoter influences the surface area of the unsupported Mo sulfide. The variation of surface areas of MoS$_2$ catalysts was in the range of few to several hundred square meters per gram depending on the precursor and condition of the synthesis [135, 136]. Alonso et al. [137] and Siadati et al. [138] reported that MoS$_2$ catalysts prepared from tetraalkylammonium thiomolybdates had surface area in the range of 60 to 329 m^2/g and 170 to 225 m^2/g, respectively.

Table 4.1 Composition and Properties of Fresh Unsupported Mo Based Sulfide
Catalysts.

Catalysts	Me/(Mo+Me)[a]	Surface Area[b] (m^2/g)	Pore Volume (cm^3/g)
MoS_2	0.00	320	0.72
$NiMoS_2$	0.43	201	0.28
$CoMoS_2$	0.43	196	0.27

a) Me/(Mo+Me) molar ratio based on metal in the precursor salts (Me = Co or Ni).

b) Samples were vacuum dried before surface area measurement.

4.1.2 Temperature Programmed Reduction

Figure 4.1 presents the TPR profiles of the unsupported MoS_2, $CoMoS_2$ and $NiMoS_2$ catalysts. The TPR profiles of all catalysts showed a well-separated peak at low temperature and one or two broad peaks at high temperature. For unsupported MoS_2 catalyst, two main peaks were observed at 235 and 524 ^{o}C, respectively. After the incorporation of the promoters (Co and Ni) into the MoS_2 catalyst, the TPR profile shifted to lower temperature for both low-temperature and high-temperature peaks. The position of the peak maxima/minima depends on the type of promoter. For the CoMo sulfide catalyst, the maximum reduction temperature peak was observed as a broad band centered between 383 and 424 ^{o}C and a low temperature peak at 198 ^{o}C. For the NiMo sulfide catalyst, three peaks were observed at 206, 366 and 439 ^{o}C, respectively. The addition of Co and Ni caused a significant downward shift (37 and 29 ^{o}C, respectively) in the peak position relative to low-temperature TPR peak of the unpromoted MoS_2 catalyst (235 ^{o}C) indicating that the addition of promoter enhanced the reducibility of Mo sulfide.
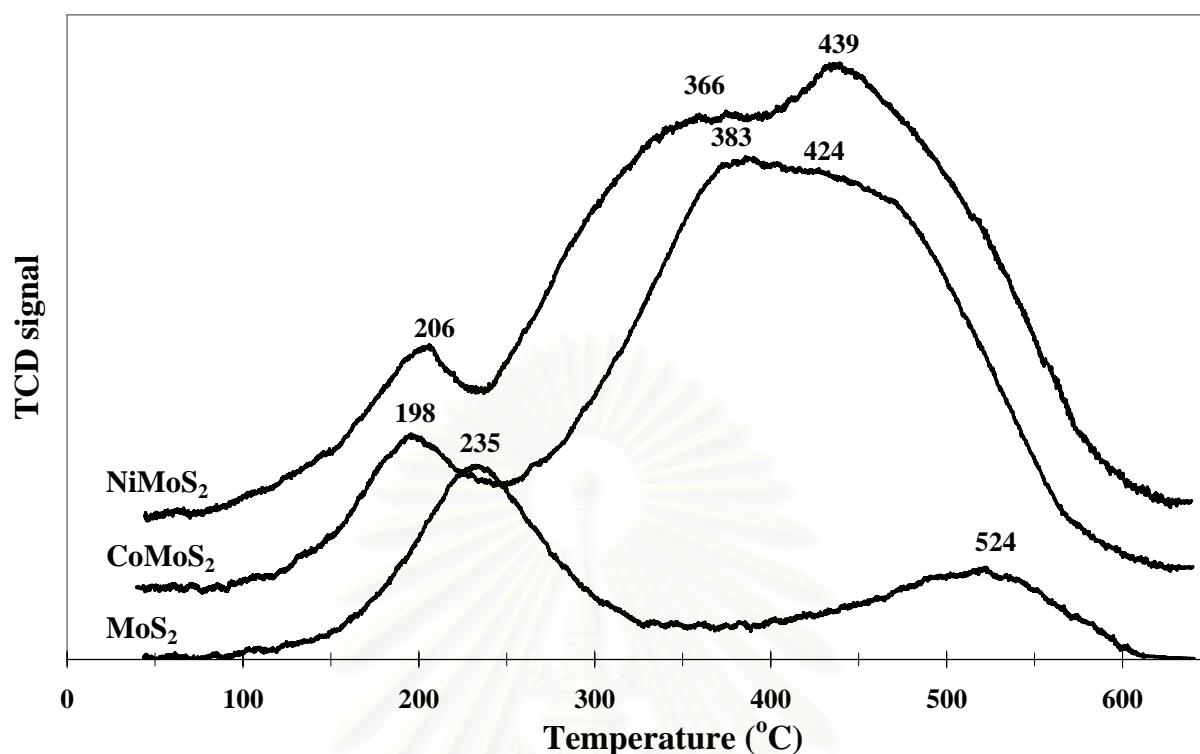
Figure 4.1 TPR patterns of unsupported MoS_2, $CoMoS_2$ and $NiMoS_2$ catalysts.

4.1.3 X-Ray Diffraction

Figure 4.2 presents the XRD patterns for the unsupported Mo sulfide catalysts before and after the addition of promoters. As compared to a commercial MoS_2 powder, both the unpromoted and promoted Mo sulfide catalysts exhibit weak XRD peaks, indicating a very poorly crystalline structure characteristic of the molybdenum disulfide. The XRD peaks became broader when the (Ni or Co) promoter was added. The intensity of most MoS_2 peaks were significantly decreased, particularly for the unsupported CoMo sulfide, the peak at $2\theta = 14.4°$, characteristic of the (002) basal planes of crystalline MoS_2 became very low. In the sulfides with promoters, the diffractions of separate Ni and Co sulfides were detected due to high loading amount of these metals indicating that the crystallized Ni_3S_4 and Co_9S_8 were formed. For the promoted sulfide catalysts, the Ni-Mo-S or Co-Mo-S phases were not reflected by any major XRD peaks. The active structure (Ni-Mo-S or Co-Mo-S phase) was possibly present as a small nano-sized particle, which cannot be detected by the XRD diffraction method [103].
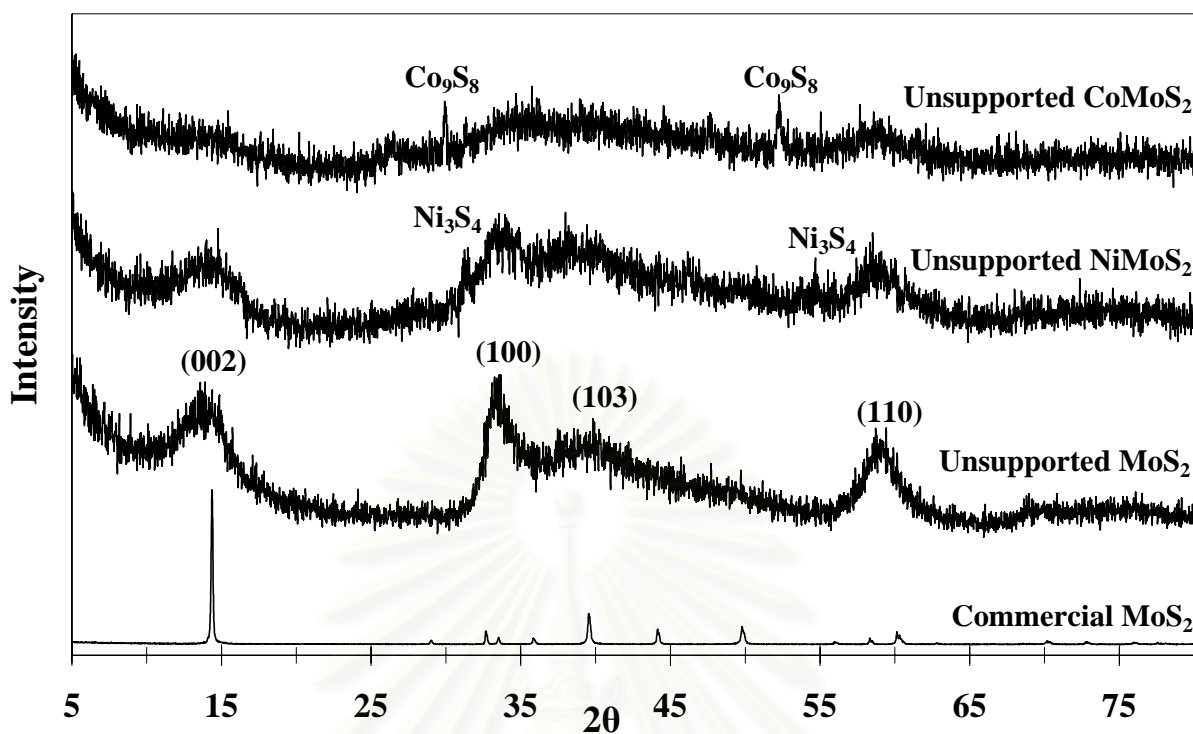
Figure 4.2 XRD patterns of three unsupported Mo based sulfide catalysts and commercial MoS_2.

4.1.4 High Resolution Electron Microscopy

Figure 4.3 presents the HRTEM photographs of the unsupported Mo sulfide catalysts with and without Ni promoter. The black thread-like fringes correspond to the MoS_2 slabs. The fringes observed in the photographs had a spacing of about 0.65 nm that was the characteristic of (002) basal planes of crystalline MoS_2. The TEM images clearly showed that the unpromoted MoS_2 catalyst had long slabs. The curvature of slabs increased while the slab length decreased upon the addition of Ni promoter. The number of stacked layer of the Ni promoted MoS_2 catalyst was more than that of the unpromoted catalyst. It can be concluded that the incorporation of Ni in to the Mo sulfide catalyst increases the number of stacked layer, while decreases the crystallite size of catalyst. The TEM images also indicated that the smaller particles were formed when the promoters were incorporated with the Mo sulfide.
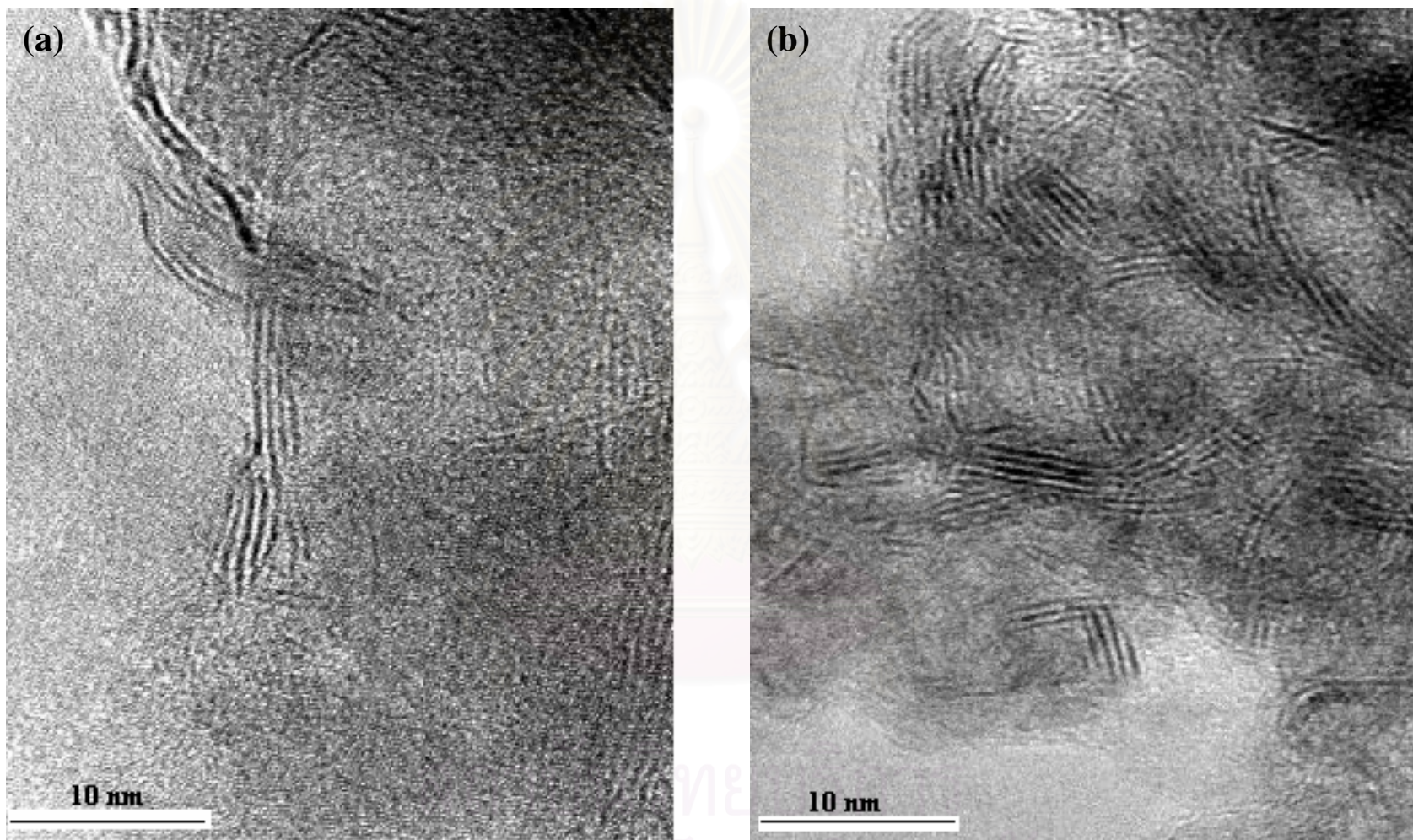
Figure 4.3 High-resolution TEM images of unsupported catalysts (a) MoS_2 (b)$NiMoS_2$.

4.1.5 Promoter Effect on Morphology of Unsupported Mo sulfide

The addition of promoter to the unsupported Mo sulfide catalyst not only changed the catalytic activity but also the porosity and the morphology of the Mo based sulfide catalyst. These changes can be clearly seen from the surface area, the HRTEM images, even the shift of low-temperature TPR peak as well as the broader XRD peak when the promoter was added. These indicate that not only a chemical such as edge decoration but also a structural such as textural or morphological promoting effect is involved.

The BET surface area of the NiMo and CoMo sulfides was lower than that of the unpromoted Mo sulfide (Table 4.1). The phenomenon of the decrease in the surface area of sulfide catalyst due to the addition of promoter was earlier reported [122, 123]. Pedraza et al. [130] also reported that the surface area decreased from 50 m^2/g to 20 - 30 m^2/g when the promoter was added into Mo sulfide catalyst. The relationship between specific surface areas and the HDS activity was not straightforward and the catalyst with larger surface area does not necessarily yield a higher HDS rate constant. This is in agreement with some studies that the catalytic activity of molybdenum sulfide catalysts was not directly related to the BET surface area but dependent on the morphology of catalysts [13]. The lack of the correlation between BET surface area and HDS activity over unsupported Mo based sulfide catalysts was earlier reported by Inamura et al. [122] and Alvarez et al. [113]

The TPR profile of sulfide catalysts contains several well separated reduction peaks. The low-temperature peak can be assigned to surface sulfur atoms (weakly bonded sulfur) whereas the ''bulk reduction'' occurs in the higher temperatures range. In the low-temperature region, the surface is reduced and the coordinative unsaturated sites (CUS) are created which are believed to be responsible for the active sites [139]. For MoS_2, apparently, the well separated low-temperature peak at 235 ^{o}C originates from sulfur atoms that are weakly bound on the catalyst surface. The signal above 327 ^{o}C corresponds to the partial reduction of the small MoS_2 crystals [125, 140]. The profile of this curve is similar to others presented in literature [141]. The behavior of this catalyst during TPR was proposed by Li et al. [142].

$$[MoS_2]_x - S \xrightarrow[<177\ ^oC]{H_2} [MoS_2]_x + H_2S \qquad \text{(surface)} \qquad (4.1)$$

$$[MoS_2]_x \xrightarrow[<400\ ^oC]{H_2} [MoS_2]_x - H \qquad \text{(surface)} \qquad (4.2)$$

$$[MoS_2]_x - H \xrightarrow[>300\ ^oC]{H_2} [Mo_xS_{2x-1}]* + H_2S \qquad \text{(surface)} \qquad (4.3)$$

$$MoS_2 \xrightarrow[>327\ ^oC]{H_2} MoS* + H_2S \qquad \text{(mass)} \qquad (4.4)$$
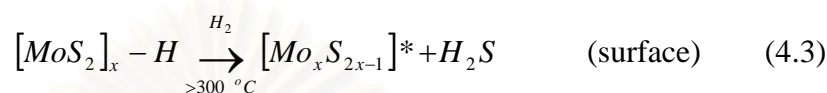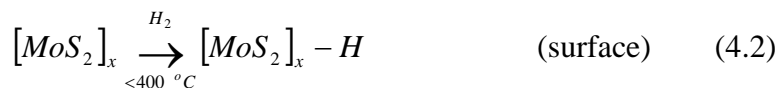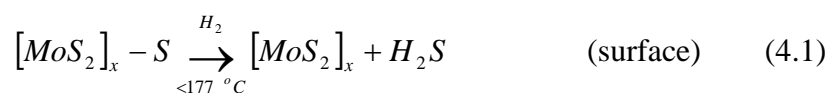
In these expression, $[MoS_2]_x$ represents MoS_2 on the surface and * represents an anionic vacancy.

The TPR results showed that the addition of Co or Ni to the unsupported Mo sulfide catalysts caused a significant downward shift of the first peak temperature during TPR. With the addition of promoter, the new TPR peaks in the high temperature range were observed. These new peak were not contributed by separated sulfide phase of promoter since the reduction of bulk separated sulfide phase began around 527 ^oC and a peak maximum was observed at 677 ^oC, as reported in the literature [140], which is much higher than the TPR temperature of new peak observed in the present work. These TPR result suggests that there is an interaction between promoter and Mo species. The lower TPR peak temperatures for Co and Ni promoted unsupported Mo sulfide catalysts imply a lower sulfur binding energy as compared to unpromoted Mo sulfide catalyst. In other words, the promoter decreased the strength of the molybdenum-sulfur-promoter bond in the sulfide itself. This is consistent with the theoretically estimated metal-sulfur bond energies indicating that the addition of Co or Ni on MoS_2 should give rise to a lower metal sulfur bond strength [143, 144]. It is generally believed for transition metal sulfide that sulfur vacancies created by means of reduction with hydrogen are responsible for the observed catalytic activity [13, 103]. This formed the basis for the bond energy model

in which there exists a correlation between the catalytic activity and the estimated metal sulfur bond strength [122]. It is clearly seen in the results that the promoted catalysts had much higher catalytic activity than unsupported Mo sulfide catalyst (Table 2). This activity variation can be rationalized in terms of the bond energy when the metal sulfur bond strengths are assessed by TPR peak temperature. This TPR result agrees with the work reported by Jacobsen et al. [141] who observed a converse relationship between the temperature of the first H_2S TPR peak of metal sulfides and the HDS activity of catalysts.

It is generally accepted that the promoter atom is located at the edges of the hexagonal MoS_2 platelets [92, 145]. It is also believed that the Co-Mo-S structure or Ni-Mo-S structure is responsible for the catalytic activity of the Co-promoted or Ni-promoted MoS_2 catalyst in the HDS reaction. As the promoter is added, it preferentially interacts with the edge of the MoS_2 crystallite surface and then forms the active species.

The XRD pattern showed that the intensity of MoS_2 peaks were decreased significantly and particularly the peak at $2\theta = 14.4°$, characteristic of the (002) basal planes of crystalline MoS_2 became very low on the unsupported CoMo sulfide. It indicated that much smaller size of (002) phase of MoS_2 was generated or/and Co or Ni places the phase of MoS_2, specifically on the (002) phase. This results in the decreasing of the length of the stack after the addition of promoter which was observed in HRTEM analysis as shown in Figure 4.3. The XRD pattern and HRTEM images showed that the addition of promoter caused the decrease in the length of the basal planes and increase in average number of layers in the stacks. This result is in agreement with previous result showing that Co decoration at the edges of MoS_2 slabs can induce an increase of the stacking height [147]. HRTEM results agreed very well with XRD analysis. In the absence of the promoters, the MoS_2 formed large crystallized particles as seen from long length slab and narrow XRD pattern. The growth of MoS_2 crystallized particles was suppressed when the promoters are incorporated. The effect of promoter on the size of MoS_2 might be explained by the decoration of promoter at the edges of MoS_2 slabs which prevents the further growth of MoS_2 crystallites.

However, not all of the promoter added results in the formation of the Co-Mo-S or Ni-Mo-S species. When all of the edges are covered, the promoter forms a separate phase of the sulfide as seen in Figure 4.2. The Ni_3S_4 and Co_9S_8 peaks were detected after the addition of promoter. These metal (Ni and Co) sulfide particles might help hydrogen adsorb and dissociate. The H species are mobile enough in the conditions of catalysis to attack the MoS_2 particles and create coordinative unsaturation site at the edges [132, 146].

In summary, the catalyst characterization efforts provided detailed and useful insights about the promoting effect on the physicochemical properties of the catalysts. The catalyst characterization experiments resulted in extensive information about the structure which enabled a better understanding of catalytic activity which is present hereafter.

4.2 Catalytic Performance of Unsupported Mo, CoMo and NiMo Sulfides

4.2.1 Nature of Catalyst Formation Mechanism

4.2.1.1 Decomposition of Thiosalts

The characterization part obviously shows that the change in the textural properties of unsupported catalysts not just due to promoter addition but it varied due to the change of the formation mechanism.

The decomposition of thiosalts has been widely observed by thermal analysis [113, 123, 148] that the evolution from thiosalt precursors to MoS_2 occurs in three steps as follow:

1. Elimination of ammonium disulfide

This step is slightly endothermic. MoS_3 is formed releasing ammonia and hydrogen sulfide to the gas phase.

$$\left(NH_4\right)_2 MoS_4 \rightarrow MoS_3 + \left(NH_4\right)_2 S \tag{4.5}$$
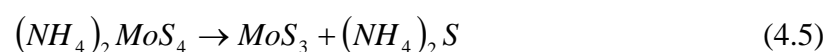
2. Elimination of sulfur

This step is notably exothermic, yielding a highly disordered – poorly crystalline – MoS_2 as it eliminates sulfur (or hydrogen sulfide, if excess hydrogen is present)

$$MoS_3 \rightarrow MoS_2(amorphous) + 1/xS_x \qquad (4.6)$$
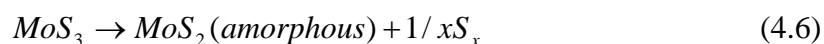
3. Aggregation and ordering of crystallites

This step involves a re-stacking process of the MoS_2 crystallites.

$$MoS_2(amorphous) \rightarrow MoS_2(crystalline) \qquad (4.7)$$
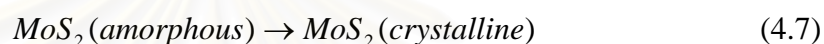
However, it is important to note that final composition of MoS_2 depends on the type of atmosphere during the thermal decomposition of the thiosalt.

4.2.1.2 Formation of Bimetallic Sulfide Catalysts

For the catalyst preparation, the reaction occurred between ATTM and promoter in the environment of hydrogen to form the bimetallic sulfide catalyst was suggested as follow [112]:

$$2[(NH_4)_2 MoS_4] + Me(NO_3)_2 \rightarrow (NH_4)_2\{Me(MoS_4)_2\} + 2NH_4NO_3 \qquad (4.8)$$
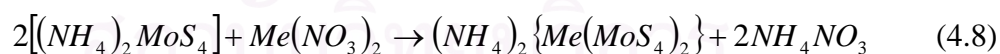
where Me is Co or Ni. In this step, the promoter cation is bonded to the thioanion containing the Mo atom.

The decomposition of the binary ammonium thiometallate obtained through reaction (4.8), in presence of hydrogen gives the binary sulfides according to the reactions

$$Me(MoS_4)_2 + 2H_2 \rightarrow Me(MoS_3)_2 + 2H_2S \qquad (4.9)$$

$$Me(MoS_3)_2 + 2H_2 \rightarrow Me(MoS_2)_2 + 2H_2S \qquad (4.10)$$
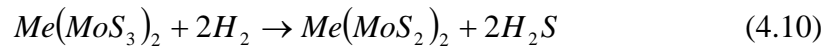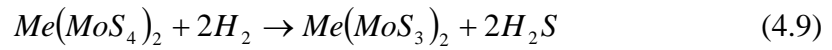
By these means, the chemical interaction produced during the formation of the binary thiometallates is maintained in the CoMo and NiMo catalysts and the electronic properties of the binary thiometallate precursors are preserved in the CoMo and NiMo catalysts. The preserving of the chemical interaction among Co or Ni and Mo atoms after the decomposition process also implies that a good dispersion of the promoter in MoS_2 is obtained, forming a large number of CoMo or NiMo sites. These sites located on the edge of MoS_2 or crystallites are proposed to act as the active sites for hydrotreating processes.

4.2.2 Overall Rate Constant and Individual Rate Constant of DBT and 4,6-DMDBT Hydrodesulfurization

The simultaneous HDS of 4,6-DMDBT and DBT was used to test the activity of the catalysts. All experiments were conducted under conditions (2.1 MPa and 300 ^{o}C) that would give conversion less than 30% in order to obtain reliable kinetic data. As a first approximation, the HDS of individual sulfur compounds follows pseudo-first-order kinetics [23, 149] whereas mixtures of gas oils and heavier oils may follow pseudo-second order kinetics [150] or a linear combination of pseudo-first order kinetics [2, 151]. Integrating the first-order rate expression for DBT and 4,6-DMDBT HDS results in the following expression:

$$\ln\left(\frac{C_{DBT}}{C_{DBTo}}\right) = -(k_1 + k_2)t \qquad (4.11)$$

$$\ln\left(\frac{C_{4,6-DMDBT}}{C_{4,6-DMDBTo}}\right) = -(k_1 + k_2)t \qquad (4.12)$$

where k_1 is the rate constant for the hydrogenation (HYD) pathway, k_2 is the rate constant for the hydrogenolysis (DDS) pathway, and $k_1 + k_2$ represents the

overall HDS rate constant of 4,6-DMDBT. This overall HDS rate constant can be obtained from the experimental data. Figure 4.4, 4.5 and 4.6 show the pseudo-first-order kinetics of 4,6-DMDBT and DBT HDS over the Mo, NiMo and CoMo sulfide catalysts, respectively.

Although the overall HDS rate constant was obtained directly from the experimental data using eq (4.11) and (4.12), the individual rate constants for each reaction pathway are not easy to measure. Some researchers have tried to estimate these values using equations derived with some assumptions [152-155]. However, these methods are not easy to use for calculating the rate constants directly from the experimental results. Since $k_1 + k_2$ values have been estimated on the basis of the experimental data, if the k_1/k_2 ratio can be estimated, the individual k_1 and k_2 values can then be calculated from the combination of the k_1/k_2 ratio and overall rate constant $(k_1 + k_2)$ values. The method of initial rates, which is widely used in kinetic analyses was used [156-158], because it does not rely on any assumptions about the reaction pathway, or the reversibility of reactions. This method was applied using the initial selectivity of primary products, i.e., the selectivity of products at close to zero conversion [159]. The k_1/k_2 ratio may be obtained directly from the initial selectivity ratio between primary products in the HYD and DDS pathways. The rate constant k_1 is proportional to the initial hydrogenation rate of DBT to THDBT, and the rate constant k_2 is proportional to the initial DDS rate of DBT to BP. In the same way, the rate constant k_1 is proportional to the initial hydrogenation rate of 4,6-DMDBT to HDMDBTs, and the rate constant k_2 is proportional to the initial DDS rate of 4,6-DMDBT to DMBP. The further detail for rate constant calculation is shown in Appendix C. The individual rate constant of DBT and 4,6-DMDBT was determined as follows :

$$\frac{k_1}{k_2} = \frac{[initial \ \ selectivity \ \ of \ \ THDBT]}{[initial \ \ selectivity \ \ of \ \ BP]} \tag{4.3}$$

$$\frac{k_1}{k_2} = \frac{[initial \ \ selectivity \ \ of \ \ HDMDBTs]}{[initial \ \ selectivity \ \ of \ \ DMBP]} \tag{4.4}$$
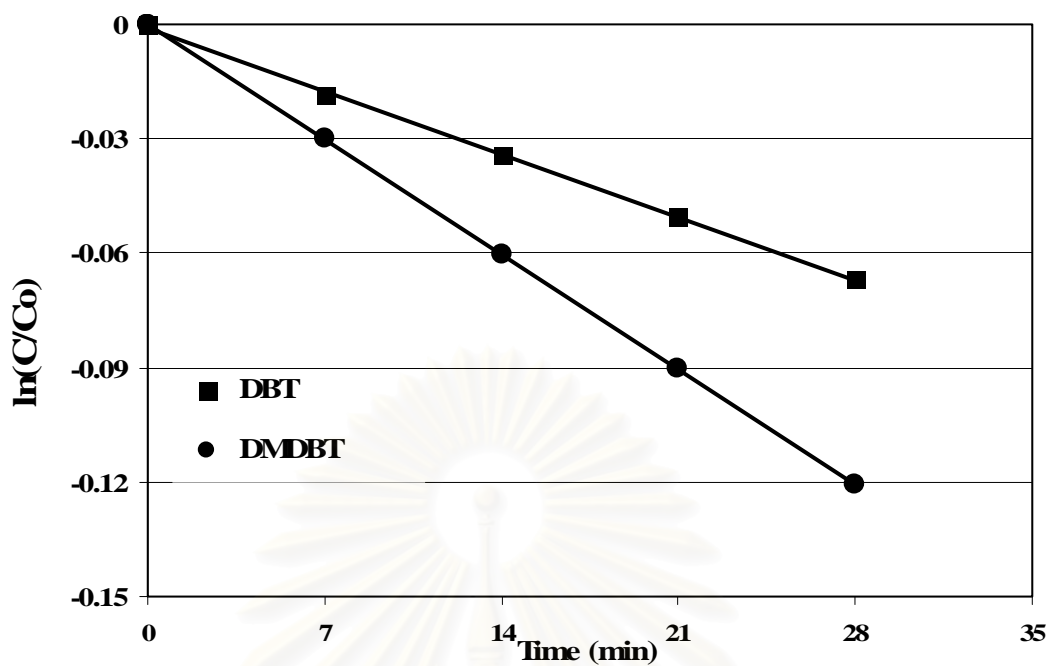
Figure 4.4 Pseudo first order kinetics of 4,6-DMDBT and DBT HDS over Mo
sulfide catalysts (HDS conditions : 2.1 MPa, 300 °C).
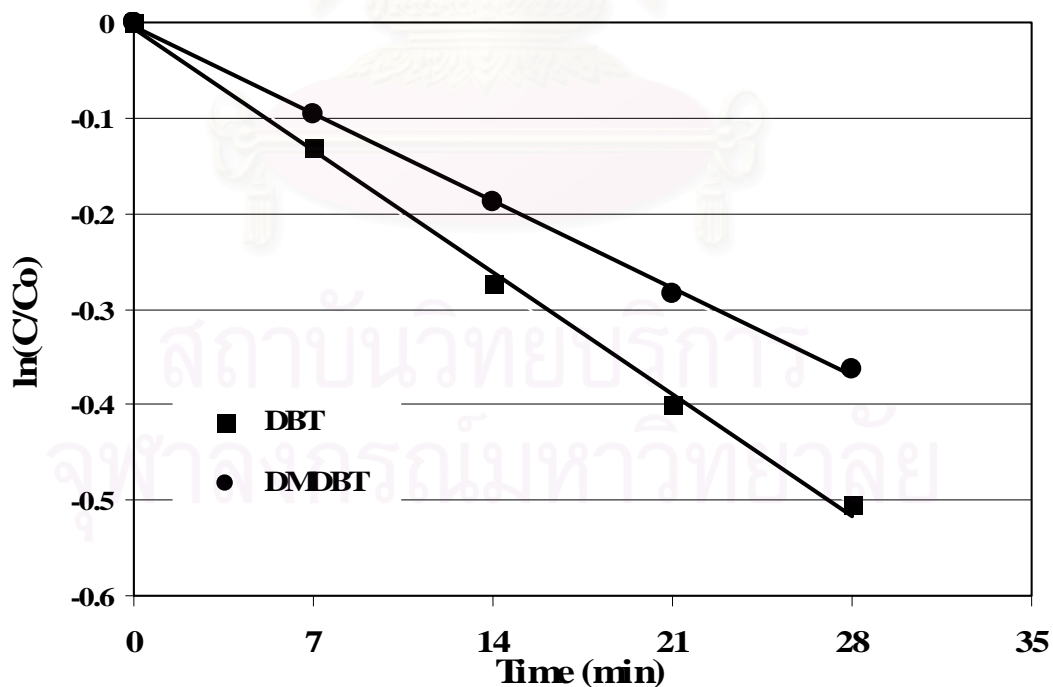
Figure 4.5 Pseudo first order kinetics of 4,6-DMDBT and DBT HDS over NiMo
sulfide catalysts (HDS conditions : 2.1 MPa, 300 °C).
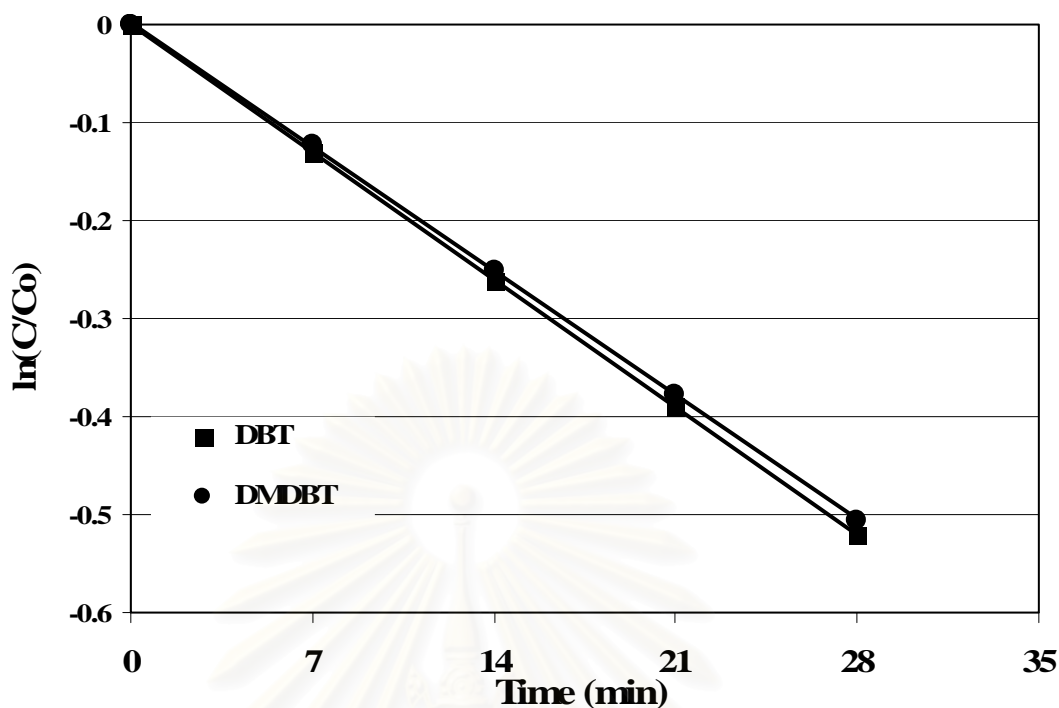
Figure 4.6 Pseudo first order kinetics of 4,6-DMDBT and DBT HDS over CoMo
sulfide catalysts (HDS conditions : 2.1 MPa, 300 $^{\circ}$C).

           4.2.3 Catalytic Activity and Selectivity for HDS of DBT and 4,6-DMDBT

        Table 4.2 shows kinetic data of 4,6-DMDBT and DBT HDS over the
Mo, NiMo and CoMo sulfide catalysts, respectively. Surprisingly, the activity of
MoS_2 catalyst for the HDS of 4,6-DMDBT was higher than that of DBT ($297.7*10^{-5}$
$s^{-1}g.cat^{-1}$ for 4,6-DMDBT and $166.3*10^{-5}$ $s^{-1}g.cat^{-1}$ for DBT). Although, for the
unsupported Mo sulfide catalyst, the rate constant of direct-desulfurization (DDS)
pathway and of hydrogenation (HYD) pathway were similar for the DBT HDS, the
rate constant of HYD pathway was clearly higher than that of DDS pathway for 4,6-
DMDBT HDS. The selectivity of HYD pathway was almost equal to one for HDS of
4,6-DMDBT as shown in Table 4.2. This result indicated that the unpromoted Mo
sulfide catalyst possessed high hydrogenation activity.

Table 4.2 Activity and Selectivity of Unsupported MoS_2, $NiMoS_2$ and $CoMoS_2$
Catalysts for Simultaneous HDS of DBT and 4,6-DMDBT.

S compounds	DBT			4,6-DMDBT		
Catalysts	MoS_2	$NiMoS_2$	$CoMoS_2$	MoS_2	$NiMoS_2$	$CoMoS_2$
k_1+k_2 10^{-5}/s gcat	166.3	1,290.0	1,316.4	297.7	920.5	1,289.5
k_1/k_2	0.9	0.4	0.1	170.4	8.8	8.1
$k_{1(HYD)}10^{-5}$/s gcat	78.2	381.9	111.3	296.0	826.2	1,147.7
$k_{2(DDS)}10^{-5}$/s gcat	88.1	908.1	1,205.1	1.7	94.3	141.7
Selectivity[a]						
S HYD	0.47	0.30	0.08	0.99	0.90	0.89
S DDS	0.53	0.70	0.92	0.01	0.10	0.11
Promoting effect[a]						
Total	1.0	7.8	7.9	1.0	3.1	4.3
On HYD	1.0	4.9	1.4	1.0	2.8	3.9
On DDS	1.0	10.3	13.7	1.0	54.3	81.6

[a] the detail for calculation is shown in appendix D

The NiMo and CoMo sulfide catalysts had higher activity than the Mo sulfide catalyst. As shown in Table 4.2, the promoting effect was around 8 for DBT HDS and 4 for 4,6-DMDBT HDS. Further detail in the calculation of promoting was presented in Appendix D. The activity of unsupported $CoMoS_2$ catalyst was higher than that of $NiMoS_2$ catalyst for the 4,6-DMDBT HDS but was almost the same for DBT HDS. For 4,6-DMDBT HDS, the promoter caused the increase in the DDS pathway selectivity while did not change the HYD pathway selectivity. For the DBT HDS, the promoter also gave the increase in the DDS pathway selectivity while decreased the HYD pathway selectivity. Therefore, over the promoted Mo sulfide catalysts, the DDS pathway became the main pathway for the HDS of DBT and HYD pathway was the predominant pathway for the 4,6-DMDBT HDS. From Table 4.2, it is obvious that the promoter not only increased the catalytic activity of the Mo sulfide catalyst but also changed the contribution on the DDS and the HYD pathways for both DBT and 4,6-DMDBT HDS. The promoting effect on the HYD pathway was much less than that on the DDS pathway for both 4,6-DMDBT and DBT HDS. It is

indicating that the promoting effect was essentially due to the enhancement of the rate of DDS pathway (or the C-S bond cleavage activity in general).

The rate constants of simultaneous HDS of DBT and of 4,6-DMDBT over the unsupported MoS_2, $NiMoS_2$ and $CoMoS_2$ catalysts and the commercial alumina supported NiMo (Cr424) and CoMo (Cr344) catalysts are shown in Figure 4.7. The activities of unsupported Mo based sulfide catalysts prepared from hydrothermal method were consistently higher than that of the commercial NiMo and CoMo alumina supported catalysts. More significantly, the HDS activity of the unsupported catalysts was five times that of the commercial catalysts for 4,6-DMDBT HDS. Although the unsupported Mo sulfide had lower activity for DBT HDS, it had higher activity for HDS of 4,6-DMDBT as compared to the commercial catalysts. This might be explained by the high hydrogenation activity of the Mo sulfide catalyst and the HYD pathway is the main pathway for the 4,6-DMDBT HDS. Both the unsupported and the commercial catalysts showed the same trend that the DDS pathway was the main pathway for DBT HDS and the HYD pathway was predominant pathway for HDS of 4,6-DMDBT. The activity of the $NiMo/Al_2O_3$ catalyst was higher than that of the $CoMo/Al_2O_3$ catalyst for the HDS of both sulfur compounds. Interestingly, the unsupported NiMo and CoMo sulfide catalysts had the same activity for DBT HDS while the CoMo sulfide catalyst had higher activity than NiMo sulfide catalyst for HDS of 4,6-DMDBT.

The ultimate goal is to synthesize catalysts for deep HDS that can remove the most refractory sulfur compounds such as alkyldibenzothiophenes. The results showed in Figure 4.7 suggested that the unsupported Mo based sulfide catalysts prepared by hydrothermal method has superiority performance to the commercial catalysts for the HDS of the refractory forms of sulfur compounds, especially 4,6-DMDBT. The improved hydrodesulfurization activity due to the higher surface area of the unsupported catalysts (about $20 - 30$ m^2/g higher than that of the commercial catalysts) is only a part of the reason for the superior performance of the unsupported Mo based sulfide catalysts. It is possible that the unsupported Mo based sulfide catalyst possesses an active phase that has superior intrinsic activity for HDS as compared to the commercial catalysts.
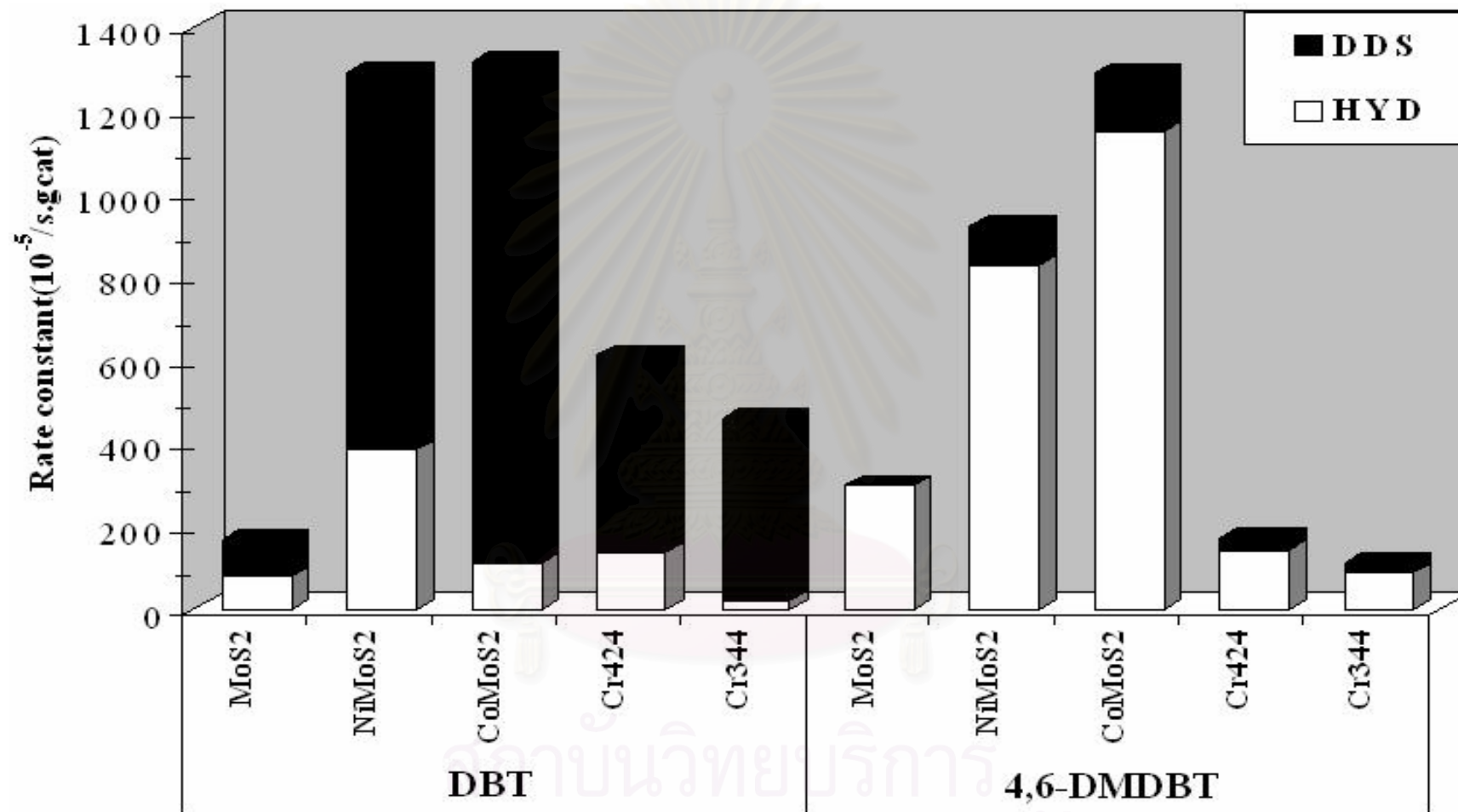
Figure 4.7 HDS rate constants for simultaneous HDS of DBT and 4,6-DMDBT over the unsupported MoS_2, $NiMoS_2$ and $CoMoS_2$ catalysts and commercial alumina-supported NiMoS (Cr424) and CoMoS (Cr344) catalysts.

The rate constant of 4,6-DMDBT HDS was higher than that of HDS of DBT over the Mo sulfide catalyst. This is mainly due to a very high rate of the hydrogenation (HYD) pathway over this catalyst (47% for DBT and 99% for 4,6-DMDBT as shown in Table 4.2.). It is probably explained by the higher adsorption capacity and stronger interaction of 4,6-DMDBT on the active site of this catalyst which can be seen from the selective adsorption results (Chapter 6). However, as generally observed, DBT was more reactive than 4,6-DMDBT on the unsupported CoMo and NiMo catalysts. In contract to other catalysts, 4,6-DMDBT was not much less reactive than DBT over all of unsupported catalysts (approximately 0.8 times compared with 2 - 6 times as reported in the literature) [160, 161]. From Table 4.2, it is clearly that the Co or Ni promoted Mo sulfide had higher activity than the unpromoted Mo sulfide for both DBT and 4,6-DMDBT HDS. It might be explained by an increased electron density not only at the Mo atoms but also at the S atom when promoter was added in the Mo sulfide as reported by Muller et al. [162]. Increasing the electron density at the S atom is expected to enhance both the activity of H_2 and the formation of more S vacancies which are believed to be the catalytic active sites [163].

The promoter also enhanced the rate constant of HYD and DDS pathways for both sulfur compounds. However, it increased the rate constant of the DDS pathway much more than that of the HYD pathway. This result is in agreement with the previous results showing that Ni or Co promotion favors the DDS pathway [45, 161, 164]. This effect might be explained by an increase in the basicity of the sulfur atoms shared between promoter Mo atoms [165]. If the C-S bond cleavage occurs through the attack of a hydrogen atom at the β position relative to the sulfur atom in the organic sulfur molecule by a sulfur anion acting as a basic site [161] as shown in Figure 4.8. Thus, an increase in the basicity would favor the C-S bond cleavage. This is in accordance with the fact that the NiMo and CoMo sulfdes are less stable than the molybdenum sulfide [59]: the sulfur atoms are less strongly bound to the metal in NiMo and CoMo sulfides, they are expected to be more basic than in molybdenum sulfide. This is also in agreement with the proposal that the promoter would increase the electron density of sulfur [163].
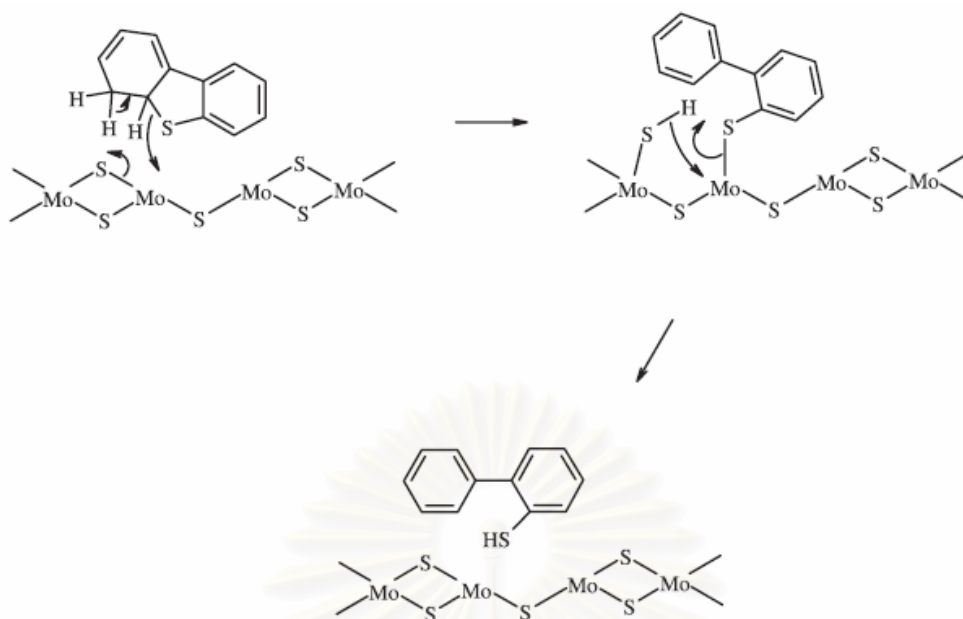
Figure 4.8 Mechanism of the C-S bond cleavage in DBT HDS via the DDS pathway [161].

Table 4.3 Turn Over Frequency (s^{-1}) of Three Unsupported Catalysts for DBT and 4,6-DMDBT on the Basis of Adsorption Capacity.

Catalyst	DBT	4,6-DMDBT
MoS_2	53	44
$NiMoS_2$	213	190
$CoMoS_2$	207	229

Table 4.3 shows the turn over frequency (TOF) of three unsupported catalysts for DBT and 4,6-DMDBT on the basis of adsorption site. The TOFs were calculated using the adsorption capacities of three catalysts (see Chapter 5) as a measurement of the number of active sites. The further detail of TOFs calculation is shown in Appendix F. The unpromoted Mo sulfide catalyst showed the lowest TOF values for both DBT and 4,6-DMDBT. The TOF values increased up to 4 times for the promoted catalysts, indicating that the active site of the promoted Mo sulfide catalyst is intrinsically more active than that of the unpromoted Mo sulfide catalyst. The promoter affects not only the number of active sites but also the activity of active sites of the unsupported Mo sulfide catalyst.

CHAPTER V

LIQUID-PHASE ADSORPTION OF DBT AND 4,6-DMDBT OVER UNSUPPORTED Mo BASED SULFIDE CATALYSTS

Much work has been conducted to understand the nature of the active sites on the surface of the Mo based sulfide catalysts. This knowledge has led to the design and synthesis of future catalysts. It is widely accepted that the coordinative unsaturated positions with the sulfur and/or anionic vacancies are associated with Mo and/or Co(Ni) ions on the edges of the MoS_2 slabs. It is responsible for the activity of catalysts in hydrodesulfurization [13, 134, 166-168]. However, quantitative measurement data of the number of active sites are still very limited in the literature. Then, the aim of this work is to study the adsorptive selectivity, capacity and mechanism for 4,6-DMDBT and DBT adsorption on the unsupported Mo, NiMo and CoMo sulfides in liquid phase system. This finding may offer a new alternative for studying the adsorption pattern of sulfur compounds on adsorption sites of the Mo based sulfide catalyst.

5.1 The Pennsylvania State University - Selective Adsorption for Removing Sulfur (PSU-SARS)

The adsorption experiments were conducted by using The Pennsylvania State University - selective adsorption for removing sulfur (PSU-SARS) which was recently proposed [1, 2, 107-111]. Figure 5.1 shows a simplified representation of PSU-SARS. The concept of PSU-SARS is that only sulfur compounds or some aromatics in liquid fuel can be adsorbed by adsorbents. For example, a liquid fuel with sulfur compounds of 0.4 wt%, aromatic of 15 wt% and saturated hydrocarbons of 85 wt% flow through adsorbent bed. More than 99 wt% liquid fuel without sulfur compound are not adsorbed and eluted out from the bed. All sulfur compounds and some of aromatics are adsorbed.
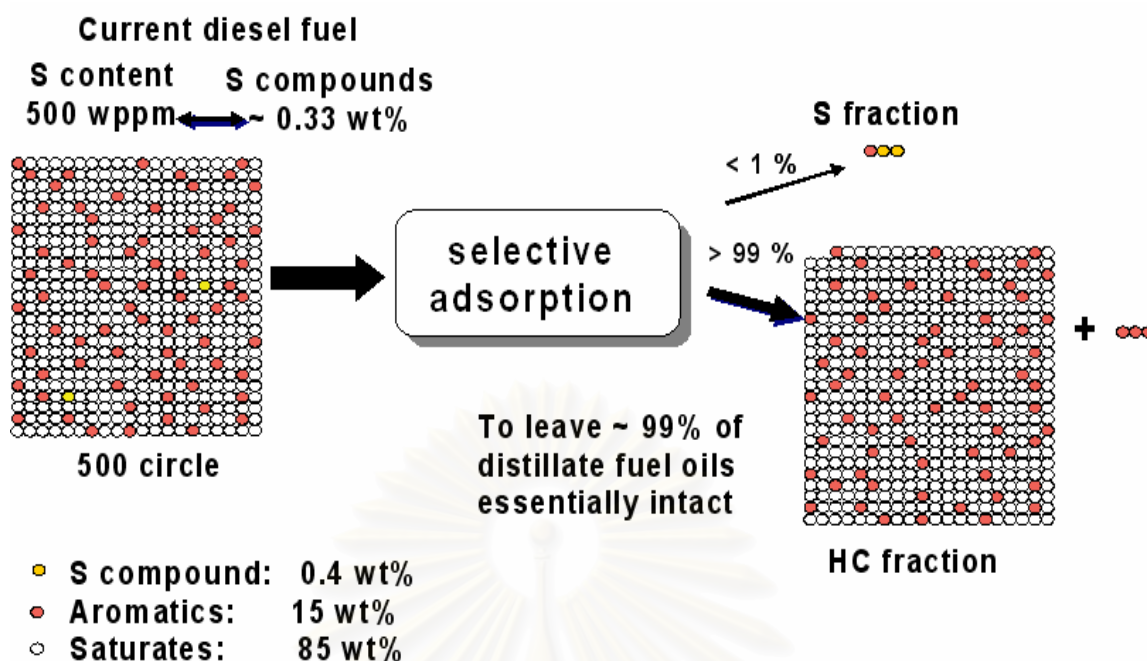
Figure 5.1 A simplified representation of PSU-SARS**.**

5.2 Measurement of Adsorption Capacities

In the liquid-phase adsorption, the model fuel was collected after passing the adsorbent bed and the concentration of each sulfur compound was measured. Then, the results were reported in plot of C/Co value (a ratio of the outlet concentration to the initial concentration in the model fuel) versus amount of treated fuel/catalyst weight called the breakthrough curve as shown in Figure 5.2. The important term are defined as follows :

The Breakthrough Point is the amount of treated fuel/catalyst weight that C/Co value starts higher than zero.

The Saturation Point is the amount of treated fuel/catalyst weight that C/Co value equal one.

The Saturation Capacity is the total adsorption capability of adsorbent that can adsorb each compound and make the C/Co value of each compound less than one.

The Breakthrough Capacity is the adsorption capacity of adsorbent that can adsorb each compound and make the C/Co value of each compound less than zero.

The replacement molecule is number of molecules of compound that have relatively lower adsorptive affinity than the subsequently breakthrough compounds and are replaced by higher adsorptive affinity compound.

The Net Capacity is the net adsorption capacity of adsorbent for each compound.

The adsorption capacity can be calculated as following equation. The further detail of the calculation of the adsorption capacity is shown in Appendix E.

The Breakthrough Capacity   =   Integration of area A   (5.1)

The Saturation Capacity   =   Integration of area (A+B)   (5.2)
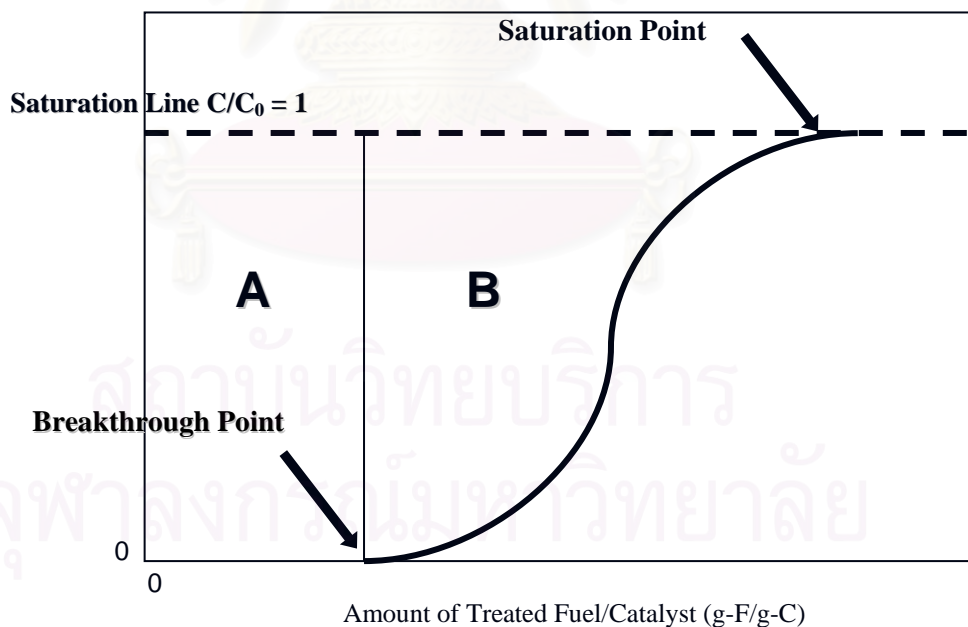
Figure 5.2 Breakthrough curve for the liquid-phase adsorption.

5.3 Liquid-Phase Adsorption over Unsupported Mo Sulfide

The liquid-phase adsorption of 4,6-MDBT and DBT over the unsupported Mo sulfide catalyst was conducted at ambient temperature and ambient pressure. The breakthrough curves of both sulfur compounds are shown in Figure 5.3. No detectable sulfur was found until 4.2 g of the treated fuel per gram of catalyst (g-F/g-C), indicating that both 4,6-DMDBT and DBT were adsorbed on the catalyst and removed from the liquid fuel. The first breakthrough compound was DBT with the breakthrough amount of 4.2 g-F/g-C. After breakthrough, The C/C_o value (a ratio of the outlet concentration to the initial concentration in the model fuel) for the DBT increased to over 1.0. After saturation point, the C/C_o value increased gradually to 1.12 and returned to 1.0 at the treated fuel amount of 25.2 g-F/g-C. When the treated fuel per gram of catalyst increased to 5.9 g-F/g-C, 4,6-DMDBT was detected in treated fuel. Then, the C/C_o value of 4,6-DMDBT increased slowly and reached saturation point at the treated fuel amount per gram of catalyst of 55.2.
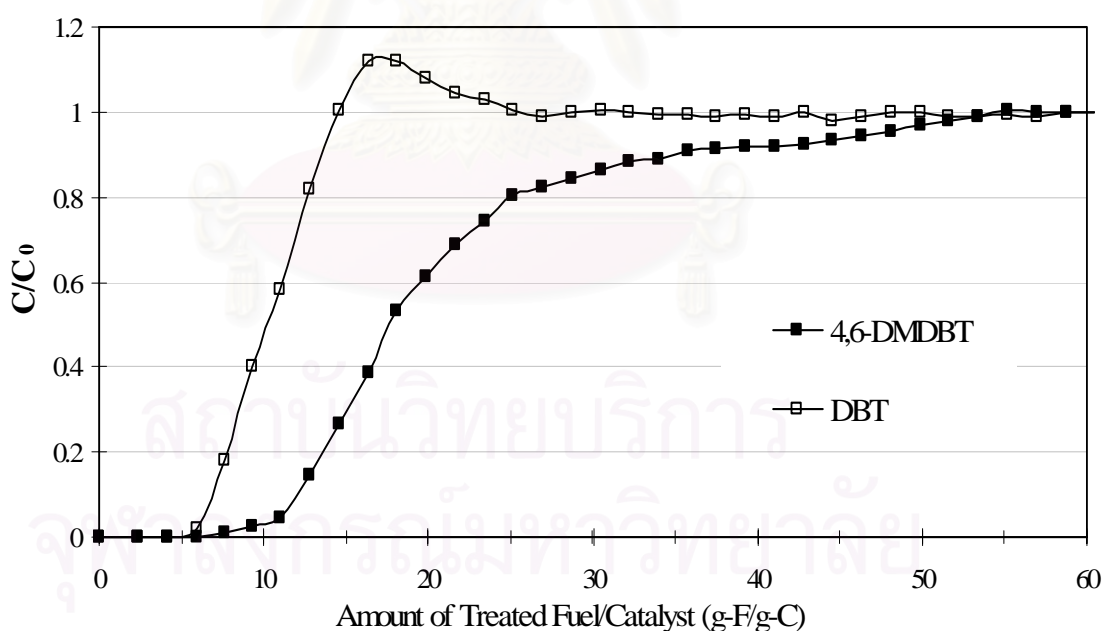
Figure 5.3 Breakthrough curves for the liquid-phase adsorption of 4,6-DMDBT and DBT at ambient temperature and pressure over the unsupported Mo sulfide catalyst.

The breakthrough, saturation and net capacities for both sulfur compounds were calculated and listed in Table 5.1 According to the breakthrough order, it is interesting that 4,6-DMDBT was adsorbed more than DBT over the unsupported Mo sulfide. The net capacity of 4,6-DMDBT was about 2.1 times higher than that of DBT.

Table 5.1 Adsorption Capacities, HDS Activities and Turn Over Frequency (TOF) of Three Unsupported Catalysts for DBT and 4,6-DMDBT on the Basis of GC-FID Analysis.

	DBT	4,6-DMDBT	Total
MoS_2			
Breakthrough (mmol/g)	0.014	0.019	0.033
Saturation (mmol/g)	0.033	0.068	0.101
Net (mmol/g)	0.032	0.068	0.100
HDS Activities (10^{-5}/s.g)	166	298	
TOF (s^{-1})	53	44	
$NiMoS_2$			
Breakthrough (mmol/g)	0.018	0.018	0.037
Saturation (mmol/g)	0.061	0.049	0.110
Net (mmol/g)	0.061	0.048	0.109
HDS Activities (10^{-5}/s.g)	1290	921	
TOF (s^{-1})	213	190	
$CoMoS_2$			
Breakthrough (mmol/g)	0.020	0.020	0.040
Saturation (mmol/g)	0.064	0.056	0.120
Net[a] (mmol/g)	0.064	0.056	0.120
HDS Activities (10^{-5}/s.g)	1316	1289	
TOF (s^{-1})	207	229	

5.4 Liquid-Phase Adsorption over Unsupported NiMo Sulfide

The breakthrough curves of 4,6-DMDBT and DBT over the unsupported NiMo sulfide catalyst are shown in Figure 5.4 No sulfur compound was detected when the treated fuel was less than 5.6 g-F/g-C. Unlike the unsupported Mo sulfide, 4,6-DMDBT and DBT broke through with the same breakthrough amount of the treated fuel. The breakthrough capacities for both compounds were 0.018 mmol/g. After breakthrough, the C/C_o value of 4,6-DMDBT increased reaching the maximum at 1.07 and then, returned to 1.0 at the treated fuel amount of 32.7 g-F/g-C. On the other hand, after breakthrough, the C/C_o value of DBT increased gradually and reached 1.0 at the treated fuel amount per gram of catalyst of 47.8. The net capacities of 4,6-DMDBT and DBT were 0.048 and 0.061 mmol/g, respectively.
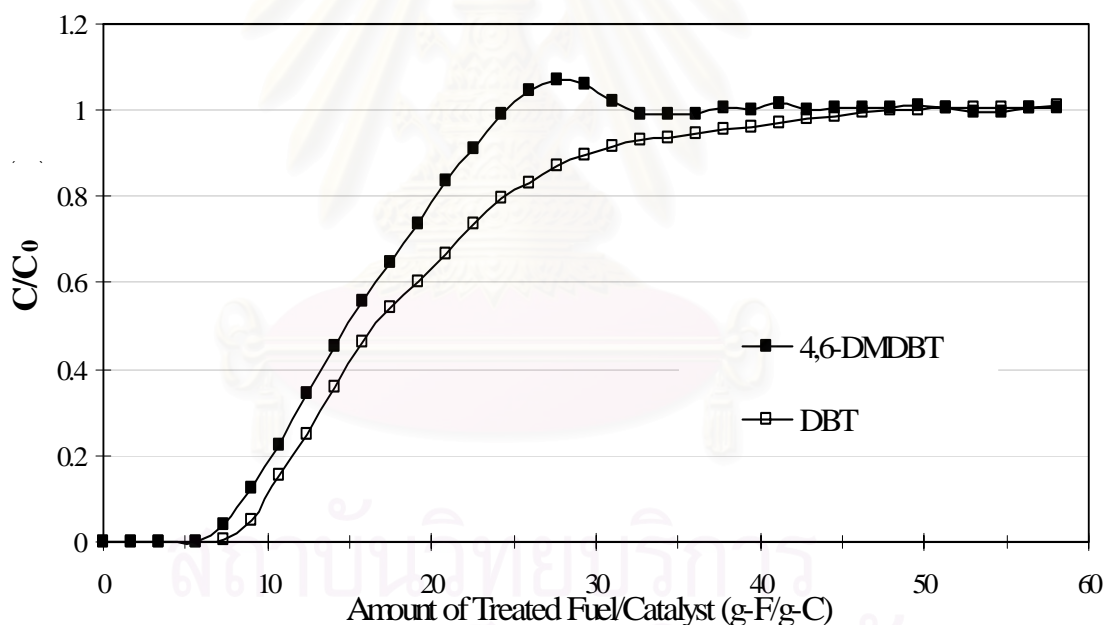
Figure 5.4 Breakthrough curves for the liquid-phase adsorption of 4,6-DMDBT and DBT at ambient temperature and pressure over the unsupported NiMo sulfide catalyst.

5.5 Liquid-Phase Adsorption over Unsupported CoMo Sulfide

The breakthrough curves of 4,6-DMDBT and DBT over the unsupported CoMo sulfide are shown in Figure 5.5. Similar to the unsupported NiMo sulfide, 4,6-DMDBT and DBT broke through with the same breakthrough amount of the treated fuel (6.1 g-F/g-C). After breakthrough, the C/C_o value of both 4,6-DMDBT and DBT increased gradually and synchronously reached 1.0 almost at the same amount of treated fuel (52.3 g-F/g-C). However, the breakthrough curve of DBT showed more inclined than that of 4,6-DMDBT indicating that the amount of DBT adsorbed was greater than that of 4,6-DMDBT over the unsupported CoMo sulfide. The net capacities of 4,6-DMDBT and DBT were 0.056 and 0.064 mmol/g, respectively.
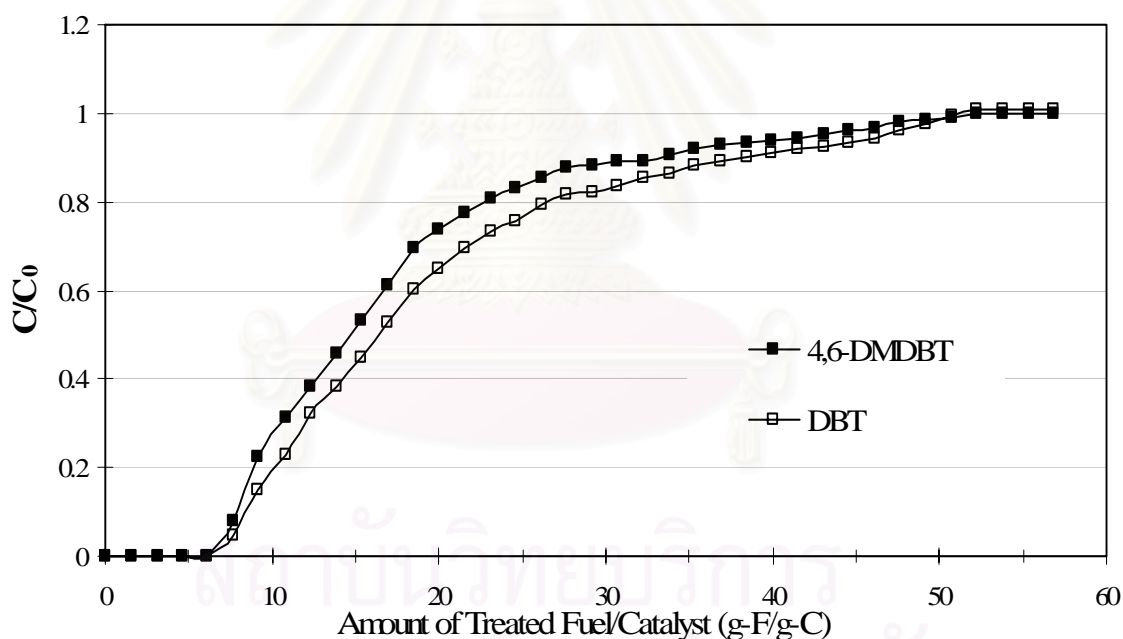
Figure 5.5 Breakthrough curves for the liquid-phase adsorption of 4,6-DMDBT and DBT at ambient temperature and pressure over the unsupported CoMo sulfide catalyst.

5.6 Comparison of Adsorption Capacity and Selectivity of Unsupported Mo, CoMo and NiMo Sulfides

Typically, adsorption performance depends on three important parameters.

1. Approachable surface
    -   Physical property
    -   Surface area
    -   Pore structure
    -   Size of adsorbate
2. Density of adsorption sites
    -   Chemical property
    -   Functional groups
    -   Coordinative unsaturated site (CUS)
3. Property of adsorption sites
    -    Chemical property
    -    Affinity force
    -    Adsorption equilibrium constant
    -    Heat of adsorption

The breakthrough curves of 4,6-DMDBT and DBT adsorption on the unsupported Mo, NiMo and CoMo sulfides showed different adsorptive selectivity for these different catalysts. The total adsorption capacities based on the catalyst weight increased in the order of CoMo > NiMo > Mo sulfide (as shown in Table 5.1). This order is consistent with the catalytic activity of these three catalysts. The unsupported Mo sulfide showed the highest adsorption capacity for 4,6-DMDBT and this capacity decreased after the addition of the promoter. On the other hand, the adsorption capacity for DBT increased when the Mo sulfide was promoted.
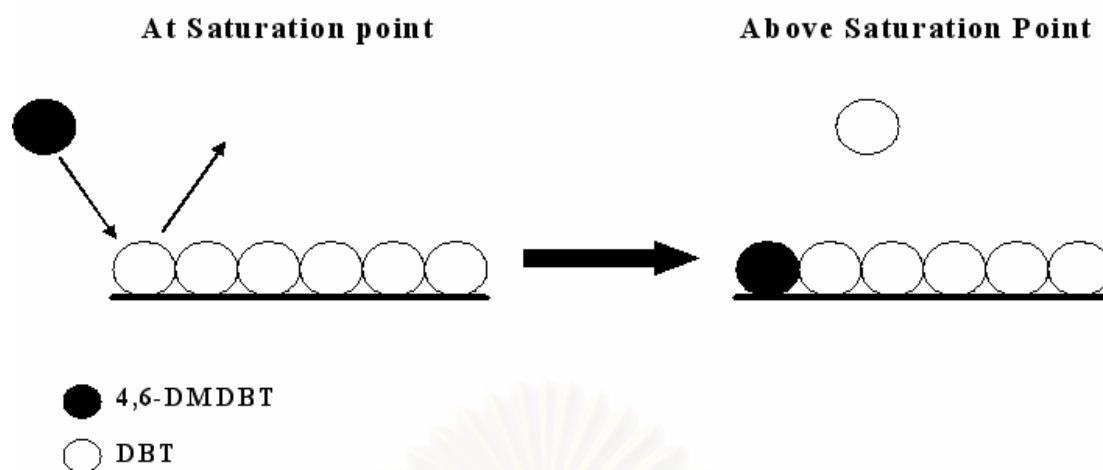
Figure 5.6 A simplified representation of displacement phenomena of DBT by 4,6-DMDBT over adsorption site of the unsupported Mo sulfide.

The adsorption of sulfur compounds on the unsupported catalysts is similar to the work previously reported by Kim et al. [169]. After passing through the saturation point ($C/C_o = 1$) the outlet concentration of some compounds increases continuously over its initial concentration in the model fuel reaching the maximum value and then, decreases gradually to the initial value. This phenomenon resulted from a partially reversible adsorption of that compound. Another reason is that the compounds have relatively lower adsorptive affinity than the subsequently breakthrough compounds, resulting in at least partly replacement of the compounds with lower adsorptive affinity by the compounds with higher adsorptive affinity. Figure 5.6 showed a simplified representation of displacement phenomena of DBT by 4,6-DMDBT over adsorption site of the unsupported Mo sulfide. At the saturation point, all adsorption sites are occupied by DBT. Since the interaction between 4,6-DMDBT and adsorption site has stronger than that of DBT, 4,6-DMDBT can kick some DBT out of the adsorption site and make an interaction with that site. This can be clearly seen from the C/C_o value is above the saturation point. As shown in Figure 5.3, the area between the breakthrough curve of the compound and line $C_t/C_o = 1$ before the saturation point represents the amount of the adsorbed molecules, while the area between the breakthrough curve and line $C_t/C_o = 1$ after the saturation point represents the amount of the replaced molecules. Comparison of these two areas provides further information about the competitive adsorption of different species on the adsorbents. The net adsorptive capacities for each compound over the three

adsorbents were calculated by subtracting the amount of the replaced molecules from the saturation capacity, and the results are listed in Table 5.1. The detail of capacity calculation is further described in Appendix F.

The adsorption of sulfur compounds on the unsupported Mo sulfide showed that 4,6-DMDBT can be adsorbed 2.1 times higher that DBT over Mo sulfide (Table 5.1). A part of the adsorbed DBT can be replaced by 4,6-DMDBT. This result indicates that the interaction of 4,6-DMDBT on the adsorption site is stronger than that of DBT. It is interesting to note that the methyl groups on the aromatic rings showed a significant and positive effect on the adsorption selectivity of Mo sulfide indicating that the methyl groups enhance the adsorption affinity or interaction through increasing the electron density of the aromatic rings since the methyl substitutent leads to the increasing of π - electron density on the aromatic rings [47]. The adsorptive selectivity agrees very well with HDS reactivity of 4,6-DMDBT and DBT on the unsupported Mo sulfide. Higher adsorption capacity and stronger interaction of 4,6-DMDBT on active site probably cause the HDS reactivity of 4,6-DMDBT higher than that of DBT over the unsupported Mo sulfide catalyst as shown in Figure 5.6.

For the unsupported NiMo sulfide, the adsorptive selectivity of DBT was higher than that of 4,6-DMDBT which reversed to the adsorptive selectivity order of the Mo sulfide. However, the replacement phenomenon was also observed in this catalyst. The amount of DBT adsorbed was greater than that of 4,6-DMDBT and a part of adsorbed 4,6-DMDBT can be replaced by DBT. Unlike on the Mo sulfide, the selective order showed that methyl groups on the 4- and 6- position of DBT strongly inhibit the adsorption of 4,6-DMDBT on NiMo sulfide. These results indicate that a direct interaction between the sulfur atom and the adsorption site on the NiMo sulfide could play an important role in the selective adsorption of DBT and 4,6-DMDBT and the two methyl groups block the approach of the sulfur atom to the adsorption site.

Like adsorption on the NiMo sulfide, DBT showed slightly higher adsorption capacity than 4,6-DMDBT on the unsupported CoMo sulfide as shown in Table 5.1. Interestingly, both DBT and 4,6-DMDBT reached the saturation point almost at the same amount of treated fuel and the replacement phenomenon was not observed. This result suggested that the methyl groups on the aromatic ring shows some negative effect to the adsorption of the sulfur compounds on the CoMo sulfide and this effect is less strong than that on the NiMo sulfide. This adsorption selectivity might explain HDS result that the HDS reactivity of DBT and 4,6-DMDBT was not much different (Table 5.1).

CHAPTER VI

HYDRODESULFURIZATION OF LIGHT CYCLE OIL USING UNSUPPORTED Mo BASED SULFIDE CATALYSTS

Light cycle oil (LCO) is a by-product of the fluid catalytic cracking process (FCC) in a petroleum refinery. The FCC process enhances gasoline production and the increasing demand for gasoline translates into increased production of LCO. Traditionally, LCO has been used as a blend-stock for home heating oil, industrial fuel oil, and diesel fuels. However, the increasing spread of natural gas in recent times for, both, heating homes and producing power has reduced demand for fuel oil and, therefore, LCO [170]. Simultaneously, diesel demand is outpacing that of other transportation fuels [171]. Therefore, refiners are now increasingly using more LCO as a blend-stock for the diesel pool. LCO has a low cetane index (typically 15–20), sulfur content as high as 3 wt.%, and 50–80 wt.% aromatics [172]. Besides its high sulfur content, the HDS of LCO is further complicated because its sulfur is distributed in the form of highly refractory dibenzothiophenes [173].

While the increasing stringency of sulfur specifications has motivated intensive HDS research, there have been few studies on HDS of real feedstocks, such as LCO. Most studies have relied on mixtures of model compounds to simulate real feedstocks [174-178]. For research on HDS of real feed-stocks, the hydrotreated or low sulfur LCO [179-185] or feedstock blends with LCO as one of the components [186, 187] were used. Some studies on HDS of typical high-sulfur content LCO had different point of view. Vanrysselberghe and Froment [188] studied the HDS of LCO over the commercial CoMo/Al$_2$O$_3$ catalyst to develop kinetic model of individual sulfur compounds. Shih et al. [189] studied the HDS of LCO over the commercial CoMo/Al$_2$O$_3$ catalyst to determine reactor temperatures for production of diesel with 500 wppm sulfur. However, there is only few research on the HDS of LCO in the literature.

From the earlier work, the activity and selectivity of unsupported Mo based sulfide catalysts strongly depended on the catalyst preparation conditions and types of promoters. The aim of the work is to study the HDS of LCO using the promoted and unpromoted Mo sulfide catalysts prepared by the hydrothermal method.

6.1 Properties of Light Cycle Oil

The LCO sample used in this study was of a particularly poor quality in terms of sulfur content and density. Table 6.1 presents the physical properties of LCO feedstock.

Table 6.1 Physical Properties of the LCO Sample

Property	Value
Sulfur content (ppm)	17,975
Nitrogen content (ppm)	535
API gravity @ 60 ^{o}F	10.3
Specific gravity (gm/ml)	0.9979
ASTM distillation (wt%)	
Initial boiling point (^{o}F)	294
5% (^{o}F)	437
10% (^{o}F)	479
20% (^{o}F)	520
30% (^{o}F)	534
40% (^{o}F)	555
50% (^{o}F)	574
60% (^{o}F)	590
70% (^{o}F)	614
80% (^{o}F)	646
90% (^{o}F)	677
95% (^{o}F)	698
Final boiling point (^{o}F)	745

All components of LCO were analyzed by GC- FID and the sulfur compounds were detected by GC-PFPD. The GC-FID and GC-PFPD chromatograms of LCO illustrate the complexity of the real fuel samples and the overlapping of hydrocarbons with sulfur compounds as shown in Figure 6.1. All sulfur species in LCO detected by GC-PFPD were identified as shown in Figure 6.2. The LCO contains the wide range of sulfur compounds, two-ring sulfur compounds, BT (benzothiophene) and three-ring sulfur compounds, DMDBT (dimethyldibenzothiophene). Most sulfur compounds were thiophenic, benzothiophenic and dibenzothiophenic in nature with different numbers of substituent chains. Major compounds are C_2-BT (specifically 2,3-DMBT) and C_1-DBT (specifically 4-MDBT) and 4,6-DMDBT, one of the most refractory sulfur compounds, is contained, as well although its amount is relatively lower than the major compounds. As shown in Figure 6.2, the retention times of different sulfur compounds correlate with their molecular weight, with short retention times for compounds of low molecular weight and long retention times for compounds of high molecular weight. Table 6.2 presents the distribution of sulfur compounds with the retention time. All the sulfur compounds are classified in 12 groups based on molecular weight.

Depauw and Froment [173] reported a detailed molecular analysis of the sulfur components in LCO sample using GC-AED and 40% of the feedstock's sulfur was present in the form of highly refractory DBTs. The results of Depauw and Froment are summarized in Table 6.3.
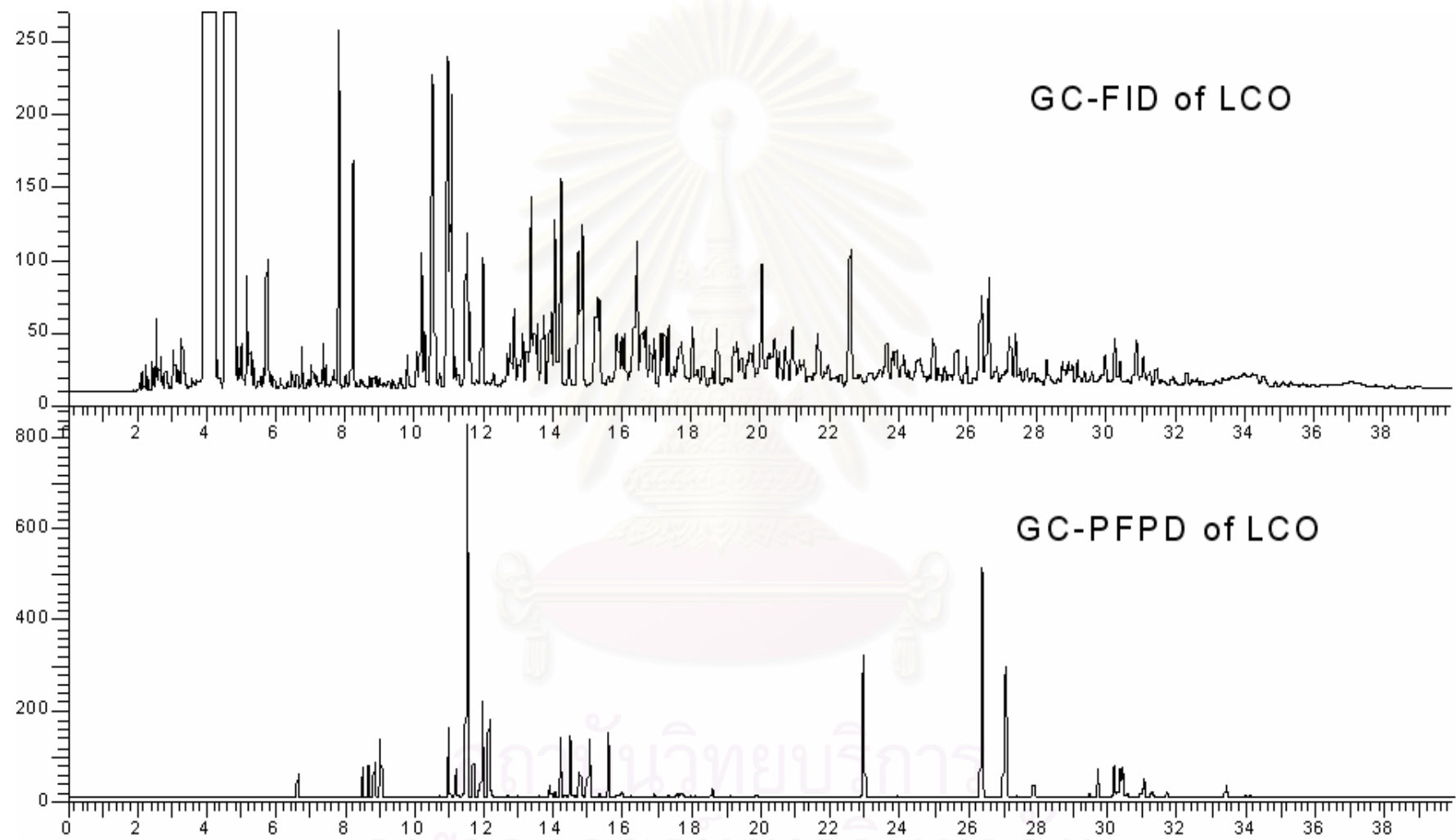
Figure 6.1 GC-FID and GC- PFPD chromatograms of LCO.
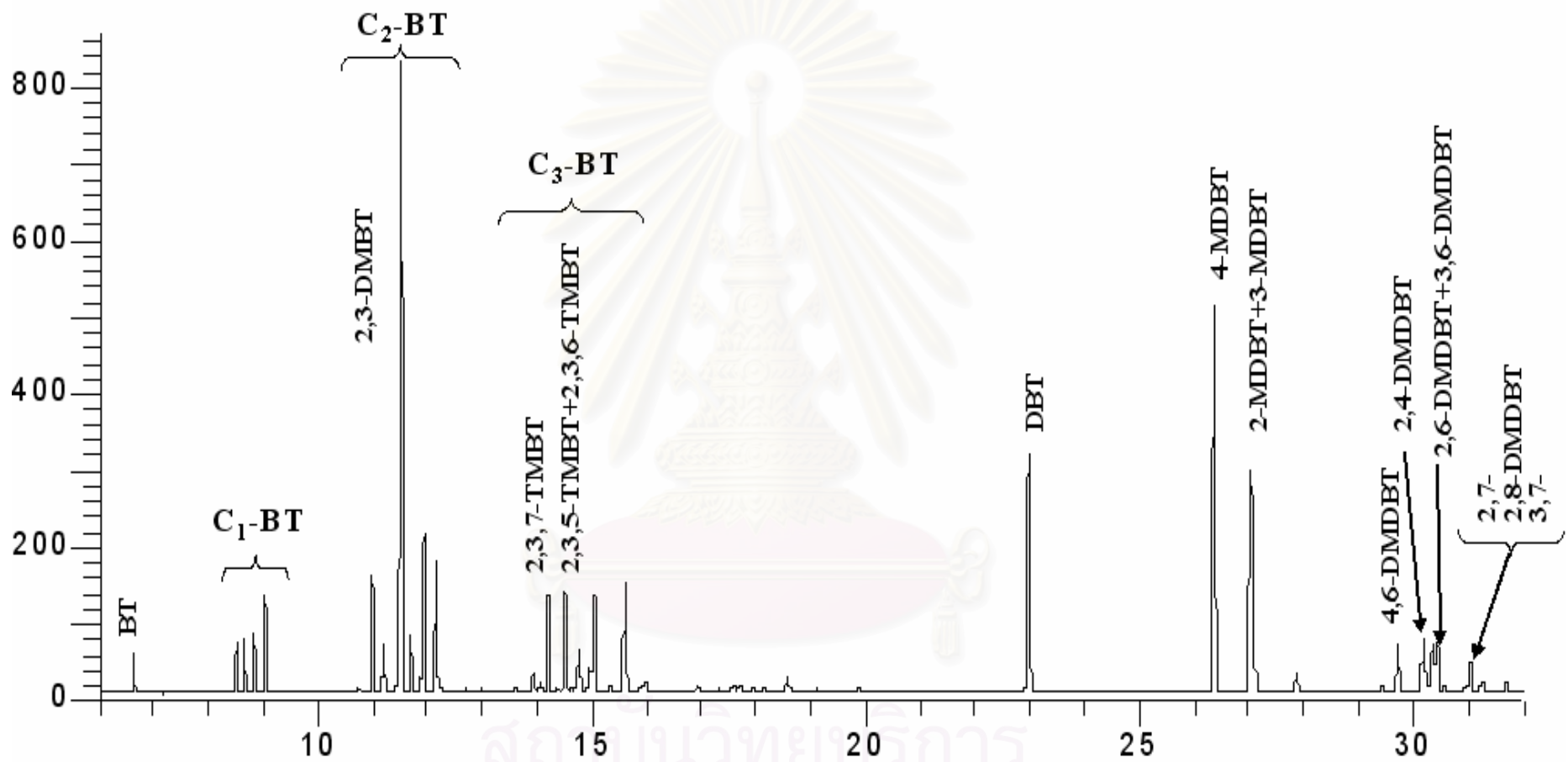
Figure 6.2 Sulfur species in LCO (the prefix Cx stands for the substituent where x indicates the number thereof).

Table 6.2 Retention Time of Various Sulfur Compounds in LCO

Group	Retention Time (min)	Possible sulfur compounds
1	6.6	benzothiophene (BT)
2	8.5-9.2	methylbenzothiophene (C_1-BT)
3	10.8-12.2	C_2-benzothiophene (C_2-BT)
4	13.6-16.2	C_3-benzothiophene (C_3-BT)
5	23	dibenzothiophene (DBT)
6	26.4	4-methyldibenzothiophene (4-MDBT)
7	27	2-methyldibenzothiophene(3-MDBT) + 3-methyldibenzothiophene (3-MDBT)
8	29.8	4,6-dimethyldibenzothiophene (4,6-DMDBT)
9	30.2	2,4-dimethyldibenzothiophene (2,4-DMDBT)
10	30.4-30.6	2,6-dimethyldibenzothiophene (2,6-DMDBT)+ 3,6-dimethyldibenzothiophene (3,6-DMDBT)
11	31-31.4	2,7-dimethyldibenzothiophene (2,7-DMDBT)+ 2,8-dimethyldibenzothiophene (2,8-DMDBT)+ 3,7-dimethyldibenzothiophene (3,7-DMDBT)
12	>32	Other unidentified heavier sulfur compounds

Table 6.3 Distribution of Various Sulfur Compound Classes in LCO

No.	Type of sulfur compound [a]	Sulfur (%)
1	C_0-benzothiophene (BT)	1.5
2	C_1-BT	10.2
3	C_2-BT	19.1
4	C_3-BT	16.2
5	C_{4+}-BT	13.1
6	C_0-DBT	3.3
7	C_1-DBT	12.5
8	C_2-DBT	11.8
9	C_{3+}-DBT	12.4

[a] The prefix Cx stands for substituents on the parent sulfur compound with x indicating the number thereof.

6.2 HDS of LCO over Unsupported Mo Based Sulfide and Commercial Catalysts

The HDS of LCO was performed to investigate whether the unsupported Mo based sulfide catalysts prepared by the hydrothermal is effective for real feedstock. The two commercial catalysts were also used for comparison. Table 6.4 shows total sulfur concentration of LCO before and after HDS. The total sulfur concentrations were determined using an Antek 9000S Total Sulfur Analyzer. LCO has very high sulfur content of 17,975 ppm which was decreased after treating over all catalysts. MoS_2 catalyst shows lowest activity. Treated LCO with $NiMoS_2$ and $CoMoS_2$ have quite the same amount of sulfur content which are much lower than that of treated LCO with two commercial catalysts. These results of real feed-stock confirm the previous results of model fuel that the unsupported Mo based sulfide catalysts prepared by the hydrothermal method have superior activity than commercial catalysts.

Table 6.4 Total Sulfur Content and % S Removal in LCO and Treated LCO over
Unsupported Mo Based Sulfide Catalysts and Commercial Catalyst.

Fuel	Catalyst	Total sulfur concentration (ppm)	% S Removal (%)
LCO	-	17,975	0.0
Treated LCO	MoS_2	13,709	23.7
Treated LCO	$CoMoS_2$	5,261	70.7
Treated LCO	$NiMoS_2$	5,443	69.7
Treated LCO	Cr344	8,616	52.1
Treated LCO	Cr424	7,938	55.8

(HDS Conditions : 350 ^{o}C 2.8 MPa 30 mins)

In order to examine the activity of catalysts, each sulfur compounds in LCO and treated LCO were analyzed by GC-PFPD. The chromatograms of LCO and treated LCO over MoS_2 are shown in Figure 6.3. The chromatograms for treated LCO over $CoMoS_2$, $NiMoS_2$, Cr344 and Cr424 are also shown in Figure 6.4. All chromatograms with complex peaks show the overlapping peak of many sulfur compounds in LCO. Thus, the determination of each sulfur compound concentration is not accurate enough for quantitative analysis. Table 6.5 presents the simple comparison of each group of sulfur compounds classified in Table 6.2. Table 6.5 also illustrates the GC-PFPD peak area of each group of sulfur compounds in LCO and treated LCO over unsupported catalysts and commercial catalysts.

From Figure 6.3 and 6.4, in all of treated LCO, some sulfur species, such as BT and C_1-BT are completely removed while others sulfur compounds are still present. The high concentration of C_2-BT in treated LCO over MoS_2 was present. The concentration of C_2-BT in treated LCO over other catalysts especially $CoMoS_2$ was detected in low amount. DBT and its derivative were present at high amount in treated LCO over all catalysts. However, for HDS of LCO, the activity of unsupported Mo based sulfide catalysts is consistently higher than that of the commercial catalyst. More significantly, the unsupported Mo based sulfide catalyst continues to be more active than the commercial catalyst for the HDS of alkyl-dibenzotiophenic sulfur compounds in LCO as seen from the lower GC-PFPD peak of alkyl-dibenzotiophenic sulfur compounds in treated LCO over the unsupported Mo based sulfide catalyst. The higher activity of the unsupported Mo based sulfide catalyst for the HDS of alkyl-dibenzotiophenic sulfur compounds is remarkable because LCO has a high concentration of both mono and diaromatics which are strong inhibitors of conventional HDS catalysts [13, 190]. It is known that aromatics and diaromatics inhibit HDS catalysts due to the strong adsorption on active sites responsible for hydrogenation activity. It is plausible that the polycyclic aromatics in LCO are adsorbed on the hydrogenation sites of the commercial catalyst and diminish its activity for the HDS of alkyl-dibenzotiophenic sulfur compounds. In contrast, the aromatics cause little inhibition of the hydrogenolysis route. Therefore, the high activity of the unsupported Mo based sulfide catalyst for the HDS of alkyl-dibenzotiophenic sulfur compounds in LCO is attributed to the different pathway preferences over each catalyst.

While the unsupported Mo based sulfide catalysts prepared by the hydrothermal method has distinct advantages catalysts have reduced absolute activities of catalysts for the HDS of PASCs in LCO was reduced compared to its activities for the HDS of the pure PASCs in model fuel. This is due to the global inhibition of the catalysts by aromatics and other non-sulfur components in LCO. Light cycle oil, typically, contains 50–80% aromatics with diaromatics content of 30–50% [172].
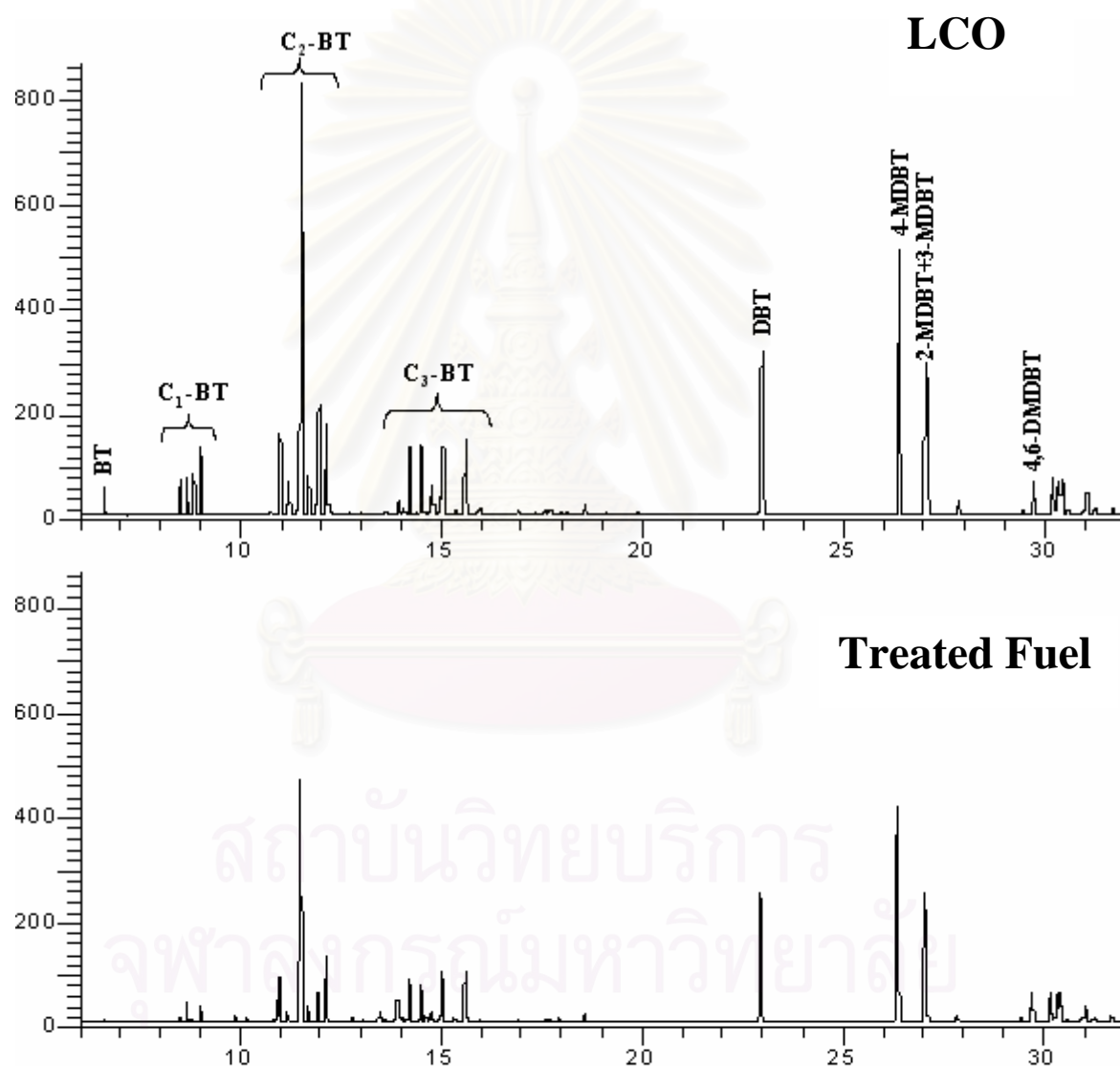
Figure 6.3 GC-PFPD chromatograms for LCO and treated LCO over MoS_2.
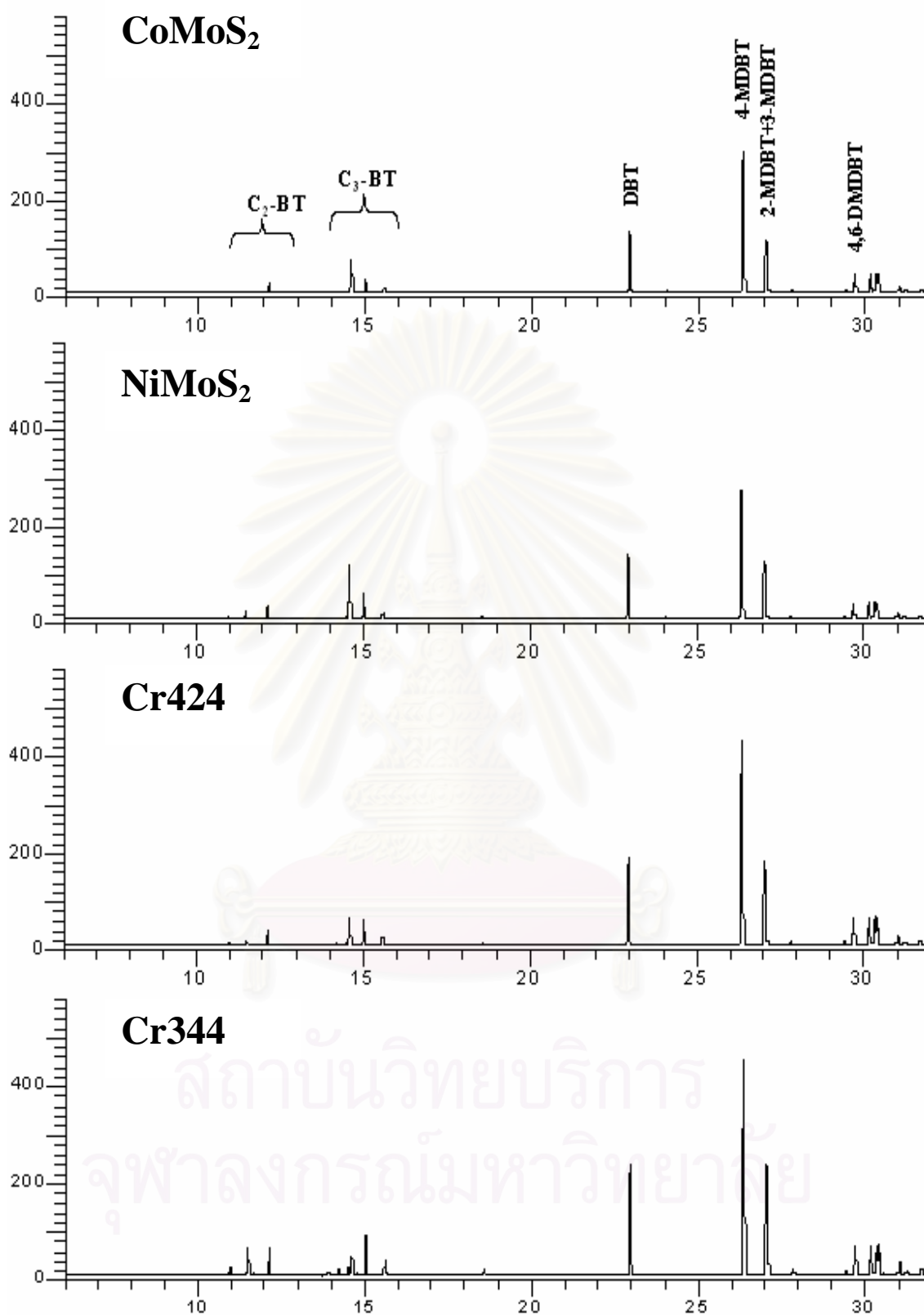
Figure 6.4 GC-PFPD chromatograms for treated LCO over CoMoS$_2$, NiMoS$_2$, Cr424 and Cr344.

Table 6.5 GC-PFPD Peak Area of Sulfur Compounds in LCO and Treated LCO

Catalyst	GC-PFPD Peak area (uV.S)					
	LCO	MoS$_2$	CoMoS$_2$	NiMoS$_2$	Cr424	Cr344
BT	84932.0	10702 (87.4)	0 (100.0)	0 (100.0)	0 (100.0)	0 (100.0)
C1-BT	822840.0	204922 (75.1)	0 (100.0)	0 (100.0)	0 (100.0)	0 (100.0)
C2-BT	4239075.0	2243705 (47.1)	58716 (98.6)	127926 (97.0)	349852 (91.7)	120870 (97.1)
C3-BT	2292215	1534814 (33.0)	334635 (85.4)	548443 (76.1)	609192 (73.4)	396846 (82.7)
DBT	1104608	812136 (26.5)	425546 (61.5)	449158 (59.3)	783037 (29.1)	623803 (43.5)
4-MDBT	1736594	1467831 (15.5)	1031004 (40.6)	990223 (43.0)	1638101 (5.7)	1517451 (12.6)
2-MDBT+3-MDBT	1619984	1354868 (16.4)	112190 (49.9)	142190 (48.0)	1277800 (21.1)	980686 (39.5)
4,6-DMDBT	209444	194745 (7.0)	111692 (46.7)	133720 (36.2)	205055 (2.1)	204146 (2.5)
2,4-DMDBT	270479	221903 (18.0)	131100 (51.5)	138509 (48.8)	232715 (14.0)	206518 (23.6)
2,6-DMDBT +3,6-DMDBT	539897	445987 (17.4)	273591 (49.3)	287240 (46.8)	488112 (9.6)	447112 (17.2)
2,7-DMDBT +2,8-DMDBT + 3,7-DMDBT	204575	122443 (40.1)	54826 (73.2)	63639 (68.9)	97263 (52.5)	97864 (52.2)

* % Peak area reduction is in the parenthesis.

CHAPTER VII

CONCLUSIONS AND RECOMMENDATIONS

7.1 Conclusions

The major conclusions of this study can be highlight in the following list and further elaborated below.

- ATTM is a promising Mo sulfide precursor for preparation unsupported HDS catalysts through hydrothermal method. The unique feature of unsupported Mo based sulfide catalysts is its superiority over the commercial catalysts and high activity for refractory S compound

- Organic solvent addition improved dispersion and increase surface area as well as increased catalytic activity

- There is strong synergetic effect of Ni and Co on the Mo sulfide catalyst.

- Effect of Promoter to Mo Sulfide

    Properties

    - Decreases the metal sulfur bond strength

    - Inhibits the growth of catalyst particle

    - Decreases surface area and pore volume

    HDS activities

    - Increases HDS activity

    - Changes catalytic activities of DDS and HYD pathways

    - Show distinctly different trend compared to comm. catalysts

- Liquid phase adsorption provide insights into the differences in behavior between MoS_2 and $CoMoS_2$/ $NiMoS_2$, and between DBT and 4,6-DMDBT and generate clear evidence for the number of active site and for correlating activity of different catalysts.

- HDS of LCO demonstrate that unsupported Mo based sulfide catalysts have superior activity than commercial catalysts for real refractory feed stock which consistent with result of model feed stock in the order of catalytic activity.

The study of unsupported sulfide catalyst is a promising research route for developing better hydrotreating catalysts. Hydrothermal preparation of transition-metal sulfides is particularly interesting, because this provides a highly active catalyst and does not require the presulfidation step. The unsupported NiMo sulfide catalysts synthesized from ATTM by the hydrothermal method exhibited the excellent catalytic activity for the simultaneous HDS of DBT and 4,6-DMDBT. For the unsupported NiMo sulfide catalysts prepared in this study, the HYD pathway was predominant as compared with the DDS pathway in the HDS of DBT as well as the HDS of 4,6-DMDBT. The unsupported NiMo sulfide catalysts present notable synergy in the HDS reaction. The maximum synergy in the HDS of DBT and 4,6-DMDBT appeared over catalyst with the Ni/(Mo+Ni) ratio close to 0.5.

The preparation conditions (H_2 pressure and temperature) have a significant effect on the HDS activity of unsupported NiMo sulfide catalyst. Although both high H_2 pressure and high temperature lead to highly active catalysts, the selectivity of NiMo sulfide catalyst is also affected in different way. Unsupported NiMo sulfide catalysts prepared at high H_2 pressure became less active for the HYD pathway, but more active for the DDS pathway. However, the NiMo catalyst prepared at high preparation temperature became less active for the DDS pathway but more active for the HYD pathway for both DBT and 4,6-DMDBT HDS. An organic solvent addition in catalyst preparation was effective for forming the high surface area and high active catalysts. This suggests that the organic solvent help to disperse ATTM and $Ni(NO_3)_2$ resulting in fine molecular dispersion of precursor molecules in aqueous solution isolated by organic solvent. Probably, the hydrothermal method with suitable conditions leads to very small (nano) size of Mo sulfide clusters and more Ni atoms could possibly incorporate into smaller Mo sulfide crystallites and form more active phase.

The unpromoted and promoted Mo sulfide (unsupported) catalysts prepared by hydrothermal synthesis method have different properties and different HDS performance. Unsupported Mo sulfide catalyst showed high surface area without using any conventional supported material. The addition of promoters (Ni or Co) resulted in significant decrease in surface area and pore volume of unsupported Mo sulfide. These catalysts have higher content of Ni or Co as compared to conventional

supported catalysts. A part of the promoters may not be coordinated in the Mo sulfide phases, but present as Co sulfide and Ni sulfide, as revealed by XRD. However, the addition of promoters generated the increase in curvature of MoS_2 slabs and the decrease in slab length on the basis of XRD and HRTEM analysis. This is probably because Ni or Co may be located on edge of MoS_2 structure and prevents the growth (or aggregation) of crystallite. The TPR also showed that the addition of promoter to the unsupported Mo sulfide catalyst causes a significant downward shift of the first peak reduction temperature which suggests the decrease in the metal sulfur bond energy. The liquid-phase adsorption of 4,6-DMDBT and DBT showed the different sulfur compound adsorption capacity, selectivity and possible adsorption mechanism over these three different sulfides. 4,6-DMDBT had higher adsorption capacity and stronger interaction with the active site than DBT over the unsupported Mo sulfide. This might explain the interesting HDS result that 4,6-DMDBT showed higher HDS reactivity than DBT over the MoS_2 catalyst. The HDS results indicated that the promoter not only increased the catalytic activity of the unsupported Mo based sulfide catalyst but also changed the contribution of the DDS and of HYD pathways. The promoter affects both the active sites number and the activity of active sites of the unsupported Mo sulfide catalysts.

The HDS of LCO was comparatively studied over commercial Al_2O_3 supported and unsupported Mo based sulfide catalyst prepared by the hydrothermal method. The unsupported Mo based sulfide catalyst demonstrates consistently higher activity for the HDS of the refractory alkyl-dibenzothiophenic sulfur compounds. Through comparative examination, the presence of aromatics in LCO appears to inhibit the HDS of the substituted DBTs. The findings of this work validate hypothesis of this research that the unsupported Mo based sulfide catalyst with its nano size particles and high activity is a promising HDS catalyst capable of hydrodesulfurization of the refractory sulfur compounds for exploring new hydroprocessing catalysts.

7.2 Recommendations

In this work unsupported Mo, CoMo and NiMo sulfide catalysts as new hydrotreating catalysts was explored. Some issues have arisen from this exploration and warrant further research are as follows:

1. Influence of nitrogen compounds on deep HDS over unsupported Mo based sulfide catalysts.

The removal of sulfur from liquid fuel to such deep level as 15 ppm will require knowledge of the influence of nitrogen compounds because the reactivity of nitrogen-containing hetero-compounds is much lower than that of PASCs [191]. Therefore, nitrogen compounds are presented in appreciable even a very low level and could significantly influence the deep HDS of PASCs. For the future research work, the effect of nitrogen compounds on catalytic activity should be investigated.

2. Effect of nobel metal (Pd, Pt and Ru) added to unsupported Mo based sulfide catalysts on HDS activity.

Transition-metal sulfides of the second and third rows (Pd, Pt and Ru) possess high activity in hydrodesulfurization. The majority of literature data confirmed that the modification of conventional Mo or CoMo/Al_2O_3 systems by noble metals led to a higher activity HDS. Therefore, newly developed unsupported Mo sulfide catalysts with promoters should be modified further with noble metal additive (Pd, Pt and Ru).

3. Deactivation of unsupported Mo based sulfide catalysts.

It is well known that the deactivation of the industrial hydro-processing catalysts is one of the major problems in the hydro-treating process. The deactivation of catalysts affects the catalyst lifetime, the catalytic activity and the product selectivity. During HDS, several complex deactivation processes occur and more studies are needed to understand the factors influencing catalysts deactivation.

4. Study the ways to make structured forms or extrudates of finely dispersed unsupported sulfide particles for fixed-bed catalytic process applications.

REFERENCES

[1] Song, C.S. An overview of new approaches to deep desulfurization for ultra-clean gasoline, diesel fuel and jet fuel. Catal. Today. 86 (2003): 211-263.

[2] Ma, X and Song, C.S. New design approaches to ultra-clean diesel fuels by deep desulfurization and deep dearomatization. Appl. Catal. B-Environ. 41 (2003): 207-238.

[3] Babich, I.V. and Moulijn, J.A. Science and technology of novel process for deep desulfurization of oil refinery streams: A review. Fuel. 82 (2003): 607-631.

[4] Knudsen, K.G., Cooper, B.H. and Topsoe, H. Catalyst and process technologies for ultra low sulfur diesel. Appl. Catal. A-Gen. 189 (1999): 205-215.

[5] Sano, Y., Choi, K., Korai, Y. and Mochida, I. Adsorptive removal of sulfur and nitrogen species from a straight run gas oil over activated carbons for its deep hydrodesulfurization. Appl. Catal. B-Environ. 49 (2004): 219-225.

[6] EPA-Diesel RIA, Regulatory Impact Analysis: Heavy-Duty Engine and Vehicle Standards and Highway Diesel Fuel Sulfur Control Requirements, United States Environmental Protection Agency, Air and Radiation, EPA420-R-00-026, December 2000.

[7] Shin, S., Yang, H., Sakanishi, K., Mochida, I., Grudoski, D. A. and Shinn, J.H. Inhibition and deactivation in hydrodenitrogenation and hydrodesulfurization of medium cycle oil over NiMoS/Al$_2$O$_3$ catalyst. Appl. Catal. A-Gen. 205 (2001): 101-108

[8] Yoshimura, Y., Yasuda, H., Sato, T., Kijima, N., and Kameoka, T. Sulfur-tolerant Pd-Pt/Yb-USY zeolite catalysts used to reformulate diesel oils. Appl. Catal. A-Gen. 207 (2001): 303-307.

[9] Swain, E.J. US crude slate gets heavier, higher in sulfur. <u>Oil Gas J</u>. 89 (1991) 59–61.

[10] Swain, E.J. US refining crude slates continue towards heavier feeds, higher sulfur contents. <u>Oil Gas J</u>. 96 (1998): 43–48.

[11] Speight, J.G. and Ozum, B. <u>Petroleum Refining Processes</u>. New York: Marcel Dekker, 2002.

[12] Brunet, S., Mey, D., Perot, G., Bouchy, C. and Diehl, F. On the hydrodesulfurization of FCC gasoline: a review. <u>Appl. Catal. A-Gen.</u> 278 (2005): 143-172.

[13] Topsoe, H., Clausen, B.S. and Massoth, F.E. Hydrotreating catalysts. in: Anderson, J.R. and Boudart, M. (Eds.). <u>Catalysis Science and Technology</u>. Vol. 11. Springer. Berlin. 1996.

[14] Shiflett, W.K.A. User's guide to the chemistry, kinetics and basic reactor engineering of hydroprocessing. <u>Proceedings of the Fifth International Conference on Refinery Processing AIChE</u> (2002): 101–122.

[15]]Bartholomew, C.H. Catalyst deactivation in hydrotreating of residua: A review. in Oballa M.C. and Shih S.S. (Eds.). <u>Catalytic Hydoprocessing of Petroleum and Distillates</u>. New York: Marcel Dekker.

[16] Kabe, T., Ishihara, A. and Qian, W. <u>Hydrodesulfurization and Hydrodenitrogenation: Chemistry and Engineering.</u> Wiley-VCH, Weinhein, 1999.

[17] Girgis, M.J. and Gates, B.C. Reactivities, reaction networks, and kinetics in high pressure catalytic hydroprocessing. <u>Ind. Eng. Chem. Res.</u> 30 (1991): 2021-2058.

[18] Schulz, H., Bohringer, W., Waller, P. and Ousmanov, F. Gas oil deep hydrodesulfurization: refractory compounds and retarded kinetics. Catal. Today. 49 (1999): 87-97.

[19] Ma, X., Sun, L., Yin, Z., and Song, C.S. New approaches to deep desulfurization of diesel fuel, jet fuel, and gasoline by adsorption for ultra-clean fuels and for fuel cell applications. Am. Chem. Soc. Div. Fuel. Chem. Prepr. 46 (2001): 648.

[20] Phillipson, J.J. Kinetics of hydrodesulfurization of light distillates. Paper Presented at the American Institute of Chemical Engineers Meeting. (1971).

[21] Frye, C.G. and Mosby, J.F. Kinetics of hydrodesulfurization. Chem. Eng. Prog. 63 (1967) 66.

[22] Kilanowski, D.R., Teeuwen, H., De Beer, V.H.J., Gates, B.C., Schuit, B.C.A. and Kwart, H. Hydrodesulfurization of thiophene, benzothiophene, dibenzothiophene, and related compounds catalyzed by sulfided CoO–MoO$_3$/γ-Al$_2$O$_3$: low-pressure reactivity studies. J. Catal. 55 (1978): 129-137.

[23] Houalla, M., Broderick, D.H., Sapre, A.V., Nag, N.K., De Beer, V.H.J., Gates, B.C. and Kwart, H. Hydrodesulfurization of methyl-substituted dibenzothiophene catalyzed by sulfided CoO–MoO$_3$/γ-Al$_2$O$_3$. J. Catal. 61 (1980): 523-527.

[24] Vasudevan, P.T. and Fierro, J.L.G. A review of deep hydrodesulfurization catalysis. Catal. Rev.-Sci. Eng. 38 (1996): 161-188.

[25] Phillipson, J.J. Kinetics of hydrodesulfurization of middle distillates, Paper Presented at the American Institute of Chemical Engineers Meeting. (1971).

[26] Gates, B.C. and Topsoe, H. Reactivities in deep catalytic hydrodesulfurization: challenges, opportunities, and the importance of 4-methyldibenzothiophene and 4,6-dimethyl-dibenzothiophene. Polyhedron. 16 (1997): 3213-3217.

[27] Kabe, T., Ishihara, A. and Tajima, H. Hydrodesulfurization of sulfur-containing polyaromatic compounds in light oil. Ind. Eng. Chem. Res. 31 (1992): 1577-1580.

[28] Ma, X., Sakanishi, K. and Mochida, I. Hydrodesulfurization reactivities of various sulfur compounds in diesel fuel. Ind. Eng. Chem. Res. 33 (1994): 218-222.

[29] Ma, X., Sakanishi, K., Isoda, T. and Mochida, I. Hydrodesulfurization reactivities of narrow-cut fractions in a gas oil. Ind. Eng. Chem. Res. 34 (1995): 748-754.

[30] Nagai, M., Urimoto, H., Uetate, K., Sakikawa, N. and Gonzalez, R. D. Desulfurization of Benzonaphthothiophenes and dibenzothiophene with a raney nicke1 catalyst and its relationshipto thex-electron density. Am. Chem. Soc. Div. Gen. Chem. Prepr. 31 (1986): 857.

[31] Givens, E.N. and Venuto, P.B. Hydrogenolysis of benzothiophenes and related intermediates over cobalt molybdena catalyst. Am. Chem. Soc. Div. Petro. Chem. Prepr: 14 (1970): 135.

[32] Houalla, M., Nag, N.K., Sapre, A.V., Broderick, D.H. and Gates, B.C. Hydrodesulfurization of dibenzothiophene catalyzed by sulfided CoO-MoO$_3$-gamma- Al$_2$O$_3$ - reaction network. AICHE J. 24 (1978): 1015-1021.

[33] Isoda, T., Nagao, S., Korai, Y. and Mochida I. HDS reactivity of alkyldibenzothiophenes in gas oil. 1. acid assisted desulfurization of 4,6 dimethyldibenzothiophene through isomerization and cracking. Am. Chem. Soc. Div. Petro. Chem. Prepr. 25 (1996): 559-562.

[34] Isoda, T., Nagao, S., Korai, Y. and Mochida I. HDS reactivity of alkyldibenzothiophenes in gas oil. 2. HDS reactivity of 4,6-dimethyldibenzothiophene and its reaction pathway over Ni loaded Y-zeolite and CoMo/Al$_2$O$_3$. Am. Chem. Soc. Div. Petro. Chem. Prepr. 25 (1996): 563.

[35] Lamuremeille, Y., Schulz, E., Lemaire, M., Vrinat, M. Effect of experimental parameters on the relative reactivity of dibenzothiophene and 4-methyldibenzothiophene. App. Catal. A-Gen. 131 (1995): 143-157.

[36] Landau, M.V., Berger, D. and Herskowitz, M. Hydrodesulfurization of methyl-substituted dibenzothiophenes: Fundamental study of routes to deep desulfurization. J. Catal. 159 (1996): 236-245.

[37] Prins, R. Hydrotreating reactions, in: Ertl, G., Knozinger, H. and Weitkamp J. (Eds.), Handbook of Heterogeneous Catalysis, Vol. 4. Wiley-VCH. Berlin. 1997.

[38] Ma, X., Kim, J.H. and Song, C. Effect of methyl groups at 4-and 6-positions on absorption of dibenzothiophenes over CoMo and NiMo catalysts, Prepr. Pap. Am. Chem. Soc., Div. Fuel Chem. Prepr. 48 (2003): 135-137.

[39] Ma, X. and Schobert, H.H. Hydrodesulfurization of heterocyclic sulfur compounds on MoS$_2$ - a computational study using ZINDO. Am. Chem. Soc., Div. Fuel Chem. Prepr. 42 (1997): 657-661.

[40] Shafi, R. and Hutchings, G. Hydrodesulfurization of hindered dibenzothiophenes: an overview. Catal. Today. 59 (2000): 423-442.

[41] Ma, X. and Schobert, H.H. Hydrodesulfurization of thiophenic compounds on MoS$_2$, a computational study using ZINDO. Am. Chem. Soc., Div. Fuel Chem. Prepr. 42 (1997): 48.

[42] Ma, X. and Schobert, H.H. Hydrogenolysis of thiophenic compounds on MoS₂— a computational modeling of heterogeneous catalysis. <u>Am. Chem. Soc. Div. Petro. Chem. Prepr.</u> 42 (1997): 657.

[43] Ma, X. and Schobert, H.H. Computational modeling on hydrodesulfurization of thiophenic compounds on MoS2 and Ni-promoted MoS₂. <u>Am. Chem. Soc. Div. Petro. Chem. Prepr.</u> 43 (1998): 24.

[44] Ma, X. and Schobert, H.H. Molecular simulation on hydrodesulfurization of thiophenic compounds over MoS₂ using ZINDO. <u>J. Mol. Catal.</u> 160 (2000): 409–427.

[45] Kabe, T., Ishihara, A. and Zhang, Q. Deep desulfurization of light oil. 2. Hydrodesulfurization of dibenzothiophene 4-methyldibenzothiophene and 4,6-dimethyldibenzothiophene. <u>Appl. Catal. A-Gen.</u> 97 (1993): 1-15.

[46] Ma, X., Sakanishi, K. Isoda, T. and Mochida I., Comparison of sulfided CoMo/Al₂O₃ catalysts in hydrodesulfurization of gas oil fractions. <u>Am. Chem. Soc. Div. Petro. Chem. Prepr.</u> 39 (1994): 622–626.

[47] Ma, X., Sakanishi, K. Isoda, T. and Mochida I. Quantum chemical calculation on the desulfurization reactivities of heterocyclic sulfur compounds. <u>Energy. Fuel.</u> 9 (1995): 33–37.

[48] Isoda, T., Ma, X. and Mochida, I. Reactivity of refractory sulfur compounds in diesel fuel. Part 1. Desulfurization reactivity of mkyldibenzothiophenes in Decalin. <u>J. Jpn. Petrol. Inst.</u> 37 (1994): 368.

[49] Mochida I., Sakanishi, K, Ma, X., Nagao, S. and Isoda, T. Deep hydrodesulfurization of diesel fuel: design of reaction process and catalysis. <u>Catal. Today.</u> 29 (1996): 185-189.

[50] Ma, X. <u>Deep hydrodesulfurization of Diesel Fuel: Chemistry and Reaction Processing Design</u>. Ph.D. Thesis, Kyushu University, Japan, 1995.

[51] Farag, H., Sakanishi, K., Mochida, I. and Whitehurst, D.D. Kinetic analyses and inhibition by naphthalene and H_2S in hydrodesulfurization of 4,6-dimethyldibenzothiophene (4,6-DMDBT) over CoMo-based carbon catalyst. <u>Energy. Fuel.</u> 13 (1999): 449-453.

[52] Ma, X., Sakanishi, K. and Mochida, I. Hydrodesulfurization reactivities of various sulfur compounds in diesel fuel. <u>Ind. Eng. Chem. Res.</u> 33 (1994): 218–222.

[53] Isoda, T., Ma, X., Nagao, S. and Mochida, I. Reactivity of refractory sulfur compounds in diesel fuel. Part 3. Coexisting sulfur compounds and by-produced H_2S gas as inhibitors in HDS of 4,6-dimethyldibenzothiophene, <u>J. Jpn. Petrol. Inst.</u> 38 (1995): 25.

[54] Shiflett, W.K. and Krenzke, L.D. Consider improved catalyst technologies to remove sulfur, <u>Hydrocarb. Process.</u> 81 (2002): 41-43.

[55] Meijburg, G. Production of ultra-low-sulfur diesel in hydrocracking with the latest and future generation catalysts, Catalyst Courier No. 46, Akzo Nobel, 2001.

[56] Plantenga, F.L. "Nebula" a Hydroprocessing Catalyst with Breakthrough Activity, Catalysts Courier No. 47, Akzo Nobel, 2002. <u>http://www.akzonobel-catalysts.com/html/catalystcourier/Courier47/c47 a3.htm</u>.

[57] <u>www.exxonmobil.com/Refiningtechnologies/pdf/h7_nebula.pdf</u>

[58] Hilton, M.R. and Fleischauer, P.D. TEM lattice imaging of the nanostructure of early-growth sputter-deposited MoS_2 solid lubricant films. <u>J. Mater. Res.</u> 5 (1990): 406-421.

[59] Chianelli, R.R. Fundamental-studies of transition-metal sulfide hydrodesulfurization catalysts. <u>Catalysis Reviews-Science and Engineering</u>. 26 (1984): 361-393.

[60] Ratnasamy, P. and Sivasanker, S. Structural chemistry of Co-Mo-alumina catalysts. Catalysis Reviews-Science and Engineering. 22 (1980): 401-429.

[61] Voorhoev, R.J. and Stuiver, J.C.M. Mechanism of hydrogenation of cyclohexene and benzene on nickel-tungsten sulfide catalysts. J. Catal. 23 (1971): 243-252.

[62] Farragher, A.L. and Cossee, P. Catalytic chemistry of molybdenum and tungsten sulfides and related ternary compounds. Proceeding of the Fifth International Congress on Catalysis. 2 (1973): 1301-1318.

[63] Ma, X. Personal communication. 2006.

[64] Daage M and Chianelli, R.R. Structure-function relations in molybdenum sulfide catalysts - the rim-edge model. J. Catal. 149 19942): 414-427.

[65] Whitehurst, D.D., Isoda, T. and Mochida, I. Present state of the art and future challenges in the hydrodesulfurization of polyaromatic sulfur compounds. Adv. Catal. 42 (1998): 345-471.

[66] Schuit, G.C.A. and Gates, B.C. Chemistry and engineering of catalytic hydrodesulfurization. AICHE J. 19 (1973): 417-438 1973.

[67] Lipsch, J.M.J. and Schuit, G.C.A. CoO-MoO$_3$-Al$_2$O$_3$ catalyst 1. cobalt molybdate and cobalt oxide molybdenum oxide system. J. Catal. 15 (1969): 163-173.

[68] Lipsch, J.M.J. and Schuit, G.C.A. CoO-MoO$_3$-Al$_2$O$_3$ catalyst 2. structure of catalyst. J. Catal. 15 (1969): 174-178& 1969

[69] Lipsch, J.M.J. and Schuit, G.C.A. CoO-MoO$_3$-Al$_2$O$_3$ catalyst 3. catalytic properties J. Catal. 15 (1969): 179-189& 1969

[70] Gates, B.C. Liquefied coal by hydrogenation. Chemtech. 9 (1979): 97-102.

[71] De Beer, V.H.J, Schuit, G.C.A, Vansintf, T.H., Vanhaand, A.C., Wolfs, M.W.J., Engelen, J.F. and Amberg, C.H. CoO-MoO$_3$-Al$_2$O$_3$ catalyst.4. pulse and continuous-flow experiments and catalyst promotion by cobalt, nickel, zinc, and manganese. J. Catal. 27 (1972): 357-368.

[72] Massoth, F.E. State of molybdena-alumina catalyst during thiophene hydrogenolysis. Journal of the Less-Common Metals. 54 (1977): 343-352.

[73] Mitchell, P.C. and Trifiro, F. Effect of sulfiding on structure of a cobalt-molybdenum-alumina hydrodesulfurization catalyst. J. Catal. 33 (1974): 350-354.

[74] De Beer, V.H.J, Vansintf, T.H, Vanderst, G.H., Zwaga, A.C. and Schuit, G.C.A. CoO-MoO$_3$ gamma Al$_2$O$_3$ catalyst 5. sulfide catalysts promoted by cobalt, nickel, and zinc. J. Catal. 35 (1974): 297-306.

[75] Voorhoev, R.J. Electron spin resonance study of active centers in nickel-tungsten sulfide hydrogenation. J. Catal. 23 (1971): 236-242.

[76] Voorhoev, R.J and Stuiver, J.C.M. Kinetics of hydrogenation on supported and bulk nickel-tungsten sulfide catalysts. J. Catal. 23 (1971): 228-235.

[77] Farragher, A.L. Solid-state chemistry and surface-structures of MoS$_2$ and WS$_2$ Am. Chem. Soc., Div. Fuel Chem. Prepr. 173 (1977): 34-34.

[78] Huisman, R., Dejonge, R., Haas, C. and Jellinek, F. Trigonal-prismatic coordination in solid compounds of transition metals. J. Solid. State. Chem. 3 (1971): 56-66.

[79] Hagenbac,G., Courty, P. and Delmon, B. Physiochemical investigations and catalytic activity measurements on crystallized molybdenum sulfide cobalt sulfide mixed catalysts. J. Catal. 31 (1973): 264-273.

[80] Grange, P., and Delmon, B. Role of cobalt and molybdenum sulfides in hydrodesulfurization catalysts – review. Journal of the Less-Common Metals. 36 (1974): 353-360.

[81] Delmon, B. New hypothesis explaining synergy between 2 phases in heterogeneous catalysis - case of hydrodesulfurization catalysts. Bull. Soc. Chim. Belg. 88 (1979): 979-987.

[82] Pirotte, D., Zabala, J.M., Grange, P. and Delmon, B. The remote-control of the active-sites of hydrodesulfurization catalysts comparison of experimental results with the model Bull. Soc. Chim. Belg. 90 (1981): 1239-1248.

[83] Furimsky, E. Role of MoS_2 and WS_2 in hydrodesulfurization. Catalysis Reviews. Science and Engineering. 22 (1980): 371-400.

[84] Topsoe, H., Candia, R., Topsoe, N.Y. and Clausen, B.S. On the state of the Co-Mo-S model. Bull. Soc. Chim. Belg. 93 (1984): 783-806.

[85] Topsoe, H. and Clausen, B.S. Importance of co-mo-s type structures in hydrodesulfurization catalysis reviews. Science and Engineering 26 (1984): 395-420.

[86] Clausen, B.S., Topsoe, H., Candia, R., Villadsen, J., Lengeler, B., Alsnielsen, J. and Christensen, F. Extended x-ray absorption fine-structure study of Co-Mo hydrodesulfurization catalysts. J. Phys. Chem. 85 (1981): 3868-3872.

[87] Topsoe, H., Clausen, B.S., Candia, R., Wivel, C. and Morup, S. In situ Mossbauer Emission-Spectroscopy studies of unsupported and supported sulfided Co-Mo hydrodesulfurization catalysts - evidence for and nature of a Co-Mo-S phase. J. Catal. 68 (1981): 433-452.

[88] Wivel, C., Candia, R., Clausen, B.S., Morup, S. and Topsoe, H. On the catalytic significance of a Co-Mo-S phase in Co-Mo-Al₂O₃ hydrodesulfurization catalysts - combined insitu mossbauer emission-spectroscopy and   activity studies. J. Catal. 68 (1981): 453-463.

[89] Candia, R., Clausen, B.S, and Topsoe, H. On the role of promoter atoms in unsupported hydrodesulfurization catalysts - influence of preparation methods Bull. Soc. Chim. Belg. 90 (1981): 1225-1232.

[90] Clausen, B.S, Lengeler, B., Candia, R., Alsnielsen, J. and Topsoe, H. EXAFS studies of calcined and sulfided Co-Mo HDS catalysts. Bull. Soc. Chim. Belg. 90 (1981): 1249-1259.

[91] Topsoe, H, Clausen, B.S, Topsoe, N.Y. and Pedersen, E. Recent basic research in hydrodesulfurization. Catalysis Industrial & Engineering Chemistry Fundamentals 25 (1986): 25-36.

[92] Topsoe, N.Y. and Topsoe, H. Characterization of the structures and active-sites in sulfided Co-Mo/Al₂O₃ and Ni-Mo/Al₂O₃ catalysts by NO chemisorption. J. Catal. 84 (1983): 386-401.

[93] Bouwens, S.M.A.M., Vanzon, F.B.M., Vandijk, M.P., Vanderkraan, A.M., De Beer, V.H.J., Vanveen, J.A.R. and Koningsberger, D.C. On the structural differences between alumina-supported comos type-I and alumina-supported, silica-supported, and carbon-supported CoMoS type-II phases studied by XAFS, MES, and XPS. J. Catal. 146 (1994): 375-393.

[94] Topsoe H., Clausen B.S., Topsoe N.Y., Hyldtoft J. and Norskov J.K. Experimental and theoretical-studies of periodic trends and promotional behaviors of hydrotreating catalysts. Am. Chem. Soc. Div. Petro. Chem. Prepr. 8 (1993) 206.

[95] Candia, R., Sorensen, O., Villadsen, J., Topsoe, N.Y., Clausen, B.S. and Topsoe, H. Effect of sulfiding temperature on activity and structures of Co-Mo/Al$_2$O$_3$ catalysts. Bull. Soc. Chim. Belg. 93 (1984): 763-773.

[96] Topsoe, H. and Clausen B.S. Active-sites and support effects in hydrodesulfurization catalysts. Appl. Catal. 25 (1986): 273-293.

[97] Bouwens, S.M.A.M., Vanzon, F.B.M., Vandijk, M.P., Vanderkraan, A.M., De Beer, V.H.J., Vanveen, J.A.R. and Koningsberger, D.C. On the structural differences between alumina-supported comos type-I and alumina-supported, silica-supported, and carbon-supported CoMoS type-II phases studied by XAFS, MES, and XPS. J. Catal. 146 (1994): 375-393.

[98] Helveg, S., Lauritsen, J. V., Lægsgaard, E., Stensgaard, I., Norskov, J. K., Clausen, B. S., Topsoe, H., and Besenbacher, F. Atomic-scale structure of single- layer MoS$_2$ nanoclusters. Phys. Rev. Lett. 84 (2000): 951-954.

[99] Lauritsen, J.V., Helveg, S., Lægsgaard, E., Stensgaard, I., Clausen, B.S., Topsoe, H. and Besenbacher, F. Atomic-scale structure of Co–Mo–S nanoclusters in hydrotreating catalysts. J. Catal. 197 (2001): 1-5.

[100] Lauritsen, J.V., Nyberg, M., Vang, R.T., Bollinger, M.V., Clausen, B.S., Topsoe, H., Jacobsen, K.W., Laegsgaard. E, Norskov, J.K. and Besenbacher, F. Chemistry of one-dimensional metallic edge states in MoS$_2$ nanoclusters. Nanotechnology 14 (2003): 385-389.

[101] Lauritsen, J.V., Bollinger, M.V, Laegsgaard, E., Jacobsen, K.W., Norskov, J.K., Clausen, B.S., Topsoe, H. and Besenbacher, F. Atomic-scale insight into structure and morphology changes of MoS$_2$ nanoclusters in hydrotreating catalysts. J. Catal. 221 (2004): 510–522.

[102] Byskov, L. S., Norskov, J. K., Clausen, B. S., and Topsoe, H. Calculations of unpromoted and promoted MoS$_2$-based hydrodesulfurization catalysts. J.Catal. 187 (1999): 109-1222.

[103] Byskov, L. S., Hammer, B., Norskov, J. K., Clausen, B. S., and Topsoe H., Sulfur bonding in MoS_2 and Co-Mo-S structures. Catal. Lett. 47 (1997): 177 - 182.

[104] Song, C.S., Yoneyama, Y. and Kondam, M.R. Method for Preparing a Highly Active, Unsupported High Surface Area MoS_2 Catalyst. US Patent No. 6451729, 2002

[105] Yoneyama, Y. and Song, C.S. A new method for preparing highly active unsupported Mo sulfide. Catalytic activity for hydrogenolysis of 4-(1-naphthylmethyl)bibenzyl. Catal. Today 50 (1999): 19-27.

[106] Yoneyama, Y. and Song, C.S. Promoting effect of H_2O addition on C-O bond cleavage and hydrogenation of dinaphthyl ether over MoS_2 catalyst in situ generated from ammonium tetrathiomolydate. Energ Fuel 16 (2002): 767-773.

[107] Ma, X., Sun, L. and Song, C.S. A new approach to deep desulfurization of gasoline, diesel fuel and jet fuel by selective adsorption for ultra-clean fuels and fuel cell applications. Catal. Today 77 (2002): 107-116.

[108] Ma, X., Sprague, M., Sun, L. and Song, C.S. Deep desulfurization of gasoline by SARS process using adsorbent for fuel cells. Am. Chem. Soc. Div. Fuel Chem. Prepr. 47 (2002): 452 World Patent WO03068892A2, 2003.

[109] Ma, X., Velu, S., Sun, L., Song, C.S., Mehdi, N. and Siva, S. Adsorptive desulfurization of JP-8 jet fuel and its light fraction over nickel-based adsorbents for fuel cell applications. Am. Chem. Soc. Div. Fuel Chem. Prepr. 48 (2003): 688.

[110] Velu, S., Ma, X. and Song, C.S. Selective adsorption for removing sulfur from jet fuel over zeolite-based adsorbents. Ind. Eng. Chem. Res. 42 (2003): 5293-5304.

[111] Ma, X., Sun, L. and Song, C. Adsorptive desulfurization of diesel fuel over a metal sulfide based adsorbent. <u>Am. Chem. Soc. Div. Fuel Chem. Prepr.</u> 48 (2003): 522.

[112] Pedraza, F. and Fuentes, S. Ni–Mo and Ni–W sulfide catalysts prepared by decomposition of binary thiometallates. <u>Catal. Lett.</u> 65 (2000): 107–113.

[113] Alvarez, L., Espino, J., Ornelas, C., Rico, J.L., Cortez, M.T., Berhault, G. and Alonso, G. Comparative study of MoS_2 and Co/MoS_2 catalysts prepared by ex situ/in situ activation of ammonium and tetraalkylammonium thiomolybdates. <u>J. Mol. Catal. A</u> 210 (2004): 105–117.

[114] Candia, R., Clausen, B.S. and Topsoe, H. The origin of catalytic synergy in unsupported Co-Mo HDS catalysts. <u>J. Catal.</u> 77 (1982): 564-566.

[115] Harris, S. and Chianelli, R.R. Catalysis by transition-metal sulfides - a theoretical and experimental-study of the relation between the synergic systems and the binary transition-metal sulfides. <u>J. Catal.</u> 98 (1986): 17-31.

[116] Nava, H., Pedraza, F. and Alonso, G. Nickel–Molybdenum–Tungsten Sulphide catalysts prepared by in situ activation of tri-metallic (Ni–Mo–W) alkylthiomolybdotungstates. <u>Catal. Lett.</u> 99 (2005): 65-71.

[117] Nava, H., Ornelas, C., Aguilar, A., Berhault, G., Fuentes, S. and Alonso, G. Cobalt–molybdenum sulfide catalysts prepared by in situ activation of bimetallic (Co–Mo) alkylthiomolybdates. <u>Catal. Lett.</u> 86 (2003): 257-265.

[118] Farag, H., Sakanishi, K., Kouzu, M., Matsumura, A., Sugimoto, Y. and Saito, I. Dibenzothiophene hydrodesulfurization over synthesized MoS_2 catalysts. <u>J. Mol. Catal. A</u> 206 (2003): 399–408.

[119] Iwata, Y., Sato, K., Yoneda, T., Miki, Y., Sugimoto, Y., Nishijima, A. and Shimada, H. Catalytic functionality of unsupported molybdenum sulfide catalysts prepared with different methods. <u>Catal. Today</u> 45 (1998): 353-359.

[120] Devers, E., Afanasiev, P., Jouguest, B. and Vrinat, M. Hydrothermal syntheses and catalytic properties of dispersed molybdenum sulfides. Catal. Lett. 82 (2002): 13-17.

[121] Afanasiev, P., Xia, G., Berhault, G., Jouguet, B. and Lacroix, M. Surfactant-assisted synthesis of highly dispersed molybdenum sulfide. Chem. Mater. 11 (1999): 3216-3219.

[122] Inamura, K. and Prins, R. The role of Co in unsupported Co-Mo sulfides in the hydrodesulfurization of thiophene. J. Catal. 147 (1994): 515-524.

[123] Weisser, O. and Labda, S. Surface Catalysts: Their Properties and Application, Pergamon. Oxford. 1973.

[124] Reddy, K.M., Wei, B. and Song, C.S. Mesoporous molecular sieve MCM-41 supported Co-Mo catalyst for hydrodesulfurization of petroleum resides. Catal. Today. 43 (1998): 261-272.

[125] Hoodless, R.C., Moyes, R.B. and Wells, P.B. Temperature programmed reduction and desorption studies of co-precipitated cobalt-molybdenum sulfide powders. Bull. Soc. Chim. Belg. 93 (1984): 673-679.

[126] Vrinat, M.L. and Demourgues, L. On the role of cobalt in sulfided unsupported Co-Mo hydrodesulfurization catalysts – kinetic studies and scanning electron-microscopic observations. Appl. Catal. A-Gen. 5 (1983): 43-57.

[127] Pratt, K.C., Sanders, J.V. and Tamp, N. The role of nickel in the activity of unsupported Ni-Mo hydrodesulfurization catalysts. J. Catal. 66 (1980): 82-92.

[128] Gachet, C., Paulus, R., Demourgues, L., Durand, C. and Toulhoat, H. Unsupported Ni-Mo sulfide catalysts - relation between the HDS and hydrogenation activities and some structural-properties. Bull. Soc. Chim. Belg. 93 (1984): 681-686.

[129] Isoda, T., Nagao, S., Ma, X., Korai, Y. and Mochida, I. Catalytic activities of NiMo and CoMo/A1$_2$O$_3$ of variable Ni and Co contents for the hydrodesulfurization of 4,6-dimethyldibenzothiophene in the presence of naphthalene. Appl. Catal. A-Gen. 150 (1997): 1-11.

[130] Pedraza, F. and Fuentes, S. Ni–Mo and Ni–W sulfide catalysts prepared by decomposition of binary thiometallates. Catal. Lett. 65 (2000): 107–113.

[131] Breysse, M., Djega-Mariadassou, G., Pessayre, S., Geantet, C., Vrinat, M., Perot, G. and Lemaire, M. Deep desulfurization: reactions, catalysts and technological challenges. Catal. Today. 84 (2003): 129-138.

[132] Delmon, B. Modification of surface-structure by spillover species - consequences in the reaction of solids and catalysis. Surf. Rev. Lett. 2 (1995): 25-41.

[133] Grange, P. and Vanhaeren, X. Hydrotreating catalysts, an old story with new challenges. Catal. Today. 36 (1997): 375-391.

[134] Prins, R. Catalytic hydrodenitrogenation. Adv. Catal. 46 (2001): 399-464.

[135] Ramanathan, K. and Weller, S. Characterization of tungsten sulfide catalysts. J. Catal. 95 (1985): 249-259.

[136] Frety, R., Breysse, M., Lacroix M. and Vrinat, M. Unsupported MoS$_2$ and WS$_2$ model catalysts - influence of textural properties on hydrodesulfurization and hydrogenation activities. Bull. Soc. Chim. Belg. 93 (1984): 671-697.

[137] Alonso, G., Berhault, G., Aguilar, A., Collins, V., Ornelas, C., Fuentes, S. and Chianelli, R.R. Characterization and HDS activity of mesoporous MoS$_2$ catalystsprepared by in situ activation of tetraalkylammonium thiomolybdates. J. Catal. 208 (2002): 359-369.

[138] Siadati, M.H., Alonso, G., Torres, B. and Chianelli, R.R. Open flow hot isostatic pressing assisted synthesis of unsupported MoS_2 catalysts. Appl. Catal. A-Gen. 305 (2006): 160-168.

[139] Afanasiev, P. On the interpretation of temperature programmed reduction patterns of transition metals sulphides. Appl. Catal. A-Gen. 303 (2006): 110-115.

[140] Scheffer, B., Dekker, N.J.J., Mangnus, P.J. and Moulijn, J.A. A temperature-programmed reduction study of sulfided Co-Mo/Al_2O3 hydrodesulfurization catalysts. J.Catal. 121 (1990): 31-46.

[141] Jacobsen, C.J.H., Tornqvist E. and Topsoe, H. HDS, HDN and HYD activities and temperature-programmed reduction of unsupported transition metal sulfides. Catal. Lett. 63 (1999): 179-183.

[142] Li, X.S., Xin, Q., Guo, X.X., Grange, P. and Delmon, B. Reversible hydrogen adsorption on MoS_2 studied by temperature-programmed desorption and temperature-programmed reduction. J. Catal. 137 (1992): 385-393.

[143] Norskov, J.K., Clausen B.S. and Topsoe, H. Understanding the trends in the hydrodesulfurization activity of the transition metal sulfides. Catal. Lett. 13 (1992): 1-8.

[144] Raybaud, P., Hafner, J., Kresse, G., Kasztelan, S. and Toulhoat, H. Structure, energetics, and electronic properties of the surface of a promoted MoS_2 catalyst: an ab initio local density functional study. J. Catal. 190 (2000): 128-143.

[145] Sorensen, O., Clausen, B.S., Candia, R. and Topsoe, H. HREM and AEM studies of HDS catalysts - direct evidence for the edge location of cobalt in Co-Mo-S. Appl. Catal. A-Gen. 13 (1985): 363-372.

[146] Grange, P. Hydrotreating catalysts, an old story with new challenges. Catal. Today. 36 (1997): 375-391.

[147] Chianelli, R.R., Ruppert, A.F., Behal, S. K., Kear, B. H., Wold A. and Kershaw, R. The Reactivity of MoS single crystal edge planes J. Catal. 92 (1985): 56-63.

[148] Brito, J.L., Ilija, M. and Hernandez, P. Thermal and reductive decomposition of ammonium thiomolybdates. Thermochim. Acta. 256 (1995): 325-338.

[149] Ma, X., Sakanishi, K., and Mochida, I. Hydrodesulfurization reactivities of various sulfur compounds in vacuum gas oil. Ind. Eng. Chem. Res. 35 (1996): 2487-2494.

[150] Sie, S.T. Reaction order and role of hydrogen sulfide in deep hydrodesulfurization of gas oils: consequences for industrial reactor configuration. Fuel Process. Technol. 61 (1999): 149-171.

[151] Girgis, M. J. and Gates, B. C. Reactivities, reaction networks, and kinetics in high pressure catalytic hydroprocessing. Ind. Eng. Chem. Res. 30 (1991): 2021-2058.

[152] Farag, H., Whitehurst, D.D., Sakanishi, K. and Mochida, I. Improving kinetic analysis of sequential and parallel reactions of hydrodesulfurization of dibenzothiophenes by establishing reasonable boundaries for reaction rate constants. Catal. Today. 50 (1999): 49-56.

[153] Da Costa, P., Potvin, C., Manoli, J.M., Lemberton, J.L., Perot,G. and Djega-Mariadassou, G. New catalysts for deep hydrotreatment of diesel fuel - kinetics of 4,6-dimethyldibenzothiophene hydrodesulfurization over alumina-supported molybdenum carbide. J. Mol. Catal. A. 184 (2002): 323-333.

[154] Ma, X., Sakanishi, K., Isoda, T. and Mochida, I. in: Occelli, M. L., Chianelli, R., (Eds). <u>Hydrotreating Technology for Pollution Control.</u> Marcel Dekker. New York, 1996.

[155] Sakanishi, K., Nagamatsu, T., Mochida, I. and Whitehurst, D.D. Hydrodesulfurization kinetics and mechanism of 4,6-dimethyldibenzothiophene over NiMo catalyst supported on carbon. <u>J. Mol. Catal. A</u>. 155 (2000): 101-109

[156] Lund, K., Fogler, H.S. and McCune, C.C. Acidization. 1. dissolution of dolomite in hydrochloric-acid. <u>Chem. Eng. Sci.</u> 28 (1973): 691-700.

[157] Schwert, G. W. Use of integrated rate equations in estimating kinetic constants of enzyme-catalyzed reactions. <u>J. Biol. Chem.</u> 244 (1969): 1278-1284.

[158] Ernst, W.R. Determination of initial reaction-rates using Wilkinson relation. <u>Int. J. Chem. Kinet.</u> 21 (1989): 1153-1160.

[159] Ma, X., Peng, Y. and Schobert, H.H. Effects of structure of the butyl chain on the pyrolysis of butylbenzenes: Molecular simulation and mechanism. <u>Am. Chem. Soc. Div. Petro. Chem. Prepr.</u> 45 (2000): 488.

[160] Kim, J.H., Ma, X., Song, C.S., Lee Y. and Oyama, S.T. Kinetics of two pathways for 4,6-dimethyldibenzothiophene hydrodesulfurization over NiMo, CoMo sulfide, and nickel phosphide catalysts. <u>Energ. Fuel.</u> 19 (2005) 353-364.

[161] Bataille, F., Lemberton, J.L., Michaud, P., Perot, G., Vrinat, M., Lemaire, M., Schulz, E., Breysse M. and Kasztelan, S. Alkyldibenzothiophenes hydrodesulfurization-promoter effect, reactivity and reaction mechanism <u>J. Catal.</u> 191 (2000) 409-422.

[162] Muller, A., Krickemeyer, E., Jostes, R., Bogge, H., Diemann E. and Bergmann, U. $[Co_4S_3(SO)(CN)_{12}]_8$ a remarkable formation of a cluster and a so ligand and its relevance to the promotor effect of HDS catalysis. J. Chem. Sci. 406 (1985): 1715-1718.

[163] Topsoe, H., Clausen, B.S., Topsoe, N., Pedersen, E., Niemann, W., Miiller, A., Bogge H. and Lengeler, B. Inorganic cluster compounds as models for the structure of active sites in promoted hydrodesulphurization catalysts. J. Chem. Soc. Faraday Trans. 83 (1987) 2157-2167.

[164] Breysse, M., Berhault, G., Kasztelan, S., Lacroix, M., Mauge F. and Perot, G. New aspects of catalytic functions on sulfide catalysts. Catal. Today. 66 (2001) 15-22.

[165] Mijoin, J., Thevenin, V., Garcia Aguirre, N., Yuze, H., Wang, J., Li, W.Z., Perot G. and Lemberton, J.L. Thioreduction of cyclopentanone and hydrodesulfurization of dibenzothiophene over sulfided nickel or cobalt-promoted molybdenum on alumina catalysts. Appl. Catal. A-Gen. 180 (1999) 95-104.

[166] Hayden, T.F., Dumesic, J.A. Studies of the structure of molybdenum oxide and sulfide supported on thin-films of alumina. J. Catal. 104 (1987): 366-384.

[167] Tauster, S.J., Pecoraro, T.A.; Chianell, R.R. Structure and properties of molybdenum sulfide - correlation of O_2 chemisorption with hydrodesulfurization activity. J. Catal. 63 (1980): 515-519.

[168] Voorhoeve, R.J.H. and Stuiver, J.C.M. Mechanism of hydrogenation of cyclohexene and benzene on nickel-tungsten sulfide catalysts. J. Catal. 23 (1971): 243-252.

[169] Kim, J.H., Ma, X., Zhou, A. and Song, C.S. Ultra-deep desulfurization and denitrogenation of diesel fuel by selective adsorption over three different adsorbents: a study on adsorptive selectivity and mechanism. Catal. Today. 111 (2006): 74–83.

[170] UOP, Diesel fuel: specifications and demand for the 21st century, 1998.

[171] De Cicco, J. and Mark, J. Meeting the energy and climate challenge for transportation in the United States, Energy Policy 26 (1998): 395-412.

[172] Song, C.S. Introduction to chemistry of diesel fuels, in: Song, C.S., Hsu, C.S. and Mochida, I.(Eds.). Chemistry of Diesel Fuels. Taylor and Francis. New York. 2000.

[173] Depauw, G.A. and Froment, G.F. Molecular analysis of the sulphur components in a light cycle oil of a catalytic cracking unit by gas chromatography with mass spectrometric and atomic emission detection. J. Chromatogr. A. 761 (1997) 231-247.

[174] Corma, A., Gonzalez-Alfaro, V. and Orchilles, A.V. Decalin and tetralin as probe molecules for cracking and hydrotreating the light cycle oil. J. Catal. 200 (2001): 34-44.

[175] Rollmann, L.D., Howley, P.A., Mazzone, D.N. and Timken, H.K.C. Model compounds for light cycle oil conversion. Ind. Eng. Chem. Res. 34 (1995): 3970-3973.

[176] Bouchy, M., Peureuxdenys, S., Dufresne, P. and Kasztelan, S. Hydrogenation and hydrocracking of a model light cycle oil feed. Part 2. Properties of a sulfided NiMo hydrocracking catalyst. Ind. Eng. Chem. Res. 32 (1993): 1592-1602.

[177] Bouchy, M. Dufresne, P. and Kasztelan, S. Hydrogenation and hydrocracking of a model light cycle oil feed. Part 1. Properties of a sulfided nimo hydrotreating catalyst, Ind. Eng. Chem. Res. 31 (1992): 2661-2269.

[178] Rankel, L.A. Using co water to hydroprocess aromatic containing feeds, Energy Fuels 6 (1992): 826-830.

[179] Corma, A. Martinez, A. and Martinez-Soria, V. Catalytic performance of the new delaminated ITQ-2 zeolite for mild hydrocracking and aromatic hydrogenation processes. J. Catal. 200 (2001): 259-269.

[180] Corma, A. Martinez, A. and Martinez-Soria, V. Hydrogenation of aromatics in diesel fuels on Pt/MCM-41 catalysts. J. Catal. 169 (1997): 480-489.

[181] Fujikawa, T., Idei, K., Ebihara, T., Mizuguchi, H. and Usui, K. Aromatic hydrogenation of distillates over SiO_2–Al_2O_3- supported noble metal catalysts. Appl. Catal. A: Gen. 192 (2000): 253-261.

[182] Fujikawa, T., Idei, K., Ohki, K., Mizuguchi, H. and Usui, K. Kinetic behavior of hydrogenation of aromatics in diesel fuel over silica–alumina-supported bimetallic Pt-Pd catalyst. Appl. Catal. A: Gen. 205 (2001): 71-79.

[183] Lecrenay, E., Sakanishi, K. and Mochida, I. Catalytic hydrodesulfurization of gas oil and model sulfur compounds over commercial and laboratory-made CoMo and NiMo catalysts: activity and reaction scheme. Catal. Today. 39 (1997): 13-20.

[184] Lecrenay, E., Sakanishi, K., Mochida, I. and Suzuka, T. Hydrodesulfurization activity of CoMo and NiMo catalysts supported on some acidic binary oxides. Appl. Catal. A-Gen. 175 (1998): 237-243.

[185] Lecrenay, E., Sakanishi, K. Nagamatsu, T., Mochida, I. and Suzuka, T. Hydrodesulfurization activity of CoMo and NiMo supported on Al_2O_3–TiO_2 for some model compounds and gas oils. Appl. Catal. B: Environ. 18 (1998): 325-330.

[186] Ancheyta-Juarez, J., Aguilar-Rodriguez, E., Salazar-Sotelo, D., Betancourt-Rivera, G. and Leiva-Nuncio, M. Hydrotreating of straight run gas oil-light cycle oil blends Appl. Catal. A: Gen. 180 (1999): 195-205.

[187] Ancheyta-Juarez, J., Aguilar-Rodriguez, E., Salazar-Sotelo, D. and Marroquin-Sanchez, G. Effect of light cycle oil on diesel hydrotreatment. Stud. Surf. Sci. Catal. 127 (1999) 343-346.

[188] Vanrysselberghe, V. and Froment, G.F. Hydrodesulfurization of dibenzothiophene on a $CoMo/Al_2O_3$ catalyst: reaction network and kinetics. Ind. Eng. Chem. Res. 35 (1996): 3311-3318.

[189] Shih, S.S., Mizrahi, S., Green, L.A. and Sarli, M.S. Deep desulfurization of distillates. Ind. Eng. Chem. Res. 31 (1992): 1232-1235.

[190] Isoda, T., Nagao, S., Ma, X., Korai, Y. and Mochida, I. Hydrodesulfurization of refractory sulfur species. part 1. selective hydrodesulfurization of 4,6-dimethyldibenzothiophene in the major presence of naphthalene over $CoMo/Al_2O_3$ and Ru/Al_2O_3 blend catalysts. Energy. Fuel. 10 (1996): 482-486.

[191] Zeuthen, P., Knudsen, K.G. and Whithust, D.D. Organic nitrogen compounds in gas oil blends, their hydrotreated products and the importance to hydrotreatment. Catal. Today. 65 (2001): 307-314.

APPENDICES

Appendix A

Reaction Products Analysis

The liquid reaction products were characterized using a Hewlett Packard 5890 Series II gas chromatograph equiped with a flame ionization detector (GC-FID). The 30 m X 0.25 mm slightly polar Restek XTI-5 column coated with 5% phenyl 95% methylpolysiloxane was used in the gas chromatograph. The GC condition and temperature program used for the analyses is described in Table A-1

Table A-1 Conditions and Temperature Program for GC-FID Analysis.

Parameters	Value
Carrier gas	Helium
Injector temperature (^{o}C)	290
Detector temperature (^{o}C)	290
Injection volume (μl)	1
Oven temperature program	
Initial temperature (^{o}C)	50
Hold time (min)	0
Final temperature (^{o}C)	240
Hold time (min)	0
Ramp rate (^{o}C/min)	5

The samples were analyzed quantitatively on the basis of response factors obtained by analyzing known concentrations. Figure A-1 provides a representative plot for the response factors of DBT and 4,6-DMDBT.

The individual sulfur compounds in the products of LCO HDS were analyzed by the Gas Chromatography - Pulsed Flame Photometric Detector (GC-PFPD). The GC condition and temperature program used for the analyses is described in Table A-2.
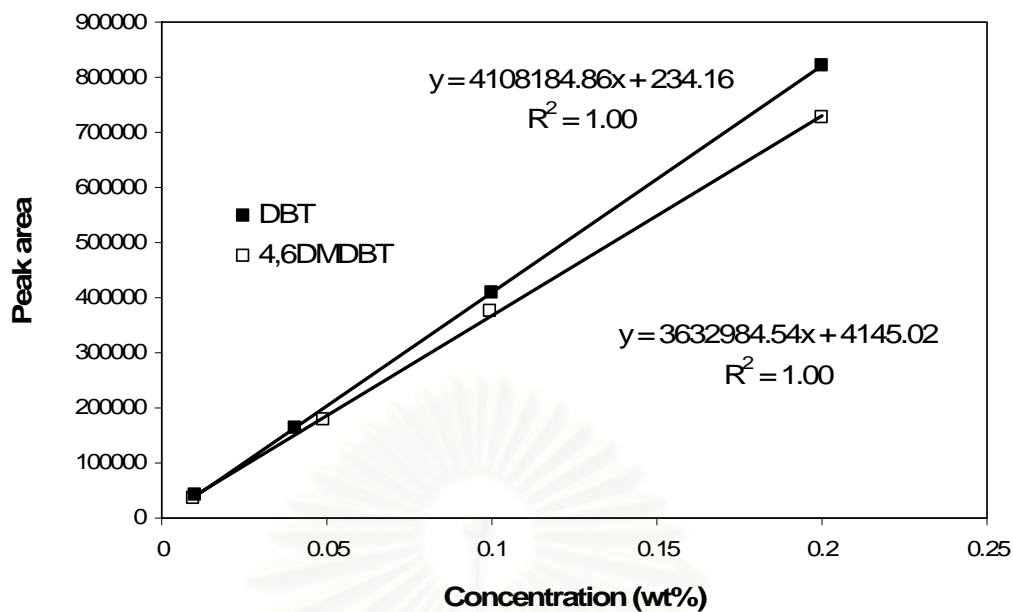
Figure A-1 A representative plot for the response factors of DBT and 4,6-DMDBT.

Table A-2 Conditions and Temperature Program for GC-PFPD Analysis.

Parameters	Value
Carrier gas	Nitrogen
Injector temperature (^{o}C)	290
Detector temperature (^{o}C)	220
Injection volume (μl)	1
Oven temperature program	
Initial temperature (^{o}C)	105
Hold time (min)	0
Ramp rate (^{o}C/min)	5
Temperature A (^{o}C)	125
Hold time (min)	0
Ramp rate (^{o}C/min)	3
Temperature B (^{o}C)	239
Hold time (min)	0
Final temperature (^{o}C)	271
Hold time (min)	0
Ramp rate (^{o}C/min)	8

Table A-3 Concentrations of DBT, 4,6-DMDBT and HDS Products in HDS Liquid Product of Unsupported NiMo Sulfide at All Catalyst Preparation Conditions

Catalyst Preparation Conditions	Concentration (wt %) in Liquid Product									
Temperature (^{o}C) / Pressure (MPa)/ Solvent amount (g)/ Ni/(Mo+Ni)	DBT	BP	THDBT	CHB	BCH	4,6-DMDBT	3,3'DMBP	THDMDBT	MCHT	3,3'-DMBCH
300 / 2.8 / 1 / 0.43	0.265	0.102	0.014	0.091	0.021	0.359	0.087	0.086	0.054	0.0040
325 / 2.8 / 1 / 0.43	0.246	0.103	0.015	0.104	0.024	0.339	0.084	0.095	0.060	0.0040
350 / 2.8 / 1 / 0.43	0.221	0.106	0.020	0.114	0.028	0.324	0.081	0.108	0.069	0.0049
375 / 2.8 / 1 / 0.43	0.192	0.109	0.016	0.137	0.028	0.295	0.070	0.135	0.087	0.0051
350 / 1.4 / 1 / 0.43	0.321	0.085	0.021	0.054	0.011	0.434	0.045	0.082	0.034	0.0050
350 / 2.1 / 1 / 0.43	0.244	0.090	0.028	0.108	0.025	0.366	0.066	0.104	0.053	0.0047
350 / 3.4 / 1 / 0.43	0.195	0.121	0.018	0.113	0.025	0.304	0.094	0.103	0.079	0.0090
350 / 2.8 / 0 / 0.43	0.254	0.109	0.022	0.093	0.018	0.394	0.058	0.102	0.040	0.0033
350 / 2.8 / 3 / 0.43	0.141	0.125	0.014	0.149	0.033	0.250	0.096	0.133	0.100	0.0067
350 / 2.8 / 1 / 0.00	0.385	0.036	0.067	0.025	0.008	0.419	0.012	0.164	0.006	0.0017
350 / 2.8 / 1 / 0.20	0.286	0.096	0.026	0.078	0.015	0.404	0.048	0.096	0.049	0.0031
350 / 2.8 / 1 / 0.33	0.260	0.099	0.019	0.092	0.020	0.362	0.055	0.112	0.057	0.0039
350 / 2.8 / 1 / 0.50	0.172	0.116	0.016	0.140	0.034	0.283	0.095	0.112	0.089	0.0059
350 / 2.8 / 1 / 0.56	0.229	0.114	0.020	0.106	0.024	0.342	0.073	0.117	0.061	0.0035
350 / 2.8 / 1 / 1.00	0.473	0.027	0.016	0.004	0.005	0.568	0.004	0.039	0.002	0.0002

Appendix B

Calculation of % Conversion and % Selectivity

The HDS activity of the catalysts was expressed in terms of weight % conversion of the sulfur compounds and was obtained using the following equation:

$$Xi = \left[\frac{(Ci, feed - Ci, product)}{Ci, feed} \right] *100 \qquad (B-1)$$

where X_i = % conversion of the component i

(DBT or 4,6-DMDBT)

$C_{i,feed}$ = concentration of component i in the reactant

$C_{i,product}$ = concentration of component i in the products

Catalyst selectivity was expressed in mole % and calculated using the following equation:

$$Yi = \left(\frac{Ci, product / MWi}{\sum_{i=1}^{n} (Ci, product / MWi)} \right) *100 \qquad (B-2)$$

where Y_i = % selectivity of the product i

$C_{i,product}$ = concentration of product i

MWi = molecular weight of product i

n = number of products in reaction (n = 4)

The products of DBT HDS are

- Biphenyl (BP)

- Tetrahydrodibenzothiophene (THDBT)

- Cyclohexylbenzene (CHB)

- Bicyclohexane (BCH)

The products of 4,6-DMDBT HDS are

- 3,3'-Dimethylbiphenyl (3,3'-DMBP)

- Tetrahydrodimethyldibenzothiophene (THDMDBT)

- Methylcyclohexyltoluene (MCHT)

- 3,3'-Dimethylbicyclohexane (3,3'-DMBCH)

Appendix C

Calculation of Overall and Individual Rate Constants

For HDS over the unsupported NiMo sulfide catalyst, only the data of DBT and 4,6-DMDBT concentration was used to calculate total and individual rate constants.

1. Total rate constants

Table C-1 presents the kinetic data for HDS of DBT and 4,6-DMDBT over unsupported Mo based sulfide and commercial catalysts. As a first approximation, the HDS of individual sulfur compounds follows pseudo-first-order kinetics. The first-order rate expressions for DBT and 4,6-DMDBT HDS are as follows :

$$\ln\left(\frac{C_{DBT}}{C_{DBTo}}\right) = -\left(k_1 + k_2\right)t \qquad (C\text{-}1)$$

$$\ln\left(\frac{C_{4,6-DMDBT}}{C_{4,6-DMDBTo}}\right) = -\left(k_1 + k_2\right)t \qquad (C\text{-}2)$$

Where k_1 =   rate constant for the hydrogenation (HYD) pathway

               k_2 =   rate constant for the direct desulfurization (HYD) pathway

            $k_1 + k_2$ =   overall HDS rate constant

The overall HDS rate constant was obtained directly from the experimental data using eq (C-1) and (C-2). The pseudo-first-order kinetics of DBT and 4,6-DMDBT HDS over unsupported NiMo sulfide catalyst is presented in Figure C-1 and slope of linear plot is total rate constant ($k_1 + k_2$).

Table C-1 Kinetic Data for HDS of DBT and 4,6-DMDBT over Unsupported Mo Based Sulfide and Commercial Catalysts

| Catalyst	Time	DBT Conversion (%)	Selectivity (%)				4,6-DMDBT Conversion (%)	Selectivity (%)			
			BP	THDBT	CHB	BCH		3,3'DMBP	THDMDBT	MCHT	3,3'-DMBCH
MoS_2	7	1.8	46.2	40.4	6.2	9.2	3	0.8	98.4	0.5	0.2
	14	3.4	45.7	39.4	6.5	8.4	5.8	1.2	95.8	1.4	1.5
	21	4.9	44.7	37.4	9.8	8.1	8.6	1.3	94.3	2.3	2
	28	6.4	40.4	33.7	13	12.8	11.3	1.6	91.7	4.2	2.5
		$k_1+k_2 = 166.3\ 10^{-5}$/s gcat and $k_1/k_2 = 0.9$					$k_1+k_2 = 297.7\ 10^{-5}$/s gcat and $k_1/k_2 = 170.4$				
$NiMoS_2$	7	12.2	57.7	22.3	16.6	3.4	9.2	10	77.5	9.7	2.8
	14	24	54.5	17.1	25.3	3	17.2	12.1	72.3	13	2.7
	21	32.9	52.6	15.8	28.8	2.9	24.7	12..9	71.4	14.7	1.1
	28	39.6	50.1	13..5	32.9	3.5	30.4	12.8	67.8	19.3	0
		$k_1+k_2 = 1290\ 10^{-5}$/s gcat and $k_1/k_2 = 0.4$					$k_1+k_2 = 920.5\ 10^{-5}$/s gcat and $k_1/k_2 = 8.8$				
$CoMoS_2$	7	12.2	79.2	7	9.2	4.6	11.5	9.4	76.9	8.7	5
	14	22.9	77	7.6	11.5	3.9	22.1	8.5	77.3	10.7	3.5
	21	32.3	75.7	7.1	13.5	3.6	31.5	8.6	77.3	13.8	0.4
	28	40.6	73.8	6.7	15.9	3.6	39.7	8.1	75.4	15.5	0.9
		$k_1+k_2 = 1316.4\ 10^{-5}$/s gcat and $k_1/k_2 = 0.1$					$k_1+k_2 = 1289.5\ 10^{-5}$/s gcat and $k_1/k_2 = 8.1$				
Cr424	7	7.9	64.6	15.6	15.1	4.7	1.3	13.6	79.5	6.3	0.7
	14	13.1	63.9	13.8	18.6	3.7	3.5	13.6	77.1	8.3	1.1
	21	16.4	63.1	13.0	20.7	3.2	4.9	12.7	77.2	8.9	1.1
	28	22.4	63.9	10.3	22.8	3.0	6.4	11.9	76.6	10.9	0.6
		$k_1+k_2 = 609.4\ 10^{-5}$/s gcat and $k_1/k_2 = 0.3$					$k_1+k_2 = 169.9\ 10^{-5}$/s gcat and $k_1/k_2 = 5.6$				
Cr344	7	4.3	87.2	4.5	3.7	4.6	1.0	17.5	74.5	8.0	0.0
	14	8.7	86.9	4.4	5.7	3.0	2.1	16.4	73.6	10.0	0.0
	21	12.0	85.9	4.2	6.6	3.3	3.0	15.3	72.8	11.6	0.3
	28	16.4	85.5	4.0	7.8	2.7	4.2	14.1	71.8	13.1	1.1
		$k_1+k_2 = 458.1\ 10^{-5}$/s gcat and $k_1/k_2 = 0.1$					$k_1+k_2 = 110.6\ 10^{-5}$/s gcat and $k_1/k_2 = 4.1$				
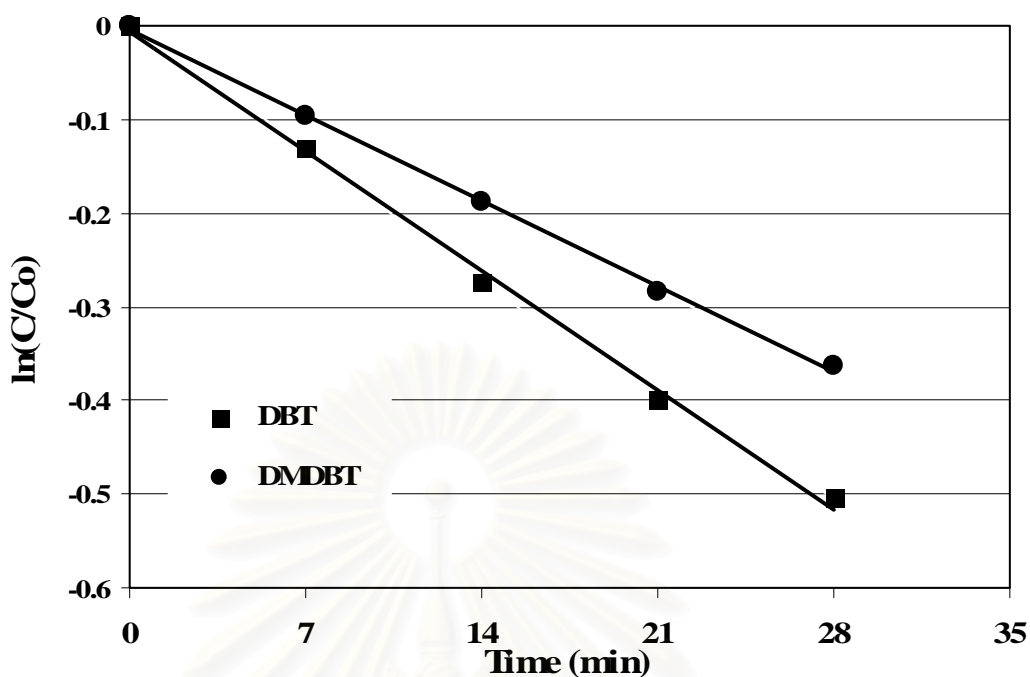
Figure C-1 Pseudo first order kinetics of 4,6-DMDBT and DBT HDS over
the unsupported NiMo sulfide catalyst.

2. Individual rate constants

We applied the method of initial rates using the initial selectivity of primary products, i.e., the selectivity of products at close to zero conversion. The k_1/k_2 ratio was obtained directly from the initial selectivity ratio between primary products in the HYD and DDS pathways. For DBT HDS, the rate constant k_1 is proportional to the initial hydrogenation rate or formation rate of THDBT, and the rate constant k_2 is proportional to the initial DDS rate or formation rate of BP. For 4,6-DMDBT HDS, the rate constant k_1 is proportional to the initial hydrogenation rate or formation rate of HDMDBTs, and the rate constant k_2 is proportional to the initial DDS rate or formation rate of DMBP.

Figure C-2 shows the plot of conversion versus selectivity for the DBT and 4,6-DMDBT HDS over unsupported NiMo sulfide catalyst. THDBT and BP clearly are the primary products, and CHB and BCH are the secondary products in

DBT HDS, because the selectivity for THDBT and BP at the zero conversion is nonzero and the selectivity for CHB and BCH at the zero conversion is zero. In the same way, THDMDBT and 3,3'-DMBP clearly are the primary products, and MCHT and DMBCH are the secondary products in 4,6-DMDBT HDS, because the selectivity for THDMDBT and 3,3'-DMBP at the zero conversion is nonzero and the selectivity for MCHT and DMBCH at the zero conversion is zero. The initial selectivity values for the primary products can be determined by extrapolation to zero conversion as shown in Figure C-2.

The individual rate constant of DBT and 4,6-DMDBT was determined as follows :

For DBT HDS
$$\frac{k_1}{k_2} = \frac{[initial\ \ selectivity\ \ of\ \ THDBT]}{[initial\ \ selectivity\ \ of\ \ BP]} \qquad \text{(C-3)}$$

For 4,6-DMDBT HDS
$$\frac{k_1}{k_2} = \frac{[initial\ \ selectivity\ \ of\ \ THDMDBTs]}{[initial\ \ selectivity\ \ of\ \ 3,3'-DMBP]} \qquad \text{(C-4)}$$

Since k_1+k_2 values have been estimated as shown in Figure C-1, $(k_1+k_2) = 1,290 * 10^{-5}$/s g.cat for DBT HDS and $920.5 * 10^{-5}$/s g.cat for 4,6-DMDBT HDS and the k_1/k_2 ratio can be estimated as shown in Figure C-2, the individual k_1 and k_2 values can then be calculated. The ratio of k_1/k_2 is equal to 0.42 for DBT HDS and 8.76 for 4,6-DMDBT HDS. The k_1 and k_2 is equal to $381.9 * 10^{-5}$/s g.cat and $908.1 * 10^{-5}$/s g.cat for DBT HDS and $826.2 * 10^{-5}$/s g.cat and $94.3 * 10^{-5}$/s g.cat for 4,6-DMDBT HDS, respectively.
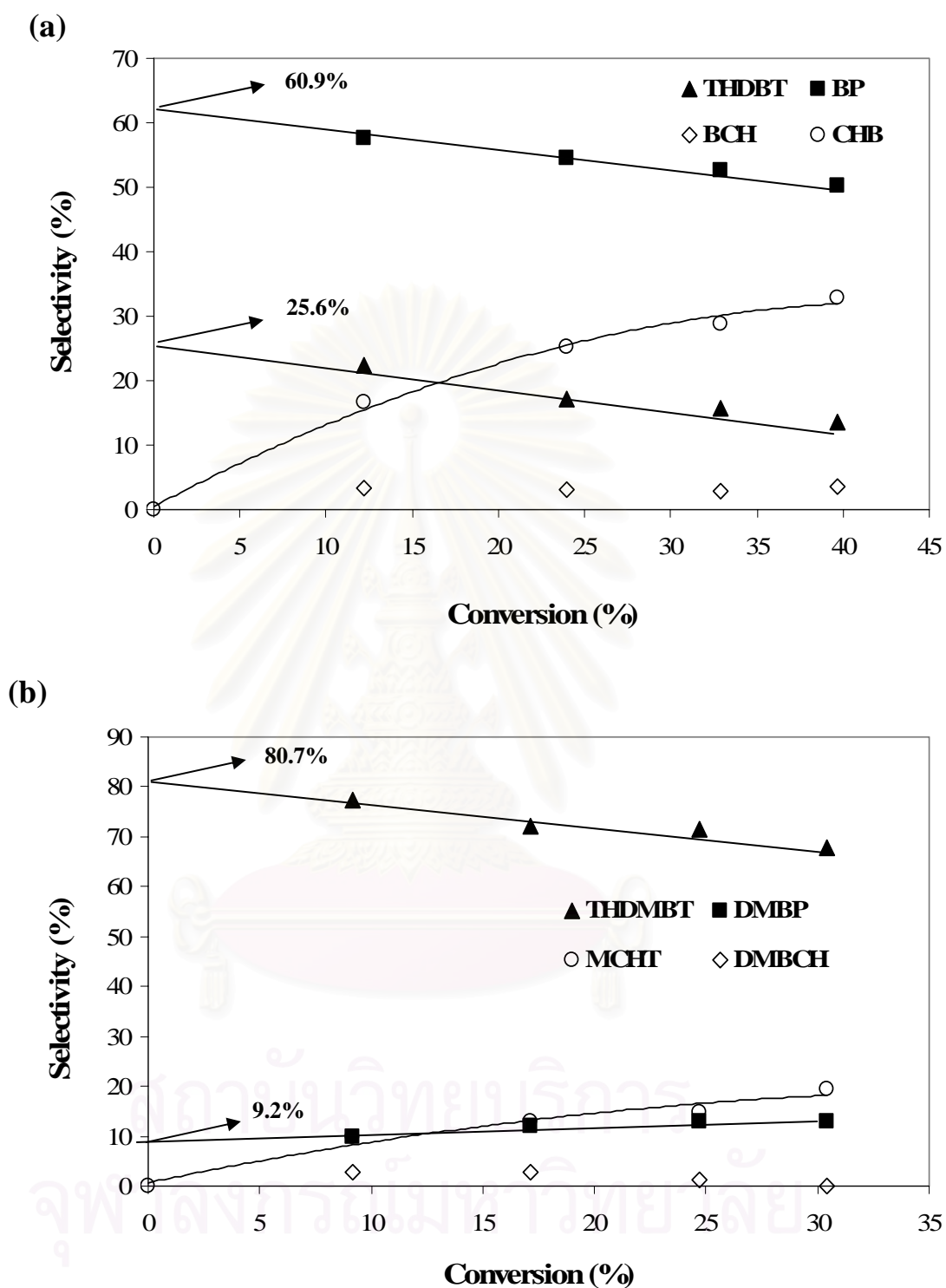
Figure C-2 Extrapolation of products of (a) HDS of DBT and (b) HDS of
4,6-DMDBT for estimating the initial selectivity of products over NiMo
sulfide catalysts.

Appendix D

Calculation of Selectivity and Promoting Effect

1. Selectivity

The selectivity for the kinetics study is the proportion between individual rate constant and total rate constant of each catalyst. It was divided into 2 types (selectivity to HYD and selectivity to DDS) and calculated using the following equation:

$$\text{Selectivity to HYD} = \frac{k_1}{(k_1 + k_2)} \qquad \text{(D-1)}$$

$$\text{Selectivity to DDS} = \frac{k_2}{(k_1 + k_2)} \qquad \text{(D-2)}$$

2. Promoting effect

The promoting effect is relative ratio of the rate constant of promoted Mo sulfide catalysts and unpromoted Mo sulfide catalysts and is determined as follows:

$$\text{Promoting effect on total rate constant} = \frac{(k_1 + k_2) \text{ of MeMoS}_2}{(k_1 + k_2) \text{ of MoS}_2} \qquad \text{(D-3)}$$

$$\text{on HYD rate constant} = \frac{k_1 \text{ of MeMoS}_2}{k_1 \text{ of MoS}_2} \qquad \text{(D-4)}$$

$$\text{on DDS rate constant} = \frac{k_2 \text{ of MeMoS}_2}{k_2 \text{ of MoS}_2} \qquad \text{(D-5)}$$

Where   Me   =   Co or Ni

       k_1 =   rate constant for HYD pathway

       k_2 =   rate constant for DDS pathway

       $k_1 + k_2$ =   overall HDS rate constant

Appendix E

Calculation of Adsorption Capacities

In the liquid-phase adsorption of DBT and 4,6-DMDBT experiments, the model fuel was collected after passing the adsorbent bed and the concentration of each sulfur compounds was determined. Then, the results were reported in plots of C/Co (ratio of the outlet concentration to the initial concentration in the model fuel) versus amount of treated fuel/catalyst weight which called the breakthrough curve as shown in Figure E-1. The important term are defined as follows :

The Breakthrough Point is the amount of treated fuel/catalyst weight that C/Co value starts higher than zero.

The Saturation Point is the amount of treated fuel/catalyst weight that C/Co value equal one.

The Saturation Capacity is the total adsorption capability of adsorbent that can adsorb each compound and make the C/Co value of each compound less than one.

The Breakthrough Capacity is the adsorption capacity of adsorbent that can adsorb each compound and make the C/Co value of each compound less than zero.

The replacement molecule is number of molecule of compound that have relatively lower adsorptive affinity than the subsequently breakthrough compounds and are replaced by higher adsorptive affinity compound.

The Net Capacity is the net adsorption capacity of adsorbent for each compound.

- The Breakthrough Capacity is area A

- The amount of the adsorbed DBT (The Saturation Capacity) is the area between the breakthrough curve of DBT and line $C_t/C_o = 1$ before the saturation point (area A+B).

- The amount of the replaced DBT is the area between the breakthrough curve and line $C_t/C_o = 1$ after the saturation point (area C).

- The Net Capacity is calculated by subtracting the amount of the replaced molecules from the saturation capacity (area (A+B) – area C).
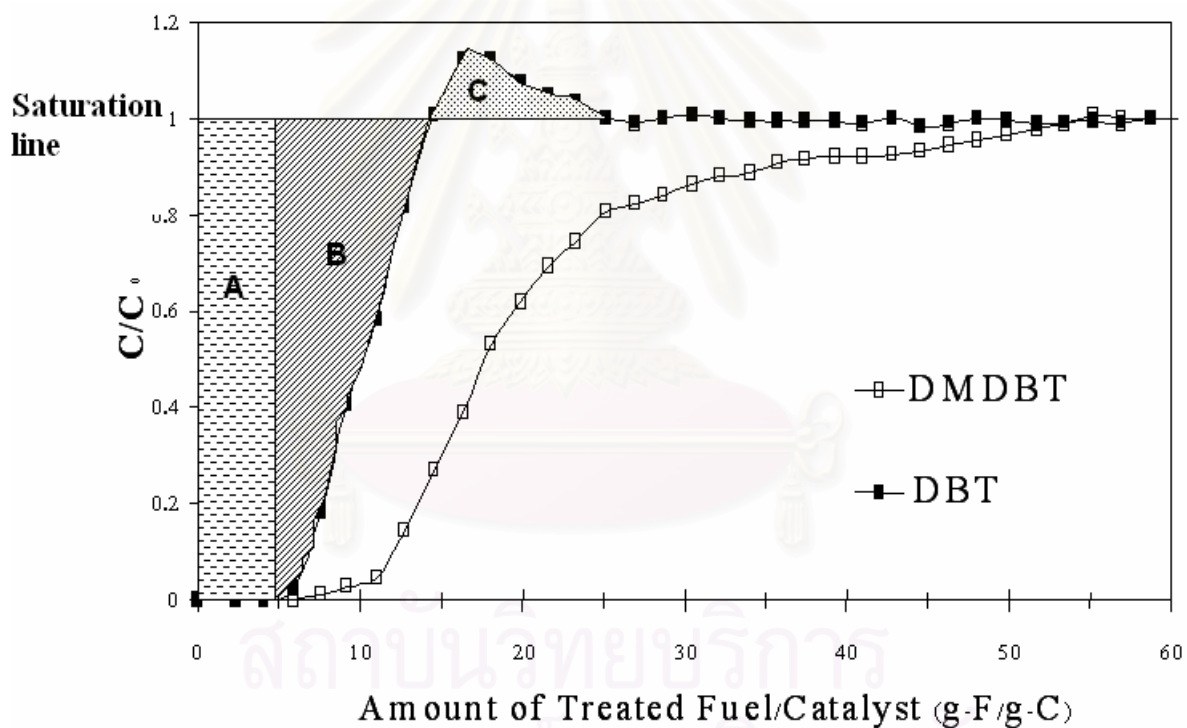

Figure E-1. The breakthrough curve of DBT and 4,6-DMDBT over the unsupported Mo based sulfide catalyst.

Appendix F

Calculation of Turn Over Frequency

Turn over frequency (TOF) in catalysis is defined as the number of molecules reacting per active site in unit time. Typically, TOF is calculated using rate constant of reaction and number of active site as shown in eq. (F-1).

$$TOF = \frac{\text{rate constant, k}}{\text{number of active site}} \qquad \text{(F-1)}$$

In this research, the TOF was calculated using the net capacity of the catalyst from selective adsorption experiment (see chapter 6) as a measurement of the number of active sites. Then, TOF presented in this research was calculated in eq. (1.2)

$$TOF = \frac{\text{rate constant, k}}{\text{net adsorption capacity}} \qquad \text{(F-2)}$$

The unit of TOF will be s^{-1}.

VITA

Miss Boonyawan Yoosuk was born on December 6, 1981 in Bangkok Thailand. She received her B.Sc. (First class honors) degree in chemical engineering from Chulalongkorn University. Boonyawan joined the department of chemical technology Chulalongkorn University as a doctoral student in 2003. She has received the Royal Golden Jubilee Scholarship from Thailand Research Fund for her Ph.D study. Boonyawan also served as a teaching assistant for undergraduate courses "Material and Energy Balances" and "Applied Mathematics in Chemical Engineering". While in graduate school, Boonyawan spent almost 2 years (2005-2007) doing research at Clean Fuel and Catalysis Program (CFCP) in The Energy Institute of The Pennsylvania State University (PSU), PA, USA. Her paper entitled "Highly Active MoS_2, $CoMoS_2$ and $NiMoS_2$ Unsupported Catalysts Prepared by Hydrothermal Synthesis for Hydrodesulfurization of 4,6-Dimethyldibenzothiophene" has been accepted for publication in "Catalysis Today". She also presented her work at 2 conferences in USA, 1 conference in the Netherlands and 1 conference in Thailand.